Politecnico di Bari

Department of Mechanics, Mathematics, and Management
MECHANICAL AND MANAGEMENT ENGINEERING
Ph.D. Program
SSD: ING-IND/13 – APPLIED MECHANICS

Final Dissertation

Electroadhesion for Soft Robotics: advancements in Soft Gripper applications

---

by
Massimiliano Mastrangelo

Supervisors:

Prof. Giuseppe Carbone

Dr. Vito Cacucciolo

Coordinator of Ph.D. Program:
Prof. Giuseppe P. Demelio

Course n°35, 01/11/2019 - 31/01/2023

LIBERATORIA PER L'ARCHIVIAZIONE DELLA TESI DI DOTTORATO

Al Magnifico Rettore del Politecnico di Bari

Il sottoscritto Massimiliano Mastrangelo, nato a Bari il 22/09/1993, residente a Bari in via P. Gobetti 6, e-mail massimilianomastrangelo@outlook.com, iscritto al 3° anno di Corso di Dottorato di Ricerca in Ingegneria Meccanica e Gestionale ciclo XXXV ed essendo stato ammesso a sostenere l'esame finale con la prevista discussione della tesi dal titolo: "Electroadhesion for Soft Robotics: advancements in Soft Gripper applications"

DICHIARA

1) di essere consapevole che, ai sensi del D.P.R. n. 445 del 28.12.2000, le dichiarazioni mendaci, la falsità negli atti e l'uso di atti falsi sono puniti ai sensi del Codice penale e delle Leggi speciali in materia, e che nel caso ricorressero dette ipotesi, decade fin dall'inizio e senza necessità di nessuna formalità dai benefici conseguenti al provvedimento emanato sulla base di tali dichiarazioni;
2) di essere iscritto al Corso di Dottorato di ricerca in Ingegneria Meccanica e Gestionale ciclo XXXV, corso attivato ai sensi del "*Regolamento dei Corsi di Dottorato di ricerca del Politecnico di Bari"*, emanato con D.R. n.286 del 01.07.2013;
3) di essere pienamente a conoscenza delle disposizioni contenute nel predetto Regolamento in merito alla procedura di deposito, pubblicazione e autoarchiviazione della tesi di dottorato nell'Archivio Istituzionale ad accesso aperto alla letteratura scientifica;
4) di essere consapevole che attraverso l'autoarchiviazione delle tesi nell'Archivio Istituzionale ad accesso aperto alla letteratura scientifica del Politecnico di Bari (IRIS-POLIBA), l'Ateneo archivierà e renderà consultabile in rete (nel rispetto della Policy di Ateneo di cui al D.R. 642 del 13.11.2015) il testo completo della tesi di dottorato, fatta salva la possibilità di sottoscrizione di apposite licenze per le relative condizioni di utilizzo (di cui al sito http://www.creativecommons.it/Licenze), e fatte salve, altresì, le eventuali esigenze di "embargo", legate a strette considerazioni sulla tutelabilità e sfruttamento industriale/commerciale dei contenuti della tesi, da rappresentarsi mediante compilazione e sottoscrizione del modulo in calce (Richiesta di embargo);
5) che la tesi da depositare in IRIS-POLIBA, in formato digitale (PDF/A) sarà del tutto identica a quelle **consegnate**/inviate/da inviarsi ai componenti della commissione per l'esame finale e a qualsiasi altra copia depositata presso gli Uffici del Politecnico di Bari in forma cartacea o digitale, ovvero a quella da discutere in sede di esame finale, a quella da depositare, a cura dell'Ateneo, presso le Biblioteche Nazionali Centrali di Roma e Firenze e presso tutti gli Uffici competenti per legge al momento del deposito stesso, e che di conseguenza va esclusa qualsiasi responsabilità del Politecnico di Bari per quanto riguarda eventuali errori, imprecisioni o omissioni nei contenuti della tesi;
6) che il contenuto e l'organizzazione della tesi è opera originale realizzata dal sottoscritto e non compromette in alcun modo i diritti di terzi, ivi compresi quelli relativi alla sicurezza dei dati personali; che pertanto il Politecnico di Bari ed i suoi funzionari sono in ogni caso esenti da responsabilità di qualsivoglia natura: civile, amministrativa e penale e saranno dal sottoscritto tenuti indenni da qualsiasi richiesta o rivendicazione da parte di terzi;
7) che il contenuto della tesi non infrange in alcun modo il diritto d'Autore né gli obblighi connessi alla salvaguardia di diritti morali od economici di altri autori o di altri aventi diritto, sia per testi, immagini, foto, tabelle, o altre parti di cui la tesi è composta.

Bari, 08/05/2023 Firma

_____

Il/La sottoscritto, con l'autoarchiviazione della propria tesi di dottorato nell'Archivio Istituzionale ad accesso aperto del Politecnico di Bari (POLIBA-IRIS), pur mantenendo su di essa tutti i diritti d'autore, morali ed economici, ai sensi della normativa vigente (Legge 633/1941 e ss.mm.ii.),

CONCEDE

- al Politecnico di Bari il permesso di trasferire l'opera su qualsiasi supporto e di convertirla in qualsiasi formato al fine di una corretta conservazione nel tempo. Il Politecnico di Bari garantisce che non verrà effettuata alcuna modifica al contenuto e alla struttura dell'opera.
- al Politecnico di Bari la possibilità di riprodurre l'opera in più di una copia per fini di sicurezza, back-up e conservazione.

Bari, 08/05/2023 Firma _____

Politecnico di Bari

Department of Mechanics, Mathematics, and Management
MECHANICAL AND MANAGEMENT ENGINEERING
Ph.D. Program
SSD: ING-IND/13 – APPLIED MECHANICS

Final Dissertation

Electroadhesion for Soft Robotics: advancements in Soft Gripper applications

---

by

Massimiliano Mastrangelo

Referees:

Prof. Shingo Maeda

Prof. Marco Fontana

Supervisors:

Prof. Giuseppe Carbone

Dr. Vito Cacucciolo

Coordinator of Ph.D. Program:

Prof. Giuseppe P. Demelio

Course n°35, 01/11/2019 - 31/01/2023

Acknowledgments

Con queste poche parole voglio esprimere il mio riconoscimento per le persone e gli avvenimenti che hanno contribuito a delineare il profilo del mio cammino di Dottorato, di cui questa tesi non è che uno dei tanti frutti che conserverò nel mio bagaglio di esperienze acquisite.

Il percorso verso il conseguimento del titolo non è stato lineare, né semplice. Molti sono stati i cambi di rotta, gli imprevisti, le delusioni, forse in numero maggiore di quanto una già perigliosa esperienza come quella dottorale ne sia naturalmente caratterizzata. Proprio per questo, però, ne risulta anche più ricca di insegnamenti per le avventure che verranno, di cui faccio tesoro.

Il Dottorato segna la fine del mio iter formativo presso il Politecnico di Bari. La scelta di candidarmi a Dottorando di Ricerca fu dettata dall'amore per il sapere, la ricerca, e la scoperta, o almeno per quella che ne era la mia visione da inesperto neolaureato. Consideravo, idealisticamente e magari erroneamente, i grandi nomi della scienza come individui capaci di conciliare rilevanti risultati scientifici con personalità lucide, vivaci, appassionate, ma soprattutto sostenute da un'integrità etica e morale tale da renderle tanto corrette nella vita quanto nel rigore del loro metodo scientifico. Ero portato a pensare che non potessero esistere i primi senza la seconda, e viceversa, che fossero interdipendenti e inseparabili. La mia seppur breve (ad oggi) esperienza nel mondo della ricerca mi ha invece insegnato che tale coincidenza è spesso non verificata. Ho imparato che si può essere bravi e appassionati ricercatori, in erba e non, senza che il proprio nome ed il proprio contributo vengano conosciuti e riconosciuti, e senza che le proprie carriere riescano a prendere il volo, per motivazioni al contrario ben note agli addetti ai lavori. Allo stesso modo, ho imparato che si può essere esperti pubblicatori e abili ricercatori, più di citazioni che di scienza, senza che nessuno dei rimanenti attributi sopracitati venga mai manifestato. Sono grato per aver ricevuto questo insegnamento, utile tanto ad illuminarmi sull'accademia che sulla vita in generale.

Ringrazio il mio tutor (mancato), Marco Donato de Tullio, per avermi mostrato il significato di amore per la ricerca e per la propria disciplina, durante il mio percorso di laurea prima e come supervisore poi.
Ringrazio il mio tutor (effettivo), Vito Cacucciolo, con cui ho avuto la possibilità di lavorare nel campo della robotica, nel quale, assieme ad altri, intendo costruire la mia carriera. Con lui ho imparato cosa significa far nascere e finalizzare un buon lavoro di ricerca, dalla formulazione di un'ipotesi alla scrittura di un contributo scientifico, e ho intrapreso la mia prima esperienza lavorativa al di fuori dell'accademia. Ho imparato molto lavorando con lui, più di quanto sia stato voluto o pianificato.
Ringrazio Shingo Maeda, e i membri del suo laboratorio, per avermi accolto e ospitato nella lontana terra giapponese, per avermi offerto gli strumenti e la disponibilità necessari alla mia ricerca durante il periodo trascorso a Tokyo, nonché per avermi dimostrato nel pratico che in Italia non esistono ristoranti di sushi.

Ringrazio i colleghi dottorandi con cui ho avuto modo di confrontarmi nel mio percorso. Ritengo lo scambio interdisciplinare e il confronto fondamentali per lo sviluppo del corretto approccio critico alle problematiche di carattere scientifico. Pertanto, non posso che essere grato anche per la minima occasione di dialogo con coloro alle prese con il mio stesso percorso formativo.
Tra i miei colleghi dottorandi, nomino in particolare gli Arduini, ovvero Simone, Michele, Alessandro, supporto e stimolo alla crescita personale prima che professionale, amici prima che colleghi.

Ringrazio i ragazzi di Omnigrasp, Davide e Fabio, i primi colleghi della mia carriera lavorativa, che alla fine del mio dottorato mi hanno regalato la fase più spensierata dell'intero percorso. Il microcosmo di Japigia è stato un'oasi rigenerante, provvidenziale per riprendere fiato alla fine dei miei studi. A proposito ringrazio anche Antonio Lassandro per il supporto logistico, e morale, e per la carica nella mia ricerca e nel mio lavoro.

Ringrazio i miei amici, i soliti noti Francesco e Simone, e Bruno (e Rossana), e Giovanni, le costanti e infaticabili presenze negli alti, nei bassi, negli arresti, nelle ripartenze. Ringrazio gli amici con cui ci siamo un po' persi di vista, il cui contributo alla mia crescita in questi anni non ho dimenticato.

Ringrazio la mia famiglia. La famiglia ti aiuta a crescere, formandoti e donandoti quelle caratteristiche di cui ti accorgi quando cresci, e quando ne necessiti. Non basterebbero queste pagine per parlarne. Posso solo dire che se sono stato in grado di completare un Dottorato di Ricerca, ma soprattutto di essere quel che sono, è per una buona parte grazie a loro.

L'ultimo dei miei ringraziamenti lo dedico a Giorgia. Nessuno avrebbe scommesso sulla possibilità di un amore tra due persone tanto diverse. E' tutto quello che io non sono, e viceversa. Colma le mie lacune e le mie incompletezze. In questi anni di lavoro mi ha ascoltato, sostenuto, incoraggiato. Il suo merito più grande è però un altro, ed è legato alla mia persona più che alla mia professione.
Giorgia ha portato la luce, dove prima c'era il buio.

Massimiliano

Abstract

This thesis advances the field of electroadhesion applied to soft robotics, with focus on electroadhesion soft grippers. The main contribution of my work regards novel insights into the influence of mechanics on electroadhesion. In the first part of the Thesis, I explored how mechanics plays a critical role in the performance of current designs of electroadhesion soft grippers. In the second and last part of Thesis, I investigated an alternative approach for the realization of a novel electroadhesion soft robotic gripper embedding hydrogel into its structure.

Despite extensive research on electroadhesion based devices has been conducted in the past, only recently the role of the mechanical features of the system has been discovered and outlined. This is particularly important for robotic devices such as electrostatic and electrohydraulic actuators, electrostatic clutches and electroadhesion grippers. In this Thesis, I focused mainly on grippers. First, I explored the relationship between mechanical and electrical parameters of the grasping system and how it influences the wrapping capabilities of an electroadhesion gripper. Despite some current designs involve the use of external actuators to ease the grasping of objects with complex shapes, passive wrapping around objects can be reached under certain conditions. In the latter case, the wrapping is based on the phenomenon of zipping, already exploited in soft electrostatic actuators. Our work allowed us to discover that the zipping of gripper's fingers on a curved object is ruled by two voltage thresholds, depending on the characteristics of the system. We experimentally validated the theoretical model and observed that actual behavior is predicted by the model, even if further investigations are needed to clarify what happens under certain conditions. The outcomes of this investigation are the starting point for determining how even more complex shape influence the object wrapping and to design grippers able to reliably grasp even the most complicated objects. The results can be useful for the advancement of electrostatic and electrohydraulic actuators as well.

The shape of the object also influences the maximum holding force of an electroadhesion gripper. When it grasps curved objects, the geometry of the object produces an exponential increase in the adhesion force. The effect has been observed in previous works, but no theoretical or systematical experimental investigations were conducted. I produced a model that considers the shape of the object and dramatically reduces the error in force prediction if compared with previous models. We also conducted a preliminary validation of the model. The first results confirm the validity of our hypotheses. Further work is required to fully validate the model. The results of the study are valuable not only for determining the capabilities of an electroadhesion soft gripper. They can easily be employed to guide the design of novel soft robotic devices such as electrostatic clutches. We aim at producing electrostatic clutches able to reduce requirements in terms of applied voltage or increase the output force, being equal other parameters.

The final part of the thesis presents the preliminary results conducted on the modulation of hydrogel friction obtained by applying voltage to it. Previous works demonstrated that hydrogel friction and adhesion respond to the application of relatively low voltages. We aim at exploiting this effect to produce the first electroadhesion soft gripper made by hydrogels. I started by investigating methods to increase water retention of hydrogel and to obtain bonding to external surfaces. Fulfilling these requirements is crucial to integrate hydrogels into a soft robot. I then produced preliminary experiments on the modulation of friction of hydrogel with applied voltage, that confirmed the hypotheses. Finally, I produced some tests on archaic prototypes of soft gripper's finger embedding hydrogel into their structure. The first experiments did not produce the expected results. The work will be carried on by improving the designs of the prototypes. Further investigations for the refinement of bonding and water retention methods will be also conducted.

Contents

List of Figures

List of tables

1. Introduction

1.1 Goal

The aim of this Thesis is to deepen the knowledge and advance the applications based on Electroadhesion (indicated as EA in the following) in the Soft Robotics field. In particular, EA soft robotic grippers have been the core of my work. However, the results of my investigation can be extended to other soft devices leveraging EA as working principle, such as soft wearables and actuators.

I mainly investigated the synergy of mechanics and electrostatics in EA soft grippers. Focusing on current designs of grippers, I studied the interplay between the mechanical and electrical features of the system composed by the gripper and the target object, and how this interplay influences the grasping task. The goal was to disclose the important role of mechanics in electroadhesion, and how it can be leveraged to create EA soft devices with improved designs.

The last part of the work included in this thesis investigated the feasibility of a novel concept of soft robotic device, capable of modulating its tribological behavior in response to an electrical stimulus when interacting with external objects. The final goal of the investigation was to include hydrogel into the structure of the robot. Previous study showed the possibility of controling adhesion and friction of hydrogels with electricity. I produced a preliminary study about the possibility of leveraging this effect in a soft robotic gripper.

1.2 Background and motivation

Traditional robotics is a mature technological field. However, in recent years the convergence of advancements in material engineering and fabrication methods has pushed the growth of a new area of study, known as soft robotics [6]. Soft robots respond to the demand for versatility arising from the expansion of robotics from conventional fields such as industry and manufacturing to novel areas such as healthcare, marine and terrestrial exploration, human-machine cooperation [7]. As the adjective suggests, the main feature differentiating a *soft* robot by its *hard* counterpart is the stiffness of its body. A soft robot is primarily composed by easily deformable matter. This allows the robot to adapt its shape and movements with respect to the environment [7]. Conventional robots made by rigid links, joints, and actuators exhibit high reliability, precision, and efficiency. Consequently, they are well-suited for designed and repetitive tasks, but lack of adaptability to unstructured environments and to different tasks [7,8]. Conversely, thanks to its intrinsic compliance, a soft robot safely interacts with humans and with its context. The ability to easily adapt to the environment due to the compliant structure rather than to complex control strategy is defined morphological computation [9]. The control of the soft robot is partially delegated to the body deformability rather than to complicated control systems.

The field of application of soft robotics is dramatically expanding in the last years. Soft robots include exoskeletons for rehabilitation [10,11] or human-machine interaction [12], surgery tools [13], locomotive terrestrial robots [14,15], swimmers [16], aerial robots [17], microrobots [18] (Figure 1.1). Soft robotic grippers are another important branch of soft robotics [19,20]. Traditional grippers are made by rigid joints and links, making the grasping extremely difficult and prone to object damage. In soft grippers, the fingers in contact with the target object are flexible and stretchable, making the grasping safe even with the most delicate objects. Additionally, the soft material allows the finger to be underactuated. Underactuation enables better conformation of the gripper to the target object [19].

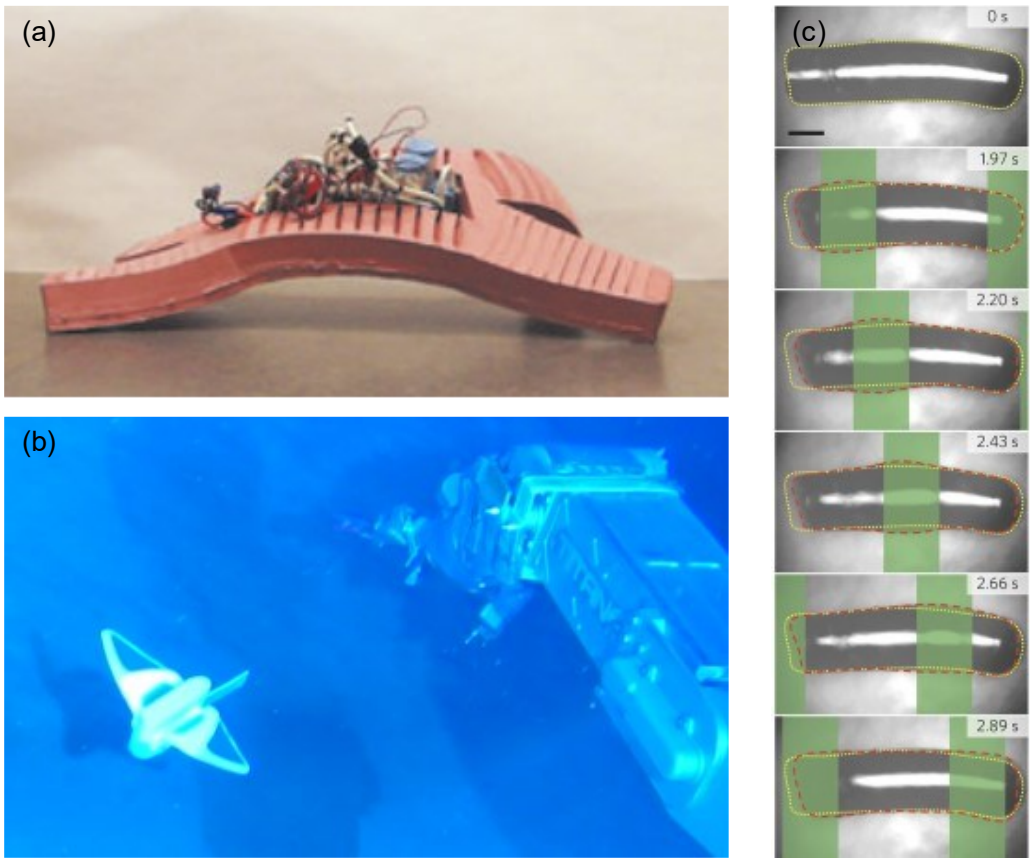

Figure 1.1 – (a) A walking, untethered soft robot. Reproduced with permission from Tolley et al. [15]. (b) A soft robot swimming at around 3000 m under the sea level. The soft robot is designed to sustain pressure of water in the Mariana Trench. Reproduced with permission from Li et al. [16]. (c) Soft microrobot moving being stimulated by light. Reproduced with permission from Palagi et al. [18].

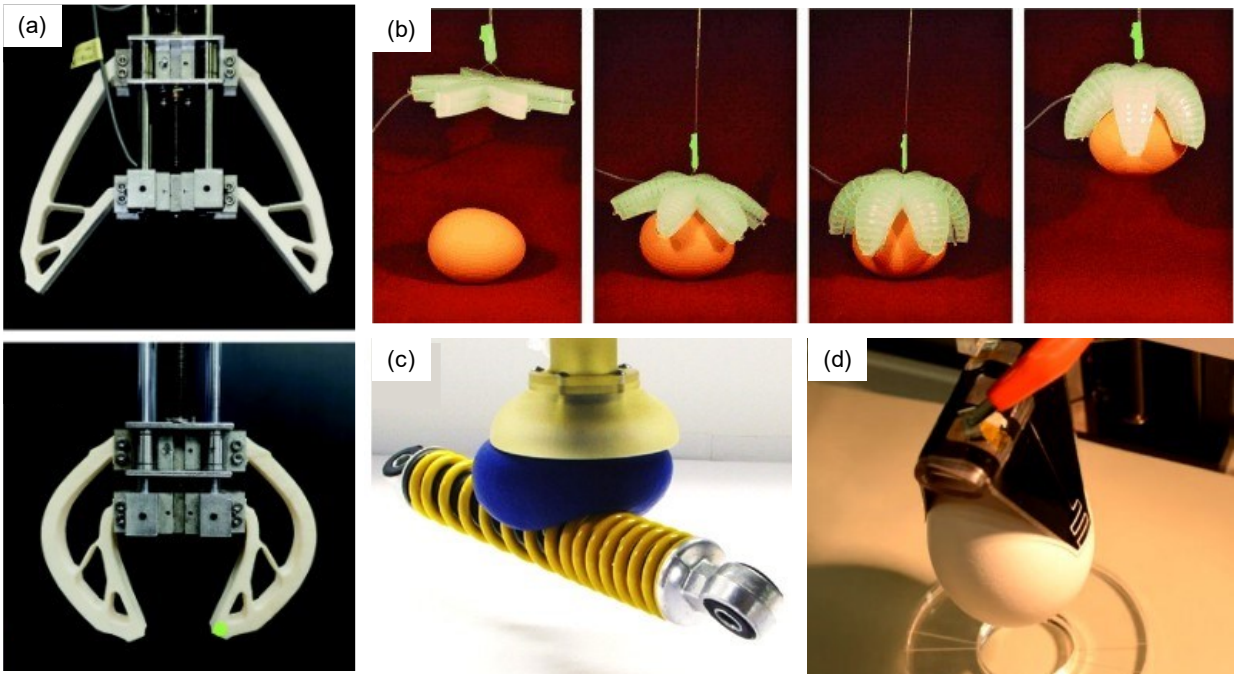

Figure 1.2 – (a) A soft gripper whose fingers passively deform under actuation and comply to the object shape. Reproduced with permission from Liu et al. [21]. (b) A pneumatically actuated gripper grasping an egg. Reproduced with permission from Ilievski et al. [22]. (c) A granular jamming gripper grasping a shock adsorber coil. Reproduced with permission from Brown et al. [23]. (d) An EA soft gripper grasping an egg. Reproduced with permission from Shintake et al. [24].

Current soft grippers typologies rely on different physical working principles. Three wide categories can be defined [19]: (1) grippers based on impactive prehension of actuated fingers; (2) grippers in which the grasping happens by controlling finger stiffness; (3) adhesion-based grippers (astrictive prehension). Common soft gripper designs include passive deformation of fingers under actuation [21], pneumatic actuation [22], granular jamming [23], EA grippers [24], and others (Figure 1.2). Among other designs, EA soft grippers present particularly advantageous features. Being based on an astrictive working principle, they grasp objects without squeezing them. They are silent, clean, low-power and low-weight. They can adapt to different tasks, from grasping fruit and vegetables [4] to textiles [25] and components for space applications [26], are self-sensing [27], hold large weights [28,29]. Moreover, they are suitable for different surface and materials properties, thanks to their adaptable working principle.

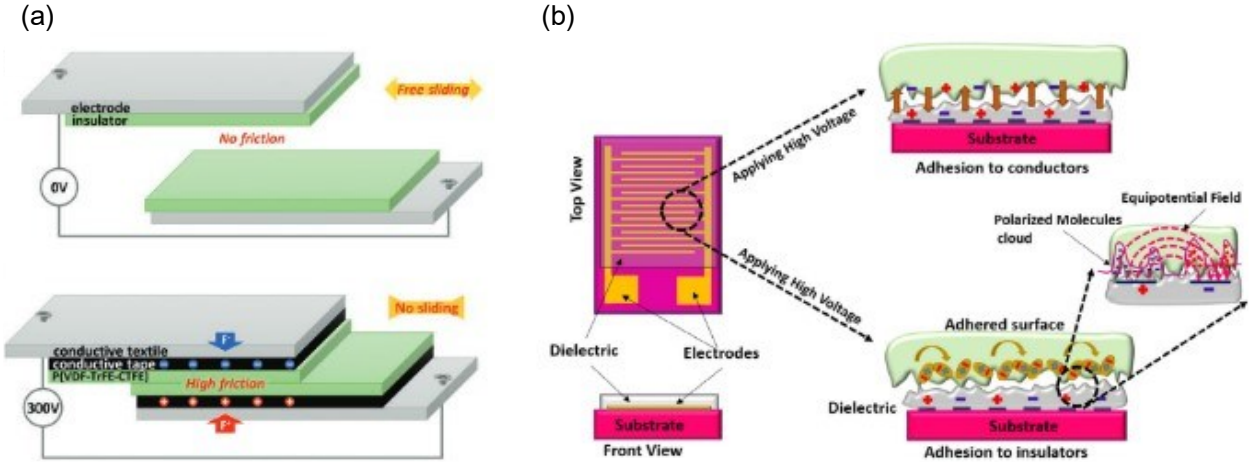

Figure 1.3 – (a) The working principle of an electrostatic clutch. When a voltage is applied between the two plates (electrodes), they attract to each other generating adhesion. Reproduced with permission from Hinchet et al. [30]. (b) The working principle of current EA soft grippers. An EA finger is a pad made by dielectric material embedding two interdigitated electrodes. When a voltage is applied to the electrodes, fringing electric fields are produced. They generate deposition of charges on the object surface by induction (conductive object) or by polarization (insulator). Charges on the object and on the electrodes attract to each other and adhesion is produced. Reproduced with permission from Rajagoplan et al. [31].

If the term adhesion refers to the force required to separate two contacting surfaces [32], electroadhesion is the attractive force between two surfaces when a potential difference is applied between them [33]. The discovery of the EA dates back to one century ago [34], when the engineers Johnsen and Rahbek observed the effect by placing a porous electrolytic material between two conductor plates at high voltage difference [31]. EA presents many advantages among other types of adhesion. It can be electrically turned on and off [35], leaves no chemical residuals on the adherends surface since it does not requires an external adhesive, works on smooth and rough surfaces (although with different outcomes in terms of adhesion forces). Today, EA finds application in many fields. For example, EA is exploited in haptic devices such as touchscreens and tactile displays, where the application of voltage to the screen induces attraction to the user finger [36–38]. In robotics, EA is used for clutches [30,39–43], wall-climbing robots [44–47], flying robots [48], soft grippers [4,49–51]. In the common design of an electrostatic clutch, the EA effect is leveraged between two planar contacting components, in which are embedded flat electrodes acting as parallel plates of a capacitor. Dielectric between the plates insulate the electrodes and ensure the electrostatic effect, responsible for preventing relative movement between the plates (Figure 1.3a). Conversely, in EA grippers both the electrodes are embedded into the gripper's finger structure. Applying a voltage to the electrodes produces a fringing electric field that exits from the finger surface and penetrates the target object. EA grippers are suited for both conductive objects and insulators. In the first case, the fringing field generates

a distribution of charges on the object surface by electrical induction. In the latter case, charges are produced by polarization of the dielectric surface. In both cases, electrostatic attraction is generated between the charges deposited on the object surface and on the electrodes, producing adhesion (Figure 1.3b).

Research on EA-based robotic systems mostly concentrated on the tribological or electrical sides of the phenomenon [52,53]. With recent works [4,28], the important role of mechanical aspects in EA has been highlighted. This Thesis aims at deepening the understanding about how the mechanics influences EA, since it can lead to exploit the full potential of current EA robotic designs. Exploiting mechanics in EA will also pave the way toward the realization of novel improved devices. For example, one of the main current drawbacks of EA robotic grippers and clutches is the use of high voltages (order of kV), that make the device bulkier and more expensive. The wise use of mechanics-based solutions could not only lead to better performances, but also to smaller and cheaper devices, being equal the resulting output.

For these reasons, in the first two Chapters of this Thesis, I focused on the role of the mechanics in current EA soft grippers design, looking for hints that could advance the field of EA-based soft robotic devices. In the third and last Chapter, I explored new possibilities based on the use of hydrogels, with the final goal of reducing voltage requirements and expand capabilities of EA soft devices. Preliminary work demonstrated the possibility of modulating friction and adhesion of hydrogels by applying relatively low voltages. Including hydrogel into an EA soft robot has the potentiality to reduce the voltage needed to control adhesion. Additionally, it could also result in augmented capabilities, enabling the device to modify its surface response, going from adhesion to lubrication.

1.3 Thesis Outline

The content of the Thesis is organized as follows:

- Chapter 2 treats the topic of passively wrapping EA grippers. The shape of the grasped object can limit the wrapping capabilities of EA soft grippers. To resolve the problem, existing solution resort to the use of external actuators that actively conform to the grasped object. The drawbacks are related to increased bulkiness of the gripper and reduced actual contact area between the gripper and the object, that is instead critical for exploiting EA effect. We discovered that with the correct choice of parameters EA grippers with fingers made by thin, soft tapes can passively wrap the object without any external actuators. We also discovered that passive wrapping depends on the interplay between the mechanical and electrical features of the system, and it is based on the physical phenomenon of electroadhesion-induced zipping.
- Chapter 3 deals with EA soft grippers producing holding forces variable with the shape of the grasped object. Starting from preliminary observations, we discovered how not only the posture of the gripper (as already demonstrated in previous works), but also the geometry of the object influences the maximum holding force of the gripper. We produced an analytical model that takes into account the shape of the target object unlike previous model. Our first experimental results confirm the validity of our hypotheses. The final outcomes of the investigation will be particularly valuable for other EA soft devices such as soft clutches.
- In Chapter 4 the preliminary work conducted on hydrogel is presented. The work aimed at fabricating the first hydrogel-based EA soft gripper. The Chapter presents the first results about the improvement of water retention capabilities of hydrogel and bonding of hydrogel to external surfaces. Both are needed to enable the inclusion of hydrogel into a soft robotic structure. Also, the results about experiments conducted on hydrogels are presented. Finally, the outcomes of the first tests conducted on archaic prototypes of a gripper finger are included.

2. Passive wrapping of curved objects with electroadhesion soft grippers: a process based on the phenomenon of zipping[1]

2.1 Introduction

The work presented in this chapter aims to investigate the wrapping capabilities of an EA soft gripper that only relies on electrostatic forces to grasp objects, without using any additional actuator. We will unveil the relationship between the mechanical and electrical features of the system composed by gripper and target object, identifying the critical parameters ruling the grasping process.

Effective grasping with EA soft grippers requires the fingers to wrap the target object and establish the largest contact interface between the fingers and the object surface. The wrapping can be actively reached through an actuator: different technologies have been proposed such as Dielectric Elastomers Actuators (also known as DEAs) [24], Fin-Ray mechanism [54], and pneumatic actuation [55] (Figure 2.1). These solutions induce the gripper to comply with the shape of the grasped object, but result in increased complexity of the manipulator, require cumbersome fabrication processes, and lead to stiffer fingers. The stiffness of the fingers is a critical parameter since it can negatively influence the actual contact area between the gripper and the object – crucial for exploiting the electroadhesion effect at a small scale – eventually resulting in limited grasping capabilities.

Without the aid of an actuator, the gripper can only leverage electrostatic forces to passively wrap the object. The absence of external actuation circumvents the issues related to complex fabrication and increased stiffness but can become challenging in some cases. Indeed, without actuation, electrostatic attraction alone is required to modify the gripper's posture and to tailor the finger even to the most complicated shapes (Figure 2.2).

We focused on the grasping of curved objects. With current passively-wrapping EA grippers architectures [4] (Figure 2.2), despite the simplicity of the regular geometry, a curved surface requires the finger to bend and lift with respect to its resting position (Figure 2.3). The electrostatic forces must provide the mechanical work to perform both operations. Our investigation shows the effects of both the elasticity of the tape and its mass properties on the wrapping behavior and can represent the starting point for extending the study to more complex geometries. Moreover, curved objects are particularly interesting since EA on curved surfaces exhibits much more higher detachment forces than on flat substrates. As we will show in Chapter 3, an EA soft gripper wrapping a curved object exponentially increases its maximum holding force with respect to the same gripper simply adhering to a flat surface [3]. Understanding how the electrostatic forces make the fingers wrap objects would pave the way for EA soft grippers holding very large weights.

[1] [1] This chapter has been Reproduced with permission from the article:
M. Mastrangelo, F. Caruso, G. Carbone, V. Cacucciolo, "Electroadhesion zipping with soft grippers on curved objects", *Extreme Mechanics Letters* (2023).

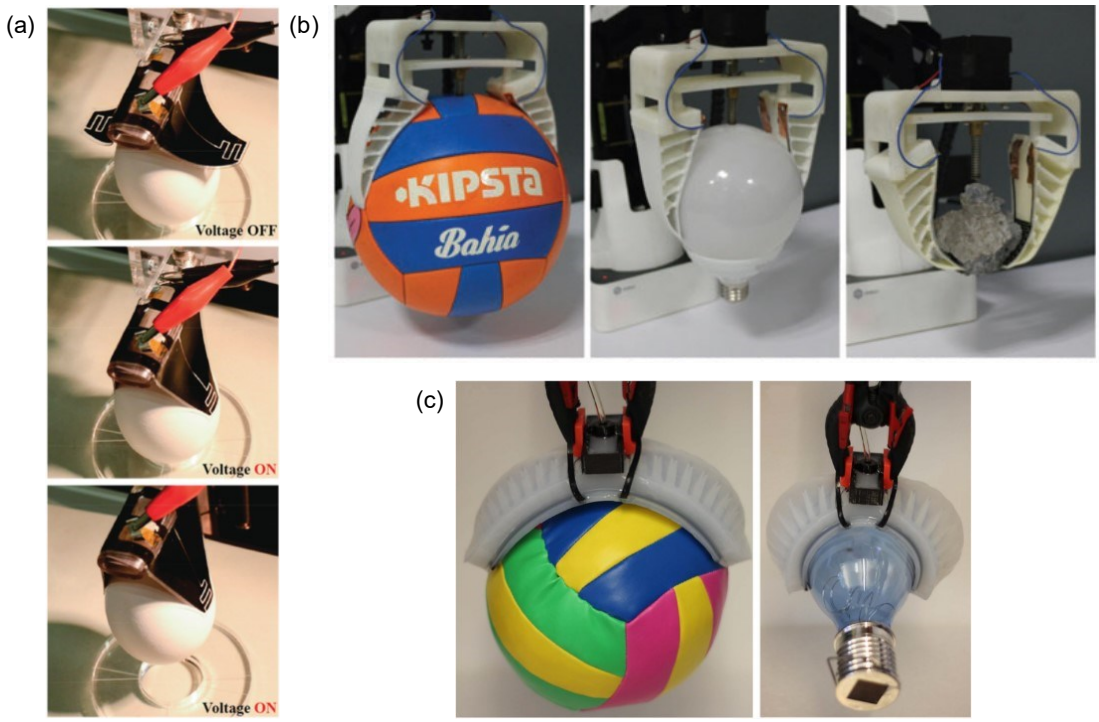

Figure 2.1 – Examples of electroadhesion gripper enhanced with external actuators. (a) The soft gripper presented in [24] merges EA with dielectric elastomers actuators. When the voltage is applied, grasping is realized through a combination of electroadhesion forces at the fingers' tip and bending deformation of the fingers toward the target object (Reproduced with permission from Shintake et al. [24]). (b) EA-augmented soft gripper from [54] adapting to different objects. Fin-Ray fingers actuated by a DC motor can grasp various objects thanks to electroadhesion augmentation (Reproduced with permission from Chen et al. [54]). (3) Soft pneumatic gripper [55] with EA electrodes embedded in the fingers (Reproduced with permission from Guo et al. [55]).

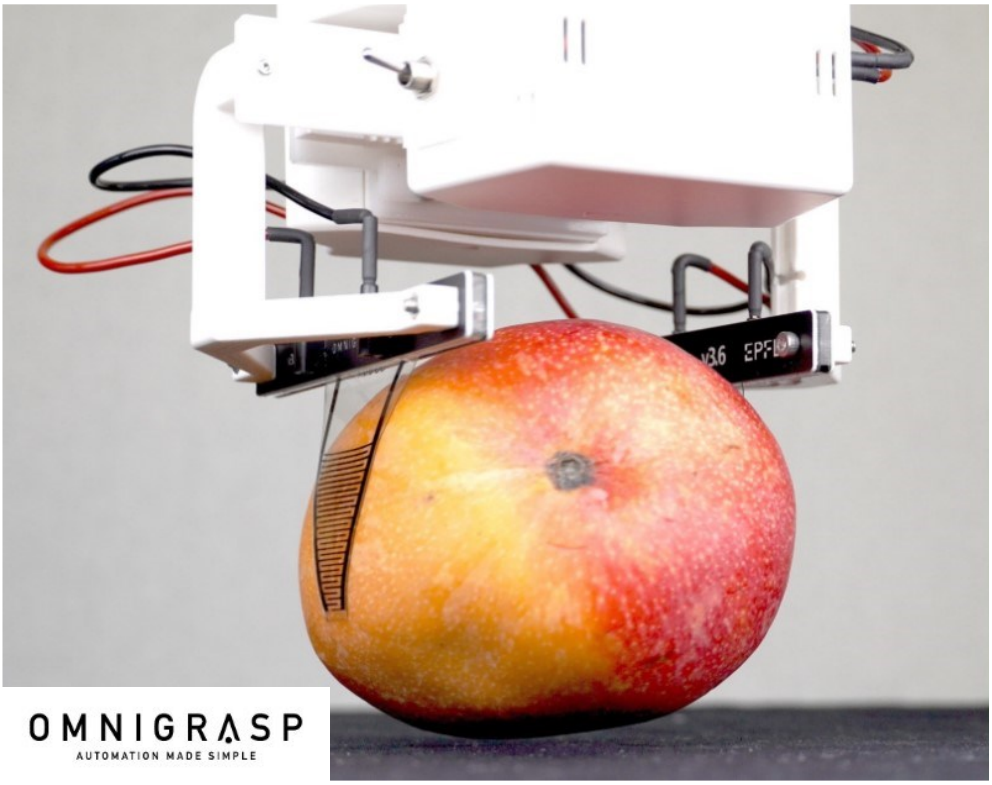

Figure 2.2 – An EA soft gripper using no external actuators to grasp a mango. Electrostatic effects alone force the gripper's finger to adapt to the object shape. Courtesy of OMNIGRASP s.r.l.

The electrostatic-induced wrapping of an object is based on the phenomenon of zipping. Electrostatic zipping is a mechanism widely used in soft actuators, such as electro-ribbon and electro-origami [56], HASELs [57], and HAXELs [58]. All these technologies share a common feature: two soft films, each containing an electrode, are made to zip together to obtain relatively large displacements. High dielectric constant liquids are placed in between the electrodes to amplify the force output. On the other hand, zipping in EA soft grippers involves the fingers of the manipulator progressively zipping over the surface of the grasped object (Figure 2.3). The electrodes are embedded in the finger's structure: no specific electric features of the object are then required for the zipping to happen, even if the properties of the grasped object (and tape) influence the process, as we will show in the following. A systematic study of the phenomenon of EA soft tapes zipping over generic surfaces was still missing. In this chapter, we propose to fill this gap.

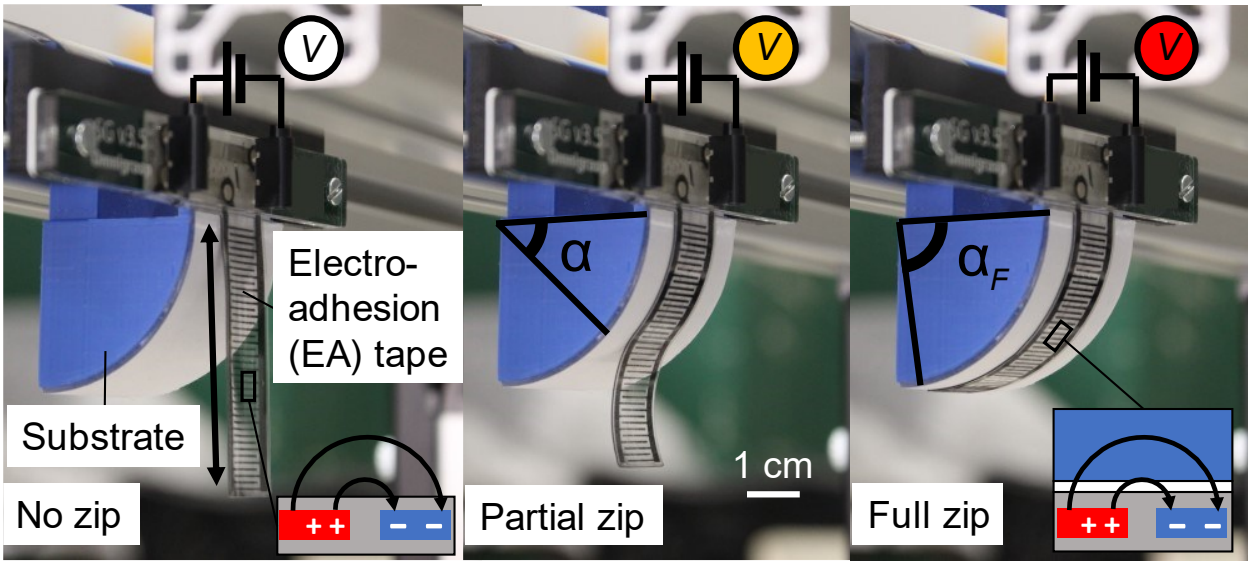

Figure 2.3 – The process of zipping of an EA soft tape on a curved object. By applying an increasing voltage to the tape, the wrapping (measured by the angle α) increases as well until full wrapping ($\alpha = \alpha_F$). Reproduced with permission from Mastrangelo et al. [1].

We present an analytical model describing the process of an EA soft tape zipping on a curved surface (Figure 2.3), quantifying the dependence of the wrapping angle on the voltage applied to the system. The derived mathematical framework accounts for features of both the gripper and the grasped object, highlighting the dependence of the phenomenon on the mechanical and electrical system features.

According to our model, the zipping is characterized by two voltage thresholds. The first one demarcates the outset of the zipping process, with no zipping happening at lower voltages. The second threshold expresses the voltage at which the tape fully collapses onto the surface, similar to a pull-in instability [59]. Between these two values, the wrapping angle increases with the applied voltage. Moreover, our model shows that the zipping does not scale with the squared ratio of the voltage to the thickness of dielectric layer covering the interdigitated electrodes ($\frac{V^2}{d^2}$), as broadly reported for EA forces, but rather with the squared voltage to the dielectric layer thickness ($\frac{V^2}{d}$). The model spotlights the mutual relationship between the mechanical and the electrical properties of the system, allowing us to produce useful tools to improve the design of future soft grippers. We will provide these tools at the end of the chapter.

We validated the model by conducting zipping tests of EA soft tapes on cylindrical objects and measuring the wrapping angle obtained in response to the applied voltage. We tested different

materials and surfaces, to account for the influence of the surface and electrical properties of the wrapped substrate. Our model does not include dynamic effects, but we also conducted experiments on the dynamic response of the system. We finally tested the capabilities of the EA tapes to wrap common curved objects such as fruits and bins.

The chapter is organized as follows. In section 2.2 we present the analytical model of the zipping of an EA tape on a curved object. We include model results in this section, and we will also discuss possible limitations of our model due to our hypotheses. Section 2.3 will present the experimental results. We include materials and methods and outcomes of experimental campaign for validating the model. We also include the results of the dynamic tests and the tests on common objects. Section 2.4 contains tools derived from the model useful for the design of improved EA soft grippers capable of wrapping curved objects and holding large weights.

Nomenclature

α = wrapping angle of the EA tape over the curved object

V = voltage applied to the tape

R = radius of the curved object

$V_{NO\ ZIP}$ = minimum voltage for the zipping to start (first threshold)

$V_{FULL\ ZIP}$ = minimum voltage for the full collapse of the tape over the object (second threshold)

ε = dielectric constant (also called relative permittivity)

W_{EL} = electrical work provided by the power supply

U_F = bending strain energy of the tape

U_G = gravitational energy of the tape

U_{EL} = electrostatic energy of the tape capacitor

U_{EA} = electroadhesion energy of the tape capacitor

M = restoring moment in the bended tape

E = tape Young's modulus

ρ = tape density

I = second moment of area of the tape section

b = tape width

t = tape thickness

L = tape length

g = gravitational acceleration

$C(\alpha)$ = capacitance of the tape, function of the zipping angle α

$\Delta\hat{c}$ = capacitance variation of the tape due to zipping, per unit length of tape

m = tape mass

BS = tape bending stiffness

γ = tape geometric factor

w = distance between interdigitated electrodes

d = thickness of the dielectric layer covering the electrodes

2.2 Analytical model of the zipping of electroadhesion soft tapes on curved objects

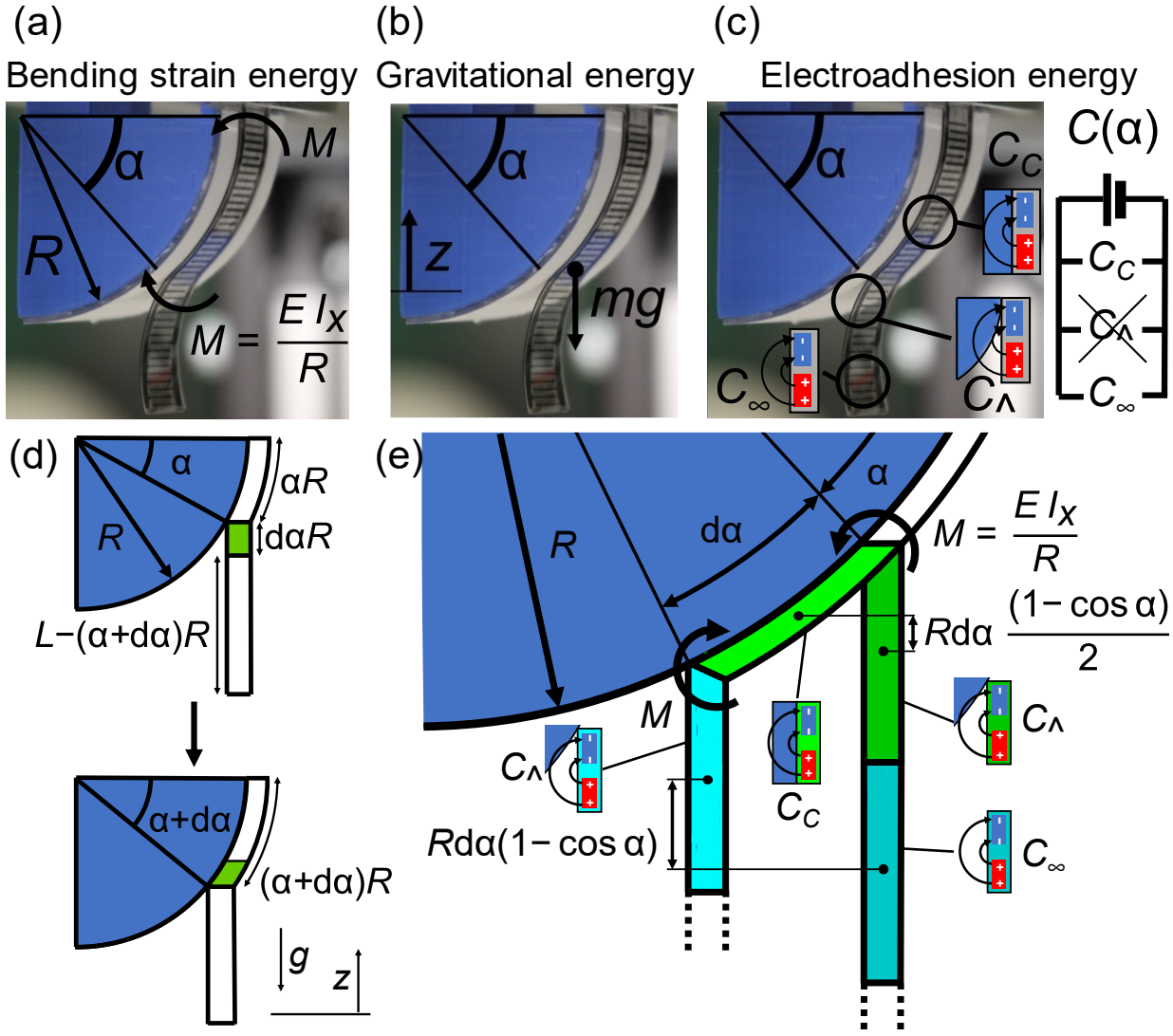

Figure 2.4 – (a-c) Energy components involved in the zipping phenomenon: (a) bending strain energy of the tape due to the restoring moment M acting in the bended tape; (b) gravitational energy due to the lifting of the center of mass of the tape m; (c) electroadhesion energy function of the applied voltage and of the capacitance $C(\alpha)$ of the tape. As we will show, the capacitance of the tape changes with respect to the material surrounding it (object or air). We define C_c the capacitance of the tape in full contact with the object and C_∞ the capacitance of the tape surrounded by air. $C(\alpha)$ depends on both C_c and C_∞ according to the wrapping angle. Any other contribute to the capacitance (as the influence of the zipping boundary) can be neglected. (d) Zipping advancement by an infinitesimal wrapping angle dα. (e) The energy variations due to the infinitesimal wrapping angle dα. Reproduced with permission from Mastrangelo et al. [1].

This section illustrates the analytical model for the zipping of an EA tape on a curved surface. The model describes the response of the gripper fingers (EA soft tapes), to the applied voltage V, in terms of the wrapping measured by the angle α, for given materials and geometries of the tape and the surface. We will present the derivation of the model based on the equilibrium of the system written in differential form, as well as an alternative approach involving the total potential energy of the system. We will show that the two approaches give the same results under equal assumptions. We will also include in the following a section dedicated to testing the limits of validity of our model and to discussing possible limitations of our model according to our

hypotheses.

We derived the model by writing the total potential energy balance of the gripping system, including the object, the tape, and the voltage supplier. The tape is modeled as a capacitor that accumulates charge over its interdigitated electrodes. The capacitance of the tape changes during the zipping according to the materials surrounding it (air or object). Energetic approaches are well-suited for electromechanical systems, as demonstrated in the cases of dielectric elastomers [60] and fluid transducers [61], since the expression of the energetic components results easier than that of the involved forces for this kind of devices. For an EA tape in our case, the energies included in the balance are the elastic energy due to the bending of the tape that conforms to the curved substrate (radius R), the gravitational energy of the tape whose center of mass lifts during wrapping, and the electrical energy of the tape and the battery (Figure 2.4a-c). We considered quasi-static effects only, so the model accounts for no dynamic or viscous effects.

2.2.1 Total potential energy balance: equilibrium of the system in differential form

To derive the equilibrium equation of the system, we considered a small perturbation to the equilibrium, quantified by the infinitesimal increment $\mathrm{d}\alpha$ of the wrapping angle (Figure 2.4d). The variation in the wrapping angle implies the following phenomena. First, the length of the section of the tape in contact with the substrate increases linearly by a quantity $R\mathrm{d}\alpha$. The capacitance of the tape is affected by the dielectric constant of the material surrounding it. Since the dielectric constant of the object is always higher than that of the air ($\varepsilon_{air} = 1$), the tape capacitance increases with the zipping. The zipping section $R\mathrm{d}\alpha$, originally in a straight position, elastically deform to conform to the curved shape of the substrate. Finally, the positions of both the portion $R\mathrm{d}\alpha$ and the rest of the unzipped tape change, so the center of mass of the tape lifts by a quantity $\mathrm{d}z(\alpha)$ (Figure 2.4e).

The increase $\mathrm{d}\alpha$ in the wrapping angle requires a certain amount of energy $\mathrm{d}W_{EL}$. For a passively wrapping gripper, this energy can only be provided by the electrical power supply. The contribute balances: the bending strain energy increase $\mathrm{d}U_F$, the gravitational energy increase $\mathrm{d}U_G$, and electrostatic energy increase of the energy stored in the capacitor $\mathrm{d}U_{EL}$. We can sum up the total potential energy balance of the system with the following equation in differential form:

$$\mathrm{d}U_{EL} + \mathrm{d}U_F + \mathrm{d}U_G = \mathrm{d}W_{EL}. \qquad (2.1)$$

The electrostatic energy of a generic capacitor can be expressed as half the product of the charge stored in the capacitor and the applied voltage, so we can write $\mathrm{d}U_{EL} = \frac{1}{2}V\mathrm{d}Q$, Q the stored charge. Similarly, the work done by a voltage supplier is the product of the charge moved by the supplier times the voltage, so $\mathrm{d}W_{EL} = V\mathrm{d}Q$. For a generic capacitor holds the relationship $V^2C = VQ$, with C the generic capacitance. The supplier work and the capacitor energy can then be expressed as CV^2 and $\frac{1}{2}CV^2$, respectively. We call electroadhesion energy the electrical energy stored in the tape capacitor $\mathrm{d}U_{EA} = \mathrm{d}W_{EL} - \mathrm{d}U_{EL} = \frac{1}{2}V\mathrm{d}Q = \frac{1}{2}V^2dC$. Equation (2.1) is rewritten as:

$$\mathrm{d}U_F + \mathrm{d}U_G = \mathrm{d}U_{EA}. \qquad (2.2)$$

Eqn. (2.2) clearly shows that the equilibrium of the EA tape on a curved object depends on the ratio between the mechanical (in terms of bending strain and gravitational energies) and electrical (the electroadhesion energy of the tape) features of the gripping system.

We now go more into the details of the terms of equation (2.2), showing how each of them is obtained and what are the system parameters that come into play.

2.2.1.1 Bending strain energy contribution

The bending of the section $R\mathrm{d}\alpha$ of the tape generates the restoring moment M, that opposes the deformation of the tape (Figure 2.4e). According to the Euler – Bernoulli theory for slender beams, the bending strain energy can be modeled as $\mathrm{d}U_F = \frac{1}{2}M\mathrm{d}\alpha = \frac{1}{2}\frac{EI_x}{R}\mathrm{d}\alpha$. E is the Young's modulus of the tape and $I_x = \frac{bt^3}{12}$ is its second moment of area. We only refer to parallelepiped-shaped tapes, with rectangular sections. We can write then:

$$\mathrm{d}U_F = \frac{1}{24}\frac{Ebt^3}{R}\mathrm{d}\alpha \qquad (2.3)$$

2.2.1.2 Gravitational energy contribution

When the wrapping increases by zipping, the gravitational energy of the tape changes since its center of mass moves to a new position. In particular, the variation of the gravitational energy of the tape is due to two contributes (Figure 2.4e). The center of mass of the zipping portion $R\mathrm{d}\alpha$ rises by a quantity $\frac{1}{2}R\mathrm{d}\alpha(1-\cos\alpha)$. The mass of this part is $R\mathrm{d}\alpha\,\rho tb$, with ρ the tape mass density. The gravitational energy of the remaining unzipped portion changes as well. We model this tape section as a straight strip, so its center of mass rises by a length $R\mathrm{d}\alpha(1-\cos\alpha)$. The mass of this part is $(L-(\alpha+\mathrm{d}\alpha)R)\rho tb$. $\mathrm{d}U_G$ then becomes:

$$\mathrm{d}U_G = \frac{1}{2}R\mathrm{d}\alpha(1-\cos\alpha)R\mathrm{d}\alpha\,\rho tbg + R\mathrm{d}\alpha(1-\cos\alpha)(L-(\alpha+\mathrm{d}\alpha)R)\rho tbg \qquad (2.4)$$

with g the gravitational acceleration.

2.2.1.3 Electroadhesion energy contribution

With the zipping advancement, a larger section of the tape contacts the substrate, and the capacitance $C(\alpha)$ of the tape increases with the angle increase $\mathrm{d}\alpha$ (Figure 2.4e). To measure the variation of the capacitance with the wrapping angle, we introduce the quantity $\Delta\hat{c}$ as the capacitance variation per unit length of the tape. By defining C_c the capacitance of the tape when fully in contact with the substrate ($\alpha = \alpha_F$) and C_∞ the capacitance of the tape when it is at infinite distance from any object, we write $\Delta\hat{c} = \frac{C_c - C_\infty}{L}$, with L = tape length. The variation in the tape capacitance when it zips by an angle $\mathrm{d}\alpha$ can then be expressed as:

$$\mathrm{d}C(\alpha) = \Delta\hat{c}R\mathrm{d}\alpha \qquad (2.5)$$

To obtain the values of C_c and C_∞, we simulated the capacitance of a semi-electrode pair of the interdigitated geometry of the tape, as done in [4]. We used COMSOL Multiphysics FEM simulator (Figure 2.5). We used a semi-electrode pair as a fundamental unit since it captures the electric field shape of the interdigitated configuration. We computed the capacitance with the semi-electrode pair in contact (a) or at infinite distance from any object (b). Then, we calculated the capacitances C_c and C_∞ by multiplying the capacitances of the semi-electrode pair by the number of pairs in the tape. The capacitance of the tape at any wrapping angle can then be expressed as $C(\alpha) = \Delta\hat{c}R\alpha + C_\infty$ (at $\alpha = 0$, the capacitance of the tape is equal to C_∞), as we suppose that it linearly increases with zipping.

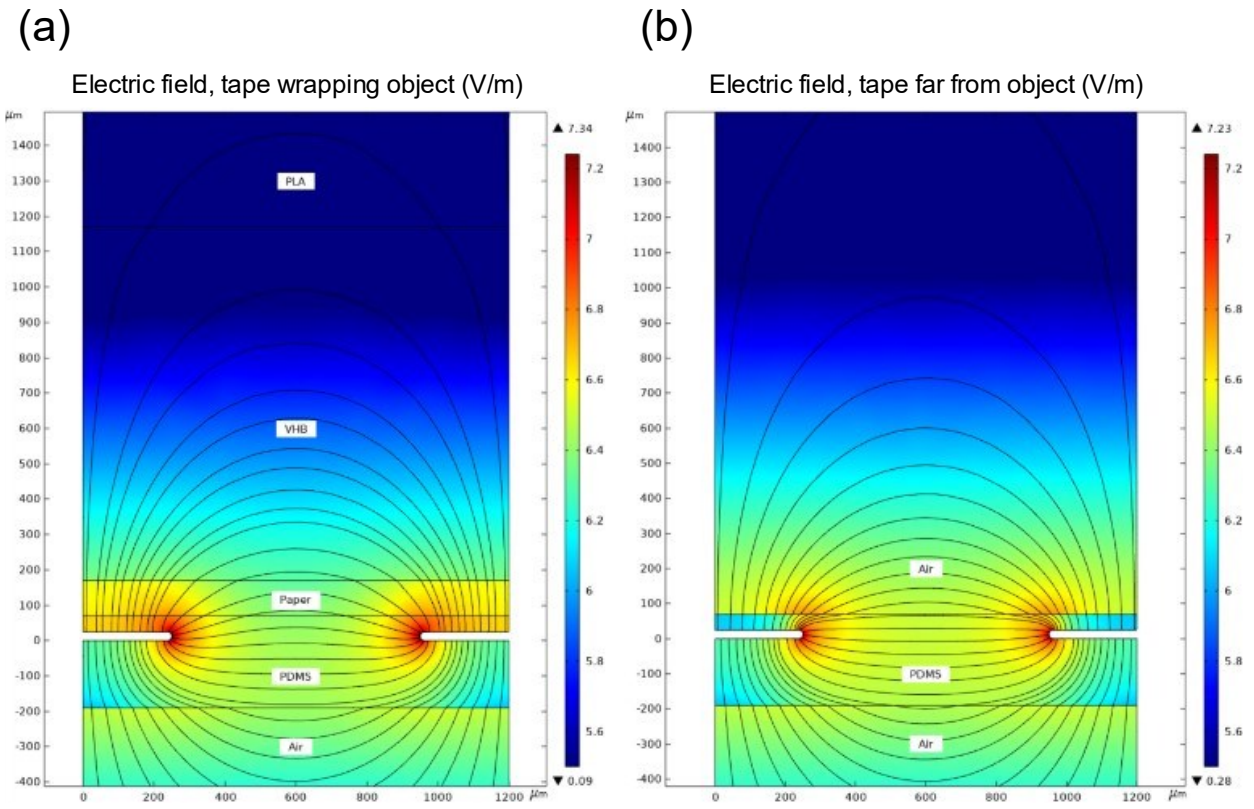

Figure 2.5 – Simulations from COMSOL Multiphysics of the electric field (norm) produced by a semi – electrode pair of the EA tape, when in contact (a) and at infinite distance from any object surrounded by air (b). We simulated the adhesion between the tape and one of the objects (PLA covered by paper and VHB tape) utilized in the experiments. Further details about the tape and the object will be provided in Section 2.3.

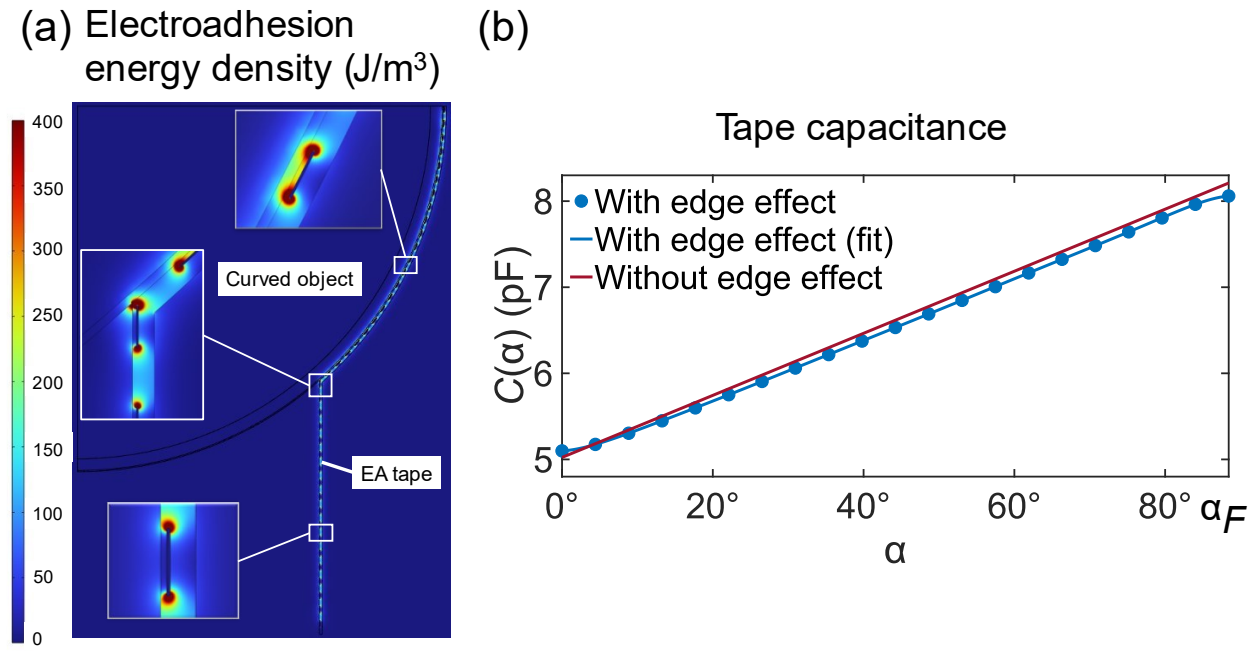

Figure 2.6 – (a) COMSOL simulation of the whole tape partially wrapped on a curved object. The electroadhesion energy density plot shows a peculiar accumulation of charges due to the edge effect at the zipping boundary, but as we found it does not greatly affect the variation of the tape capacitance with zipping. (b) Comparison between tape capacitances obtained with the two described approaches. We found that the edge effect does not modify the variation of the capacitance with α, so we neglected its contribution and wrote $C(\alpha) = \Delta\hat{c}R\alpha + C_\infty$. Reproduced with permission from Mastrangelo et al. [1].

Since the unzipped section of the tape is not actually at infinite distance from the substrate, we tested the validity of eqn. (2.5) by comparing the value of capacitance obtained by using eqn. (2.5) with the results coming from a different approach. We computed the capacitance of the whole tape at different wrapping angles by using COMSOL (Figure 2.6a). By doing so, we implicitly included in the computation the effects of the finite distance between the unzipped tape and the object.

The comparison between the results of the two approaches shows that no significant differences arise (Figure 2.6b). This means that the electrostatic influence of the unzipped tape on the zipping process is very small, and its contribution can be accounted for as coming from a tape at infinite distance from the object. Moreover, full-tape simulations showed that at the zipping boundary a small concentration of the electrostatic field is produced. The accumulation of charges at the boundary produces indeed a variation in the whole tape capacitance, but our simulations shows that the effect is constant with the wrapping angle, and the increase of the capacitance with the zipping angle is not affected by this phenomenon. Based on these results, we concluded that the infinitesimal increase in the tape capacitance with zipping can be effectively expressed by eqn. (2.5). The variation of the electroadhesion energy with zipping is finally expressed as:

$$\mathrm{d}U_{EA} = \frac{1}{2}\Delta\hat{c}V^2 R\mathrm{d}\alpha \qquad (2.6)$$

2.2.2 Relationship between applied voltage and wrapping angle

Eqn. (2.3, 2.4, 2.6) allowed us to rewrite the potential energy balance in differential form as (eqn. (2.2)):

$$\frac{1}{24}\frac{Ebt^3}{R}\mathrm{d}\alpha + \frac{1}{2}R\mathrm{d}\alpha(1-\cos\alpha)R\mathrm{d}\alpha\,\rho tbg + R\mathrm{d}\alpha(1-\cos\alpha)(L-(\alpha+\mathrm{d}\alpha)R)\rho tbg = \frac{1}{2}\Delta\hat{c}V^2 R\mathrm{d}\alpha \qquad (2.7)$$

By excluding higher order terms, we rewrote eqn. (2.7) obtaining:

$$\frac{1}{24}\frac{Ebt^3}{R} + (L-\alpha R)\rho tbgR(1-\cos\alpha) = \frac{1}{2}\Delta\hat{c}RV^2 \qquad (2.8)$$

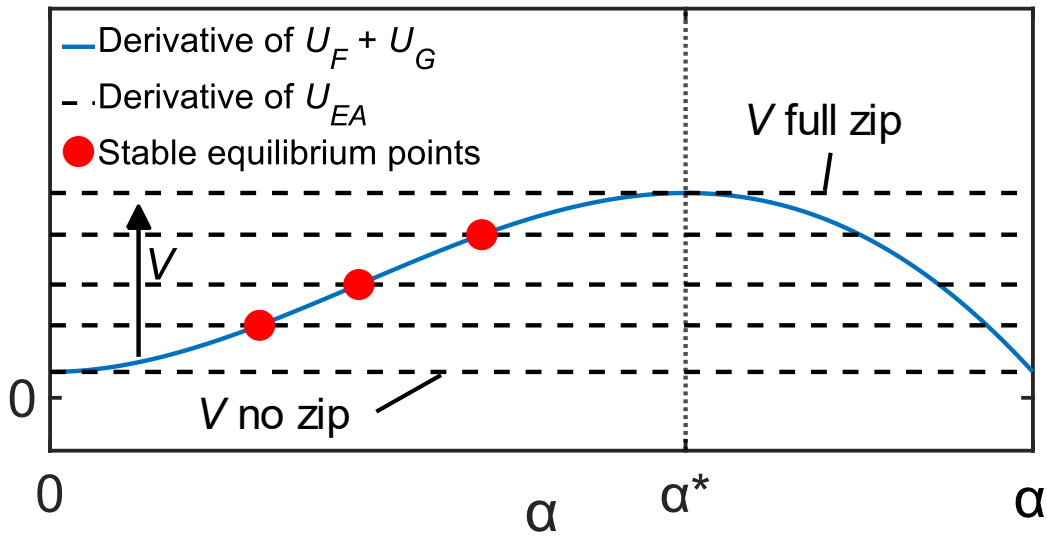

Figure 2.7 – Potential energy components derivatives (eqn. 2.8). The electroadhesion term increases with the applied voltage. Red points in the graph are the stable equilibrium points of the system. No equilibrium is possible until the voltage is equal to $V_{NO\ ZIP}$. Stable equilibrium proceeds toward higher wrapping angles with increasing voltage, until full wrapping ($V > V_{NO\ ZIP}$). Reproduced with permission from Mastrangelo et al. [1].

Eqn. (2.8) expresses the equilibrium states of the wrapping system, in terms of derivatives of the components of the total potential energy of the system. Figure 2.7 shows the allowable states as intersection points between the graphs of the LHS and RHS of the equation. The RHS is plotted for different values of the applied voltage. No equilibrium point exists until V reaches a minimum value. This is because even if the derivative of the gravitational energy (second addendum of LHS) is null when $\alpha = 0$, the derivative of the bending strain energy is constant and independent on the wrapping angle. The derivative of the electroadhesion energy (RHS) needs to match the bending contribute for the zipping to start. The value of the minimum voltage threshold ($V_{NO\ ZIP}$) can be calculated by eqn. (2.8) at $\alpha = 0$:

$$V_{NO\ ZIP} = \frac{1}{R}\sqrt{\frac{1}{12}\frac{Ebt^3}{\Delta\hat{c}}} \qquad (2.9)$$

First, eqn. (2.9) shows that the mass of the tape does not influence $V_{NO\ ZIP}$. Moreover, higher bending stiffness leads to higher $V_{NO\ ZIP}$, and higher $\Delta\hat{c}$ leads to lower values, as well as a smaller object radius.

Eqn. (2.8) also gives the relationship between applied voltage and wrapping angle. By rearranging (2.8), at equilibrium:

$$V = \sqrt{\frac{2}{\Delta\hat{c}}\left[\left(\frac{L}{R} - \alpha\right)\rho tbgR(1 - \cos\alpha) + \frac{1}{24}\frac{Ebt^3}{R^2}\right]} \qquad (2.10)$$

The wrapping angle increases with the applied voltage, but the increase is nonlinear due to the gravitational term. Additionally, stable equilibrium points are only possible when the wrapping angle $\alpha < \alpha^*$. Beyond that point, the applied voltage is sufficient to induce the full zipping of the tape. This phenomenon is similar to an electrostatic pull-in instability, very common in electromechanical systems [60,62], and it is due to the shape of the gravitational term. $\frac{dU_G}{d\alpha}$ has a maximum in $\alpha = \alpha^*$, so when the applied voltage overtakes the value needed to get α^*, the tape fully collapses over the object. The limit voltage value is then the minimum voltage to get full zipping. We call it $V_{FULL\ ZIP}$ and we calculated it by substituting $\alpha = \alpha^*$ in equation (2.10). The angle α^* is obtained by the stability condition $\frac{d^2(U_G+U_F)}{d\alpha^2} = \frac{d^2U_{EA}}{d\alpha^2}$ that gives:

$$\rho tbgR[(L - \alpha R)\sin\alpha + R\cos\alpha - R] = 0. \qquad (2.11)$$

The stability condition is satisfied for $\alpha = 0$ (trivial case) and $\alpha = \alpha^*$. If we recall that $\alpha_F = \frac{L}{R}$, one gets in the nontrivial case:

$$\alpha_F = \alpha^* + \frac{1 - \cos\alpha^*}{\sin\alpha^*} \qquad (2.12)$$

The stability condition in the nontrivial case then implies that there is a relationship between the limit angle α^* and the full wrapping angle α_F, and that this relationship appears to be constant and independent from any physical parameters. This is because both bending strain energy and EA energy are linear with the wrapping angle, and then disappear in the second derivative. Conversely, the gravitational energy nonlinearly depends on the wrapping angle. Thus, α^* depends only on the shape of the gravitational energy function. We resolved eqn. (2.12) numerically for $\alpha_F < 90°$, and found that for this limit case the limit angle can be approximated as $\alpha^* = 0.65\alpha_F$: independently on any parameter except that for the ratio $\alpha_F = \frac{L}{R}$, the angle at which the instability occurs is nearly proportional to the wrapping angle. The result is particularly interesting for a soft

gripper since with current configurations α_F is always < 90°. By substituting $\alpha = \alpha^* = 0.65\alpha_F$ in equation (2.10) we get an expression for $V_{FULL\ ZIP}$:

$$V_{FULL\ ZIP} = \sqrt{\frac{2}{\Delta\hat{c}}\left[0.35\rho tbLg\left(1-\cos\left(0.65\frac{L}{R}\right)\right)+\frac{1}{24}\frac{Ebt^3}{R^2}\right]}. \qquad (2.13)$$

Conversely to $V_{NO\ ZIP}$, $V_{FULL\ ZIP}$ is influenced by both the bending stiffness and the mass density of the tape.

As anticipated in the Introduction, eqn. (2.8, 2.9 and 2.13) show that electrostatic zipping does not scale with with $\frac{V^2}{d^2}$, with d the thickness of dielectric layer covering the interdigitated electrodes, as broadly reported for EA forces. According to our model, given that for a generic capacitor C is inversely proportional to the distance between the electrodes, EA zipping rather appears to scale with the squared voltage to the dielectric layer thickness ratio $\frac{V^2}{d}$.

2.2.3 Alternative approach for the derivation of the equilibrium equation

Finally, we propose an alternative formulation for the equilibrium of the system, obtained by writing the total potential energy of the system (function of α and V). The alternative approach allows to identify the equilibrium points of the system by writing the total potential energy and calculating its derivative.

Rather than writing the balance in differential form, here we write the total potential energy of the system, following methods already developed for dielectric elastomers actuators [63] and zipping actuators [64]. The total potential energy of the system is the sum of three contributes: the bending strain energy, the gravitational energy and the electroadhesion energy. One can write:

$$U_T(\alpha, V) = U_F(\alpha) + U_G(\alpha) - U_{EA}(\alpha, V). \qquad (2.14)$$

2.2.3.1 Bending strain energy contribution

Consider the tape wrapping the object by an angle α. The tape is subject to a pure homogeneous moment M due to the deformation imposed by the constant curvature of the object (Figure 2.4a and 2.8a). The associate bending strain energy is:

$$U_F(\alpha) = \frac{1}{2} M\alpha. \qquad (2.15)$$

According to Euler-Bernoulli slender beam theory, the restoring moment can be expressed as $M = \frac{EI_x}{R}$, with E = tape Young's modulus, R = object radius, $I_x = \frac{bt^3}{12}$ = second moment of area of the tape section with respect to the x-axis (Figure 2.8a), b = tape width, t = tape thickness. By recalling eqn. (2.15) one gets (Figure 2.8d):

$$U_F(\alpha) = \frac{1}{24} \frac{\alpha E b t^3}{R}. \qquad (2.16)$$

2.2.6.2 Gravitational energy contribution

The gravitational energy of the tape during zipping is $U_G(\alpha) = mgz(\alpha)$, with m = tape mass, g = gravitational acceleration, $z(\alpha)$ = vertical coordinate of the tape center of mass (Figure 2.4b and 2.8b). Define $m = \rho btL$, with ρ = tape density, L = tape length. Consider the auxiliary reference system z' in Figure 2.8b. When $\alpha = 0$ the gravitational energy in this reference system can be written as:

$$U'_G(\alpha = 0) = mgz'(\alpha = 0) = \frac{\rho btLgL}{2}. \qquad (2.17)$$

In the zipped state, the gravitational energy is the sum of two contributes, coming from the zipped (1) and the unzipped (2) sections, respectively:

$$U'_G(\alpha) = m_1(\alpha) g z'_1(\alpha) + m_2(\alpha) g z'_2(\alpha) \qquad (2.18)$$

with $m_1(\alpha)$ and $z'_1(\alpha)$ the mass and the z'-coordinate of the center of mass of the zipped section, and $m_2(\alpha)$ and $z'_2(\alpha)$ the mass and the z'-coordinate of the center of mass of the unzipped section.

We can rewrite eqn. (2.18) as:

$$U'_G(\alpha) = R^2 bt\rho g \int_0^{\alpha} \sin\theta \, d\theta + (L - \alpha R) bt\rho g \left(R \sin\alpha + \frac{L - \alpha R}{2} \right) =$$

$$bt\rho g \left[R^2 (1 - \cos\alpha) + (L - \alpha R) \left(R \sin\alpha + \frac{L - \alpha R}{2} \right) \right]. \qquad (2.19)$$

By switching to the reference system z, since $z = \frac{L}{2} - z'$ (Figure 2.8b), one gets:

$$U_G(\alpha) = \frac{\rho btLgL}{2} - U'_G(\alpha), \qquad (2.20)$$

and finally:

$$U_G(\alpha) = \frac{\rho btLgL}{2} - R^2 bt\rho g \int_0^{\alpha} \sin\theta \, d\theta - (L - \alpha R) bt\rho g \left(R \sin\alpha + \frac{L - \alpha R}{2}\right) =$$

$$\rho btLg \left[\frac{L}{2} - \frac{R^2(1 - \cos\alpha) + (L - \alpha R)\left(R \sin\alpha + \frac{L - \alpha R}{2}\right)}{L}\right]. \qquad (2.21)$$

2.2.6.3 Electroadhesion energy contribution

The total electrical energy of the system is the sum of the energy stored in the voltage supplier (modeled as a battery) $Q_b V$ and in the EA capacitor $\frac{1}{2}QV = \frac{1}{2}CV^2$. During the zipping process, charges move from the battery to the capacitor. However, the total electrical charge of the system is constant and equal to $Q_T = Q_b + Q$. The total electrical energy of the system can be written as $V\left(Q_b + \frac{1}{2}Q\right) = VQ_T - \frac{1}{2}VQ$. Since the quantity VQ_T is constant, we can neglect it and only consider as the total electrical energy $U_{EL} = -U_{EA}(\alpha, V) = -\frac{1}{2}VQ = -\frac{1}{2}C(\alpha)V^2$, with $C(\alpha)$ the capacitance of the tape. $U_{EA}(\alpha, L)$ is the electroadhesion energy, the electrical energy stored in the tape capacitor.

$C(\alpha)$ is the sum of two contributions (Figure 2.4c). The first contribution comes from the zipped portion of the tape. Given C_c the capacitance of the tape when fully wrapped around the object, when the tape is partially adhered to the object (wrapping angle = α), the contribution coming from the zipped section is $C_c \frac{\alpha R}{L}$. C_∞ is conversely the capacitance of the tape at infinite distance from any object. The second contribute to $C(\alpha)$ is then $C_\infty \frac{L - \alpha R}{L}$. The total electroadhesion energy then becomes (Figure 2.8f):

$$U_{EA}(\alpha, V) = \frac{1}{2}C_\infty V^2 + \frac{1}{2}(C_c - C_\infty)\frac{\alpha R}{L}V^2. \qquad (2.22)$$

2.2.6.4 Total potential energy

By merging eqn. (2.14, 16, 21, 22) one gets (Figure 2.8c):

$$U_T(\alpha, V) = \frac{1}{24}\frac{\alpha E b t^3}{R} + \rho btLg \left[\frac{L}{2} - \frac{R^2(1 - \cos\alpha) + (L - \alpha R)\left(R \sin\alpha + \frac{L - \alpha R}{2}\right)}{L}\right] - \frac{1}{2}C_\infty V^2$$

$$- \frac{1}{2}(C_c - C_\infty)\frac{\alpha R}{L}V^2. \qquad (2.23)$$

By deriving (2.23) with respect to α one obtains the equilibrium as already expressed by eqn. (2.8).

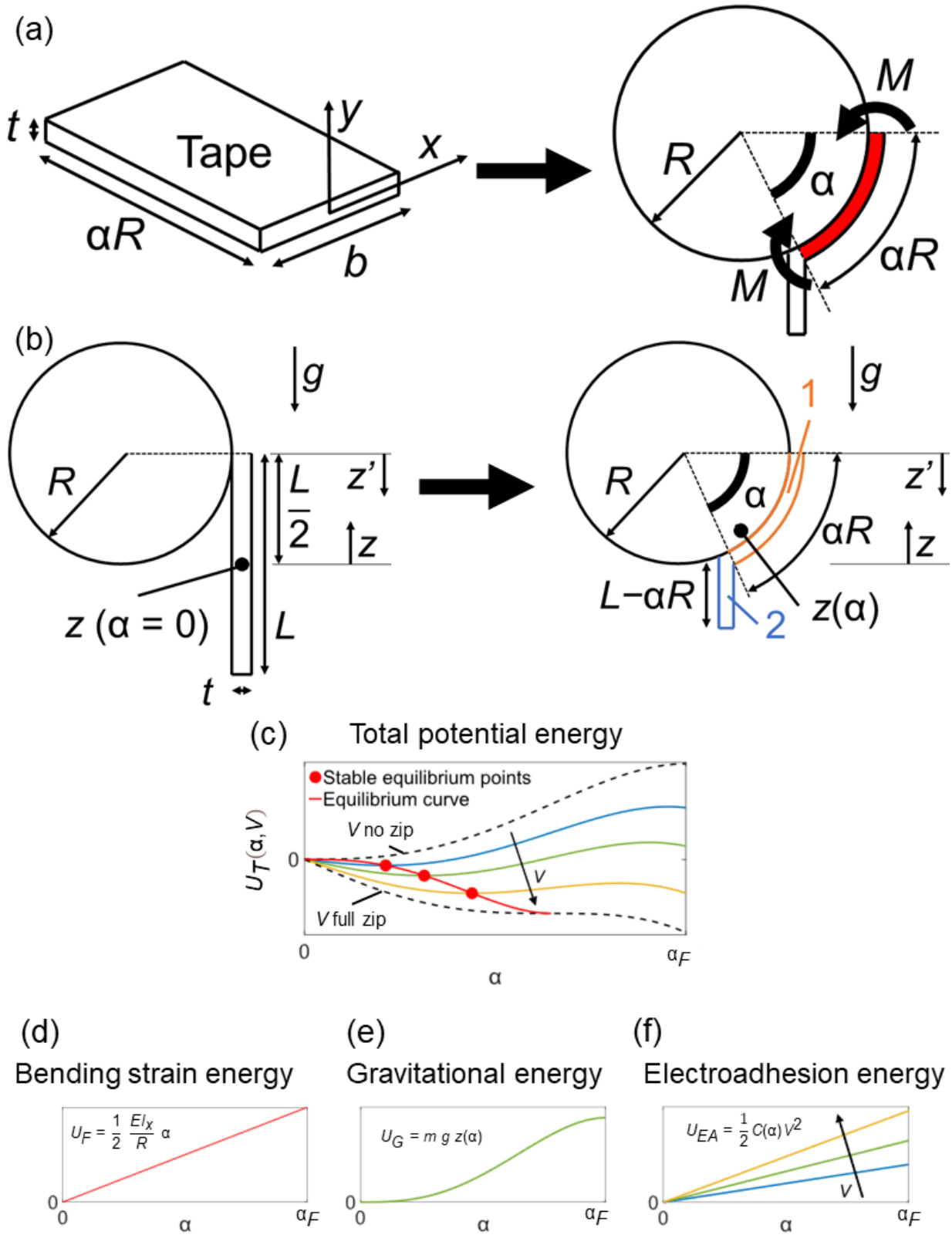

Figure 2.8 – (a) The undeformed section αR of the tape beam, and the same section (red) subject to bending. (b) When undeformed, the gravitational energy of the tape is 0 in the z-reference system. When zipped, the gravitational energy is the sum of the contributions from sections 1 and 2. (c) The total potential energy of the system (eqn. 2.14, 23). (d) The bending strain energy term (eqn. 2.16). (e) The gravitational energy term (eqn. 2.21). (f) The electroadhesion energy term (eqn. 2.22). Reproduced with permission from Mastrangelo et al. [1].

2.2.4 Limitations of the model

In the previous Sections we presented the results of our theoretical investigation on wrapping of EA tapes on curved objects, based on the phenomenon of zipping. Our model is based on several assumptions, made to keep the equations simple and ready to use. In this section, we discuss the validity of these assumptions and possible limitations of our model due to the underlying hypotheses.

We assumed the unzipped section of the tape hanging straight down, then neglecting the bending stiffness of this part and the strain energy related to its deformation. The assumption does not affect the value of $V_{NO\ ZIP}$ since the tape is undeformed until the zipping starts and works well for our tape and for relatively small wrapping angles: the bending stiffness of our tape is negligible if compared to the weight of the unzipped section, that can be considered straight and perpendicular to the ground. When the zipping advances, the bending stiffness of the tape becomes more important. The unzipped section of the tape is visibly curved, and its center of mass is lifted if compared to the model assumptions (Figure 2.1a-c). The unzipped part then contains bending strain and gravitational energy, that could influence the zipping behavior.

To test the validity of our model, we investigated the case of EA tape with very high bending stiffness compared to its weight, that is the opposite with respect to the current hypotheses of our model. Under this assumption, we can calculate the additional contributes of the gravitational and bending straight energy of the unzipped portion of the tape and estimate their influence on the zipping behavior of the system.

If the weight-to-bending stiffness ratio is large, the unzipped tape hangs straight down (Figure 2.9a, left) and the gravitational energy of the whole tape is expressed by eqn. (2.21): $U_{G,1} = \rho btLg\left[\frac{L}{2} - \frac{R^2(1-\cos\alpha)+(L-\alpha R)\left(R\sin\alpha+\frac{L-\alpha R}{2}\right)}{L}\right]$. With low weight-to-bending stiffness ratio, we assume that the unzipped section of the tape is tangent to the curved surface (Figure 2.9a, right). The gravitational energy of the tape becomes:

$$U_{G,2} = \rho btLg\left[\frac{L}{2} - \frac{R^2(1-\cos\alpha)+(L-\alpha R)\left(R\sin\alpha+\frac{L-\alpha R}{2}\cos\alpha\right)}{L}\right] \quad (2.24)$$

The only difference between the two limit cases is the factor $\cos\alpha$ that multiplies the last term.

We can compare the derivatives of the mechanical (bending strain plus gravitational) energy for the two cases of: (1) unzipped tape hanging straight down and (2) unzipped tape tangent to the curved object. Figure 2.9b shows the comparison. The green line indicates the mechanical energy derivative for the unzipped tape hanging straight down (Figure2.9a, left), the blue line shows the same quantity for the case of unzipped tape tangent to the object (Figure 2.9a, right). The dotted lines indicate the derivative of the electroadhesion energy at various voltages, unchanged in both configurations. We observe that the $V_{FULL\ ZIP}$ is nearly unchanged in both configurations, while the critical angle α^* at which full zip happens is lower with the unzipped tape tangent to the object ($\alpha_2^* < \alpha_1^*$). In the real case, the unzipped tape is at an intermediate configuration between the two limit cases (neither fully hanging straight down nor tangent). We can conclude that the additional contribution to the real case's gravitational energy would have negligible influence on the zipping behavior (in terms of voltage thresholds).

For what concerns the bending strain energy, we can calculate the bending strain energy contribute coming from the unzipped section of the tape modeling it as a cantilever beam attached at the zipping front. The length of the beam is $L - \alpha R$. The beam is subject to the gravitational load. The

vector g makes an angle α with the longitudinal axis of the beam. The distributed load acting on the beam is $w = \rho btg \sin\alpha$. The energy of the deformed beam is:

$$U_{bs} = \int_0^{L-\alpha R} \frac{M^2 dx}{2EI}. \qquad (2.25)$$

$M = 0.5wx^2$ is the bending moment acting on the beam. By solving eqn. (2.25) one gets:

$$U_{bs} = \frac{(\rho btg)^2}{40EI} (\sin\alpha)^2 (L - \alpha R)^5. \qquad (2.26)$$

By differentiating eqn. (2.26) with respect to the wrapping angle we obtain the derivative of the additional bending energy component U_{bs}:

$$\frac{dU_{bs}}{d\alpha} = \frac{(\rho btg)^2}{40EI} (L - \alpha R)^4 \sin\alpha \, [2(L - \alpha R)\cos\alpha - 5R\sin\alpha]. \qquad (2.27)$$

To test the validity of our model we calculated $\frac{dU_{bs}}{d\alpha}$ and compared it to the other components of the derivative of the total potential energy of the system, in the limit case of high bending stiffness of the tape. We used a value of the Young's modulus that would produce a maximum deflection of 5% with respect to the beam length on our tape in a cantilever configuration when subjected to its own weight. The maximum deflection can be calculated in this case as:

$$\delta_{MAX} = \frac{mgL^3}{8E_{hb}I_x}. \qquad (2.28)$$

With our tape length (48 mm), a 5% deflection corresponds to 2.4 mm. With our data, we get that the required bending stiffness is $E_{hb} \cong 492$ MPa. Figure 2.9c compares the derivatives of the potential energy components. The mechanical energy derivative is plotted in case of high stiffness-to-weight ratio (red line) and in case of low stiffness-to-weight ratio (green line). The gravitational contribute is accounted for by means of eqn. (2.24) (high stiffness-to-weight ratio case). The case for high stiffness-to-weight ratio includes the contribute coming from the unzipped portion of the tape. The figure shows that the mechanical energy derivatives for the two cases have negligible differences in terms of $V_{FULL\ ZIP}$. We conclude that the additional contribute to the bending strain energy coming from the unzipped tape in the case of high bending stiffness has negligible influence on the zipping behavior, and that the assumptions of our model appear adequate to explain the zipping phenomenon.

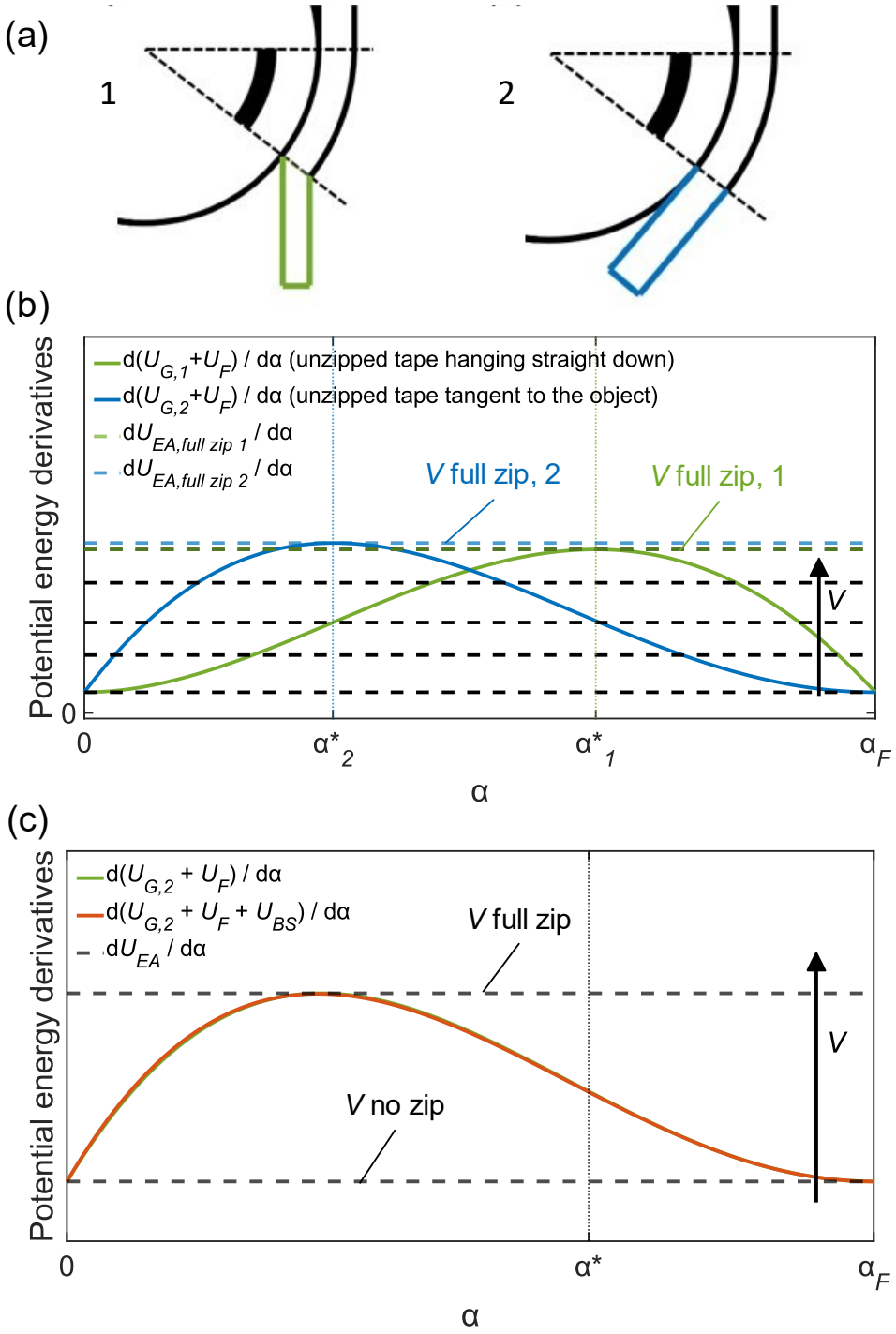

Figure 2.9 – (a) The configuration of the unzipped tape in the limit cases of (1) low stiffness-to-weight ratio (unzipped tape hanging straight down) and (2) high stiffness-to-weight ratio (unzipped tape tangent to the curved object). (b) Comparison between mechanical (bending strain plus gravitational) energy derivatives of the tape in the cases of (1) unzipped tape hanging straight down (green line) and (2) tangent to the curved object (blue line). In the latter case, the critical angle at which the full zipping happens is lower than in the first case, but the difference between $V_{FULL\ ZIP}$ in the two cases is negligible. (3) Comparison of the mechanical energy derivatives of the tape calculated with and without the contribute coming from the bending strain energy of the unzipped tape, in case of large bending stiffness of the tape. The additional term negligibly affects the voltage thresholds of the zipping phenomenon. Reproduced with permission from Mastrangelo et al. [1].

2.3 Zipping experiments

We validated the model by conducting zipping tests of EA soft tapes on curved objects. We measured the wrapping angle α in response to the application of the voltage V to the tape. We performed zipping experiments in various conditions and with different objects. The details of the chosen materials and methods, as well as the results of the experiments, are reported in the following Sections.

2.3.1 Model validation

2.3.1.1 *Materials and Methods*

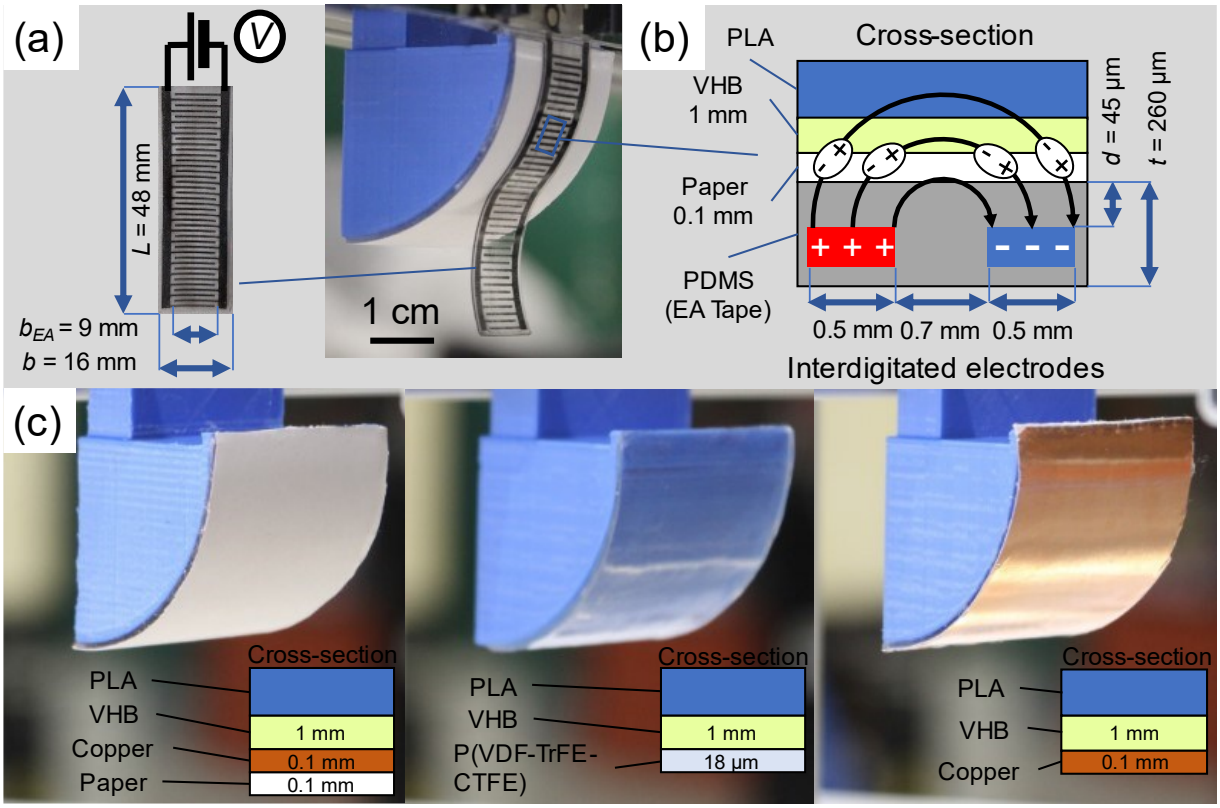

Figure 2.10 – (a) The interdigitated tape utilized in the experiments. (b) Cross-section of the interdigitated tape wrapping a paper-covered cylindrical object. (c) From left to right: PLA cylindrical object covered by a double layer of copper (internal) and paper (external); PLA cylindrical object covered by P(VDF-TrFE-CTFE); PLA cylindrical object covered by copper. Each coating is manually applied and bonded to the object with VHB tape. Reproduced with permission from Mastrangelo et al. [1].

The tested substrates are custom-made 3D-printed PLA (Polylactic Acid) cylindrical objects (Figure 2.10). We used object with radii of 30 and 45 mm. For the value of the dielectric constant of PLA, we refer to the value reported in [65] ($\varepsilon_{PLA} = 3$). We chose to coat the PLA with different materials to test the dependence of the zipping phenomenon on the electrical and surface properties of the substrate. First, we chose a 0.1 mm-thick copper layer coating to study the behavior of the tape on a conductive material. In another set of experiments, we covered the copper with a 0.1 mm-thick paper layer to investigate the influence of a dielectric layer ($\varepsilon_{PAPER} = 3$ [66]) placed between the tape and the conductive substrate, and also to test the effect of a rough surface. We also tested an object with a pure paper coating (no conductive substrate) and, as a comparison for the full dielectric case, a 18 µm-thick P(VDF-TrFE-CTFE), characterized by a higher dielectric constant ($\varepsilon_{PVDF} = 30$, PolyK Technologies [67]) and a smoother surface if compared to paper (Figure 2.10c). Each coating is manually applied to the object, and bonded to it using a 3M VHB 4910 adhesive (1 mm-thick, $\varepsilon_{VHB} = 4.7$ [68]).

As EA tapes we used custom-made rectangular stripes (48 mm-long, 16 mm-wide, 26 μm-thick) made by PDMS (Polydimethylsiloxane, Sylgard 184 produced by Dow Corning, $\varepsilon_{PDMS} = 2.7$) (Figure 2.10a). The tape embeds interdigitated electrodes made by carbon loaded PDMS. The electrode width is 0.5 mm, and the pitch between the electrodes is 0.7 mm (Figure 2.10b). The electrodes are separated from the adhered substrate by a 45 μm-thick PDMS layer. The tapes are fabricated by blade casting and curing in the oven at 80 °C of the PDMS backing and the PDMS-carbon composite for the electrodes. Then, laser ablation is conducted to shape the electrodes and finally blade casting and curing of the covering PDMS insulating layer. The volume fraction of the electrodes with respect to the whole tape is small, so we assumed homogeneous material properties equal to that of the PDMS: Young's modulus E = 3.9 MPa [69] and density ρ = 1030 kg/m^3 [70].

We started each zipping test by placing the tape in a vertical position, tangent to the object. We applied the voltage and measured the resulting wrapping angle. We tested the quasistatic response of the tape to the applied voltage since the model does not account for dynamic effects. We varied the voltage slowly (200 V every 10 s). We never applied a voltage exceeding 4 kV in any test, to prevent electrical breakdowns. An electrical breakdown of an insulator occurs when the electric field applied to it surpasses a limit value, and suddenly current flows through it. The breakdown limit for the Sylgard 184 PDMS is 100 kV/mm [71], and applying 4 kV means that only 45 kV/mm are applied to the insulating layer between the electrodes, well below the field limit. We also tested both DC and AC voltage (in the form of a 10 Hz bipolar square wave). We used a DC-HVDC (Direct Current to High Voltage Direct Current) converter (XP Power A series) and high-voltage optocouplers (VMI OC 100G).

2.3.1.2 *Experimental results (quasistatic experiments)*

We conducted the following tests to validate the model and investigate the behavior of the EA tape: quasi-static tests with different radii, substrates, load conditions and electric supply modes (AC and DC); cyclic tests of zipping and unzipping. We repeated the tests three times to get reliable results. The showed graph reports the mean and the standard deviation of the data.

First, we tested the behavior of the EA tape with different object dimensions, in both AC and DC cases, in quasistatic conditions (Figure 2.11). As predicted by the model, the zipping phenomenon is characterized by two voltage thresholds that define the intervals in which the tape doesn't move at all, constantly zips over the object with increasing voltage and it's fully wrapped on the object, respectively. This behavior is confirmed by our experiments. With both radii and under different voltage conditions, the wrapping angle increases with the applied voltage, but only after a certain value is applied to the tape. The wrapping angle increases until full wrapping. Moreover, the model also predicts the influence of the object radius R on the wrapping behavior, that we observed also in our experiments: $V_{NO\ ZIP}$ and (more markedly) $V_{FULL\ ZIP}$ increase if the radius decreases, as expected.

The trend of the experimental data is captured with good accuracy by the model, especially considering that we didn't fit any parameter in the model, that only contains physical quantities. Nevertheless, some general discrepancies exist between the model and the observed data, that we attribute to the following reasons. The EA tape tested in the experiments is intrinsically non-flat. The PDMS band presents a non-zero gaussian curvature, due to the fabrication process (see Section 2.3.1.1). Moreover, for simplicity we modeled the unzipped section of the tape as a straight line. This approximation becomes less reliable with the proceeding of the zipping, as we discussed in Section 2.2.4.

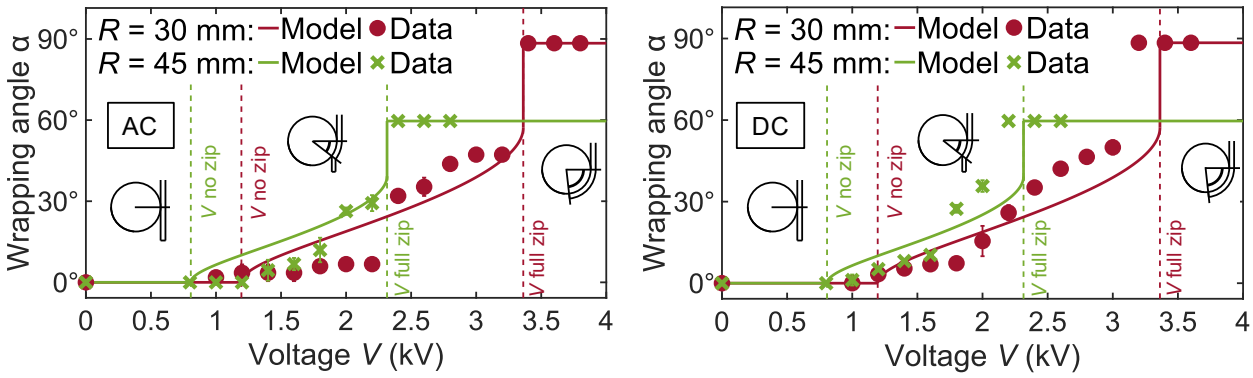

Figure 2.11 – validation of the zipping model for an EA tape wrapping curved objects (radii 30 and 45 mm) covered by paper, for both AC (left) and DC (right) voltage. Reproduced with permission from Mastrangelo et al. [1].

We also observed that under DC voltage the tape zips at lower voltages than in the AC case. We attribute the divergence to the phenomenon of the building up of charges in the dielectric layer of the tape under the application of a DC voltage for a prolonged time. The event is well documented in literature since it affects other EA-based robotics systems such as electrostatic clutches [30]. Space charges accumulation is commonly solved indeed using periodically reversed voltage polarity.

We also tested the tapes under full cycles of wrapping (Figure 2.12). We let the EA tape wrap the object under the application of an increasing voltage and then we decreased the voltage again to investigate the unzipping behavior, for both AC and DC. According to the model (eqn. 2.8 and 2.23), the nonlinearity of the system potential energy implies hysteresis of the wrapping angle with respect to the applied voltage. If the tape reaches full wrapping, the tape would remain wrapped even if the applied voltage is decreased, until reaching again $V_{NO\ ZIP}$. This is not true if the tape only partially wraps the object: by decreasing the voltage in this case, the tape is expected to unwrap accordingly (wrapping and unwrapping are specular processes in this case).

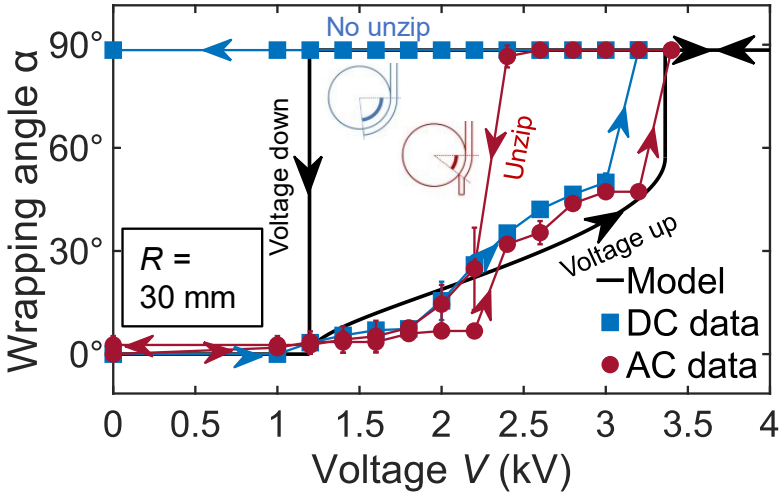

Figure 2.12 – Zipping and unzipping cycles, both AC and DC voltages. Object radius = 30 mm. Object covered by paper. Reproduced with permission from Mastrangelo et al. [1].

The hysteresis of the tape is captured by our experiments, but we observed some discrepancies with respect to the model. The unzipping process with AC voltage happens at higher voltage than model predictions. The model prediction is that unzipping should happen for $V \leq V_{NO\ ZIP}$, due to the nonlinearities of the total potential energy function (eqn. 2.23 and Figure 2.8c). We attribute this discrepancy to the shape of the total potential energy function. The potential energy of the

tape around the full wrapping angle α_F becomes flatter with lower voltages. This phenomenon decreases the range of stability of the full wrapping configuration. The AC voltage induces oscillations of the tape, whose dynamic effects are not included in the total energy of the system. We consider these oscillations as the cause for the earlier detachment of the tape. Conversely, in the DC case no vibrations of the tape are produced. We additionally observed that the tape remains wrapped even when the voltage is totally removed. We attributed this outcome again to the building up of space charges in the dielectric, but also to dry adhesion effects generated by the prolonged exposure to the voltage generating electrostatic normal pressure between the tape and the object. This effect is mitigated with AC voltage since the pressure is periodically removed and reapplied.

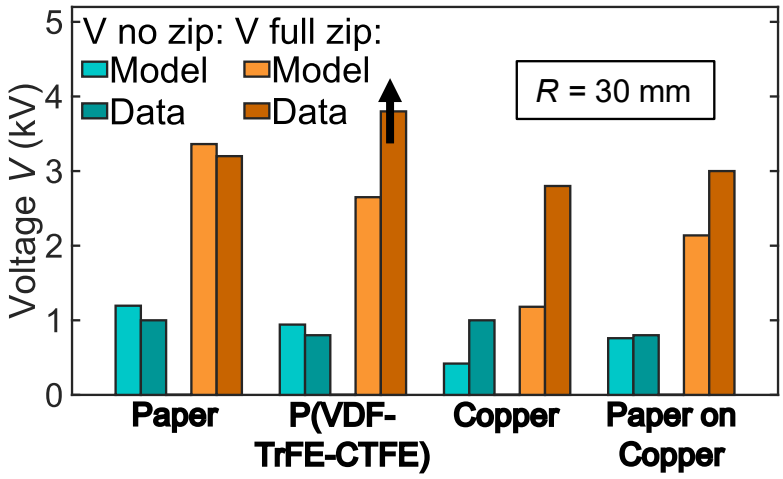

Figure 2.13 – Comparison between model results and data of zipping experiments on objects with different surface and material properties. Reproduced with permission from Mastrangelo et al. [1].

The experiments presented until now have been conducted with EA tapes wrapping paper-covered objects. This is since paper normally does not stick to the PDMS of the tape: we tried to minimize dry adhesion and insulate electrostatic effects. The experiments with paper showed very good agreement with the analytical model. To account for the influence of different surface and electrical properties, we repeated quasistatic tests with the objects described in Section 2.3.1.1 (Figures 2.10c): PLA cylindrical objects coated by (1) 0.1 mm-thick copper, (2) 0.1 mm-thick copper covered by 0.1 mm-thick paper, (3) 18 µm-thick P(VDF-TrFE-CTFE), all bonded with 1 mm-thick VHB on 30 mm-radius objects (Figure 2.13). We only tested DC voltage. For every object, we repeated the COMSOL simulations described in Section 2.2.1.3 to obtain the updated values of C_c of the tape and calculated $\Delta\hat{c}$ (recall that $\Delta\hat{c} = \frac{C_c - C_\infty}{L}$, L = tape length) to insert in eqn. 2.10. The critical parameter for the variation of the tape capacitance is the dielectric constant of the object. P(VDF-TrFE-CTFE) has a very high constant with respect to paper ($\varepsilon_{PVDF} = 30$ vs $\varepsilon_{PAPER} = 3$), so C_c is very high too and both $V_{NO\ ZIP}$ and $V_{FULL\ ZIP}$ are consequently decreased with respect to the paper case (eqn. 2.9 and 2.13). Our experiments confirm the decrease in $V_{NO\ ZIP}$, but experimental $V_{FULL\ ZIP}$ is over 40% higher than our model predictions. We do not know the reason behind this behavior yet. An explanation could be the complex polarization dynamics of P(VDF-TrFE-CTFE), making the tape unable to wrap the object in only 10 s.

Electroadhesion works with both insulators and dielectrics (even if according to different physical mechanisms). Then we tested the zipping behavior on a cylindrical object covered by a 0.1 mm-thick copper layer. According to our FEM simulations electrostatic forces between the tape and the object are even higher than with P(VDF-TrFE-CTFE) in this case, and the calculated $V_{NO\ ZIP}$ and $V_{FULL\ ZIP}$ are furtherly lower. Data observations show instead that the beginning and the completion of wrapping happen at voltages higher than predictions, only slightly lower than the

values needed in the paper case. Again, we cannot draw any conclusions about these observations: the model does not account for the dynamics of charges that can influence the zipping process, and with the copper coating not only the electrical but also the surface properties of the object are modified.

To restore the affinity with the paper case, we decided to cover the copper-coated object with an additional external 0.1 mm-thick layer of paper. In this case predicted electrostatic forces are higher than the paper-alone case, but lower than the copper case, and $V_{NO\ ZIP}$ and $V_{FULL\ ZIP}$ lie between the values obtained in those cases. The experimental error with the predicted $V_{NO\ ZIP}$ is strongly reduced, even if $V_{FULL\ ZIP}$ shows a 40% discrepancy with the prediction (yet compared to 200% error for the copper case). The reduction in the observed divergence could be due to the use of a rough surface as in the paper case, or to a mitigation effect of charges dynamics operated by the paper layer.

Lastly, we tested the wrapping capabilities of an EA tape in a load-lifting configuration, similarly to an electrostatic actuator task [56,57] (Figure 2.14a). We attached a small mass (1 g) to the tape tip and performed a quasistatic experiment as described for the previous cases (200 V every 10 s, DC voltage). The radius of the object was 45 mm and it was covered with paper. The total potential energy equilibrium is modified by the contribute coming from the hanging mass. The potential energy of the system is expressed in this case as:

$$U_T(\alpha, V) = \frac{1}{24}\frac{\alpha E b t^3}{R} + \rho b t L g \left[\frac{L}{2} - \frac{R^2(1-\cos\alpha) + (L-\alpha R)\left(R\sin\alpha + \frac{L-\alpha R}{2}\right)}{L}\right] - \frac{1}{2}C_\infty V^2 - \frac{1}{2}(C_c - C_\infty)\frac{\alpha R}{L}V^2 + PgR(\alpha - \sin\alpha). \qquad (2.29)$$

The shape of the total potential energy curves (Figure 2.14b) is modified with respect to the case with no mass (Figure 2.8c). The system still exhibits equilibrium angles that increase with the applied voltage but is characterized by no instabilities. The full zip angle is reached by continuously increasing the applied voltage and no pull-in phenomenon is expected. Moreover, $V_{NO\ ZIP}$ is not affected by the mass, since as already shown (eqn. 2.9) it only depends on the electrostatic and bending contributes. Conversely, $V_{FULL\ ZIP}$ is strongly affected by the added load, as expected (eqn. 2.13). Finally, no hysteresis between zipping and unzipping is expected with a mass attached at the tape tip. For this case, model and data show a very good agreement (Figure 2.14c).

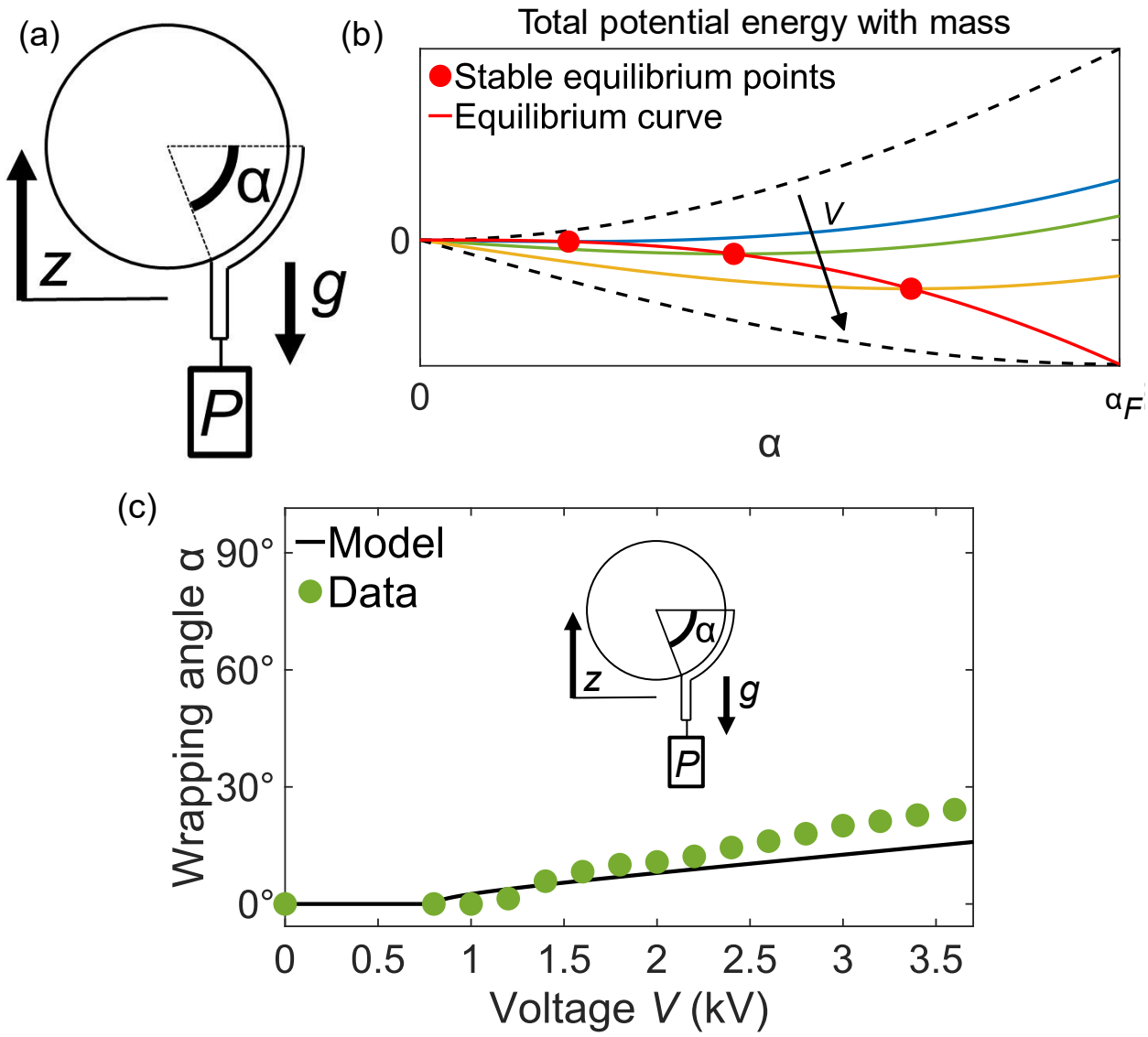

Figure 2.14 – validation of the zipping model in a load lifting configuration. (a) The zipping system with a small mass (1 g) attached to the tape tip. (b) The total potential energy of the system with the mass. (c) Comparison between model and experimental results. Reproduced with permission from Mastrangelo et al. [1].

2.3.2 Dynamic experiments

Despite the analytical model does not account for dynamics effect, we also tested the wrapping of the EA tape under dynamics conditions. Time response is in fact very important for EA soft grippers and their applications in real scenarios as industrial applications, where a fast yet reliable grasping is required. The experiments tested the tape under the repeated application of increasing (by 400 V each time) voltage steps (3 seconds on, followed by 3 seconds off). We only tested 30 mm radius, paper-coated cylindrical objects.

Results (Figure 2.15) show that the tape can fully wrap the object only when a voltage equal to 3.2 kV is applied. This value is very similar to the $V_{FULL\ ZIP}$ predicted by the quasistatic model (~3.2 kV) for the object we used. When the voltage is furtherly increased (3.6 kV), the wrapping is faster: we measured a 90%-time response of nearly 0.419 s for the zipping and 0.328 s for the unzipping.

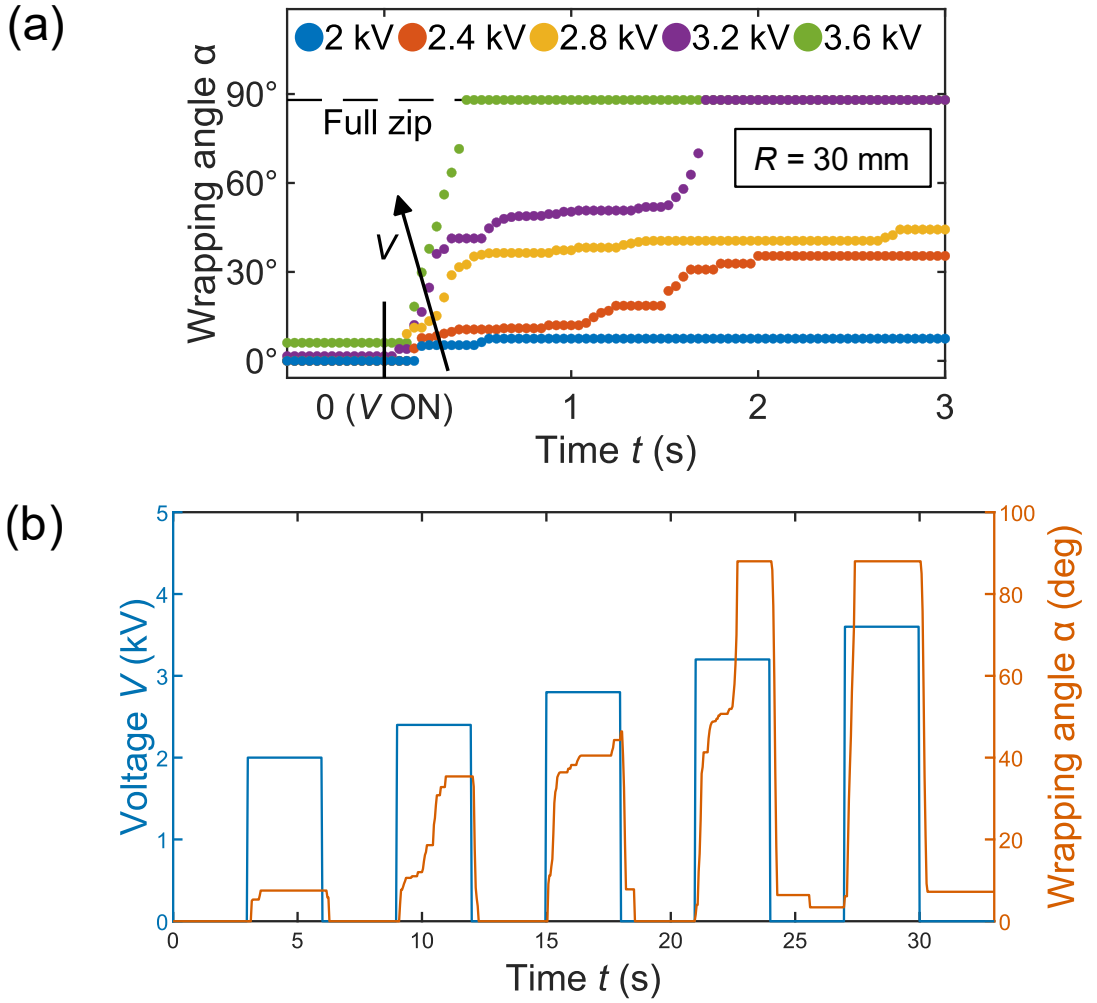

Figure 2.15 – (a) Dynamical tests of the zipping of an EA tape on a 30 mm paper-covered curved object (see Section 2.3.1.1). Only when a voltage equal to 3.2 kV is applied (like the $V_{FULL\ ZIP}$ value predicted by the model for the quasi-static case) the tape fully wraps the object. For higher voltage (3.6 kV) the wrapping is faster. (b) Complete zipping and unzipping cycles (3 sec voltage on, 3 sec voltage off). Reproduced with permission from Mastrangelo et al. [1].

2.3.3 Tests on common objects

Finally, we tested the zipping of the tape on various common objects (Figure 2.16). As in the previous experiments, we placed the tape in vertical position, tangent to the object. Then we applied 4 kV and recorded the zipping process. For each of the tested object, the wrapping angle of the tape reached α_F. However, with spherical objects the tape was unable to fully contact the surface. A sphere is characterized by a nonzero Gaussian curvature, in contrast with the cylinder case for which the Gaussian curvature is zero as a planar surface. This means that the tape is only required to bend to conform to a cylindrical object, but a deformation in the surface plane (stretching or compression) and a consequent variation in the Gaussian curvature is needed to conform to a spherical one. Further investigation is needed to quantify the effect of the nonzero Gaussian curvature on the zipping behavior, since our model does not account for the mechanical energy required for the stretching of the tape.

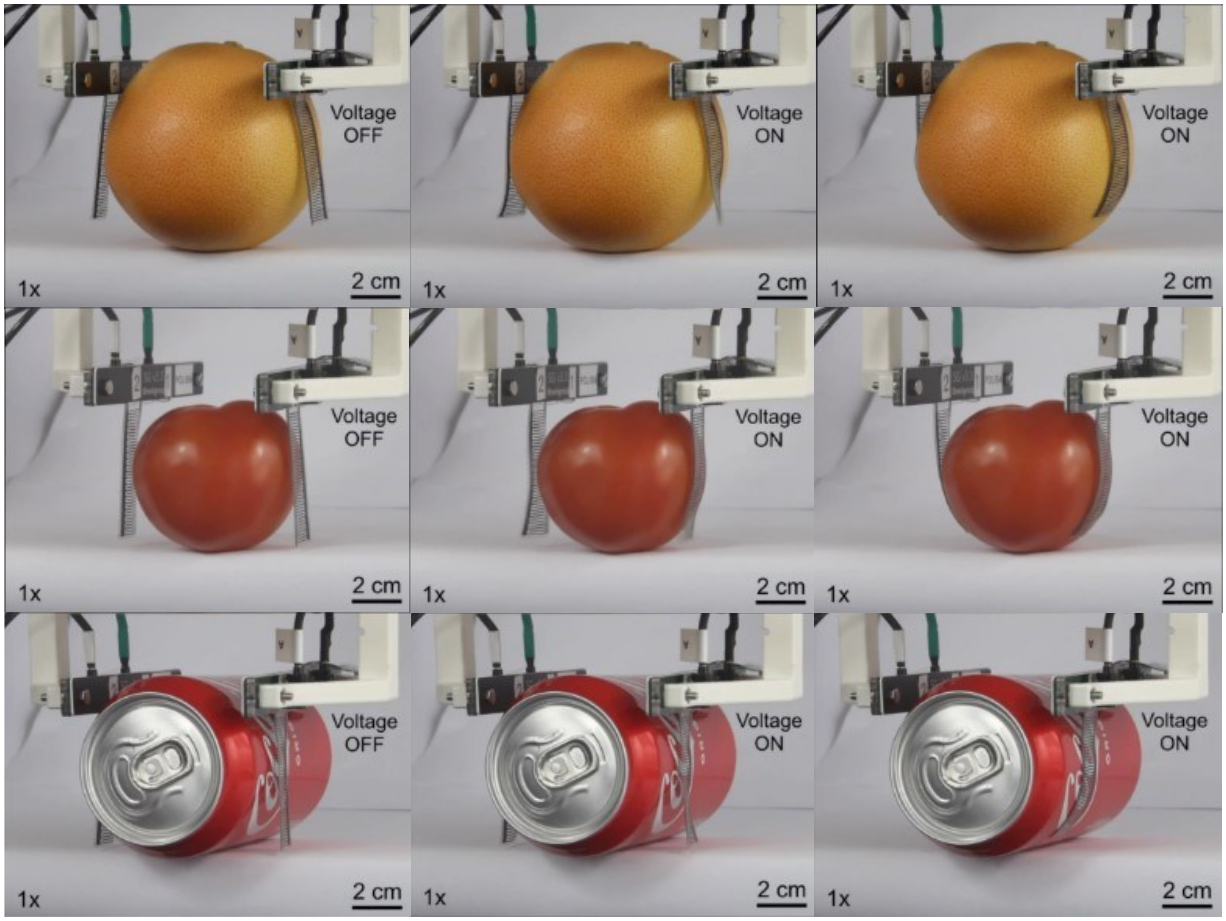

Figure 2.16 – Video frames of the tests conducted on three common objects: an orange, a tomato, and a can. We applied 4 kV at 10 Hz during each test. From left to right: no voltage applied, tape at rest; as soon as 4 kV voltage is applied, the zipping starts; end of the zipping, tape fully wrapped on the object. Reproduced with permission from Mastrangelo et al. [1].

2.4 Tools for the design of a passively wrapping EA soft gripper

The analytical model presented in Section 2.2 highlighted the main system features influencing the wrapping of an EA soft tape on a curved object. The process happens with the tape progressively zipping on the object, under the application of an increasing voltage. The ratio between the mechanical (elastic and mass) and electrical properties of the system determines the zipping advance, affecting the voltage thresholds that define the wrapping phases.

By recalling eqn. (2.9, 2.13), $V_{NO\ ZIP}$ and $V_{FULL\ ZIP}$ are expressed as $V_{NO\ ZIP} = \frac{1}{R}\sqrt{\frac{1}{12}\frac{Ebt^3}{\Delta\hat{c}}}$ and $V_{FULL\ ZIP} = \sqrt{\frac{2}{\Delta\hat{c}}\left[0.35\rho tbLg\left(1-\cos\left(0.65\frac{L}{R}\right)\right)+\frac{1}{24}\frac{Ebt^3}{R^2}\right]}$. We can simplify both the equations by defining some useful parameter to clarify the mutual relationship between the energy terms in eqn. (2.8). By defining $\frac{Ebt^3}{12}$ as the bending stiffness BS of the tape, we get:

$$V_{NO\ ZIP} = \frac{1}{R}\sqrt{\frac{BS}{\Delta\hat{c}}}. \qquad (2.30)$$

Similarly, by defining $\gamma = 0.70R^2\left(1-\cos\left(0.65\frac{L}{R}\right)\right)$ the geometric factor of the system and by recalling that the tape mass is equal to $m = \rho tbL$, we obtain:

$$V_{FULL\ ZIP} = \frac{1}{R}\sqrt{\frac{mg\gamma + BS}{\Delta\hat{c}}}. \qquad (2.31)$$

The whole wrapping can be then described by the relationship between the bending stiffness BS, the mass m and the geometry γ of the system, as well as $\Delta\hat{c}$, the capacitance variation per unit length of the tape.

This section reports design tools that show how the electric features of the system, accounted for by the quantity $\Delta\hat{c}$, can be tuned by controlling the characteristic of the interdigitated electrodes of the tape, and how the wrapping response of the gripper is affected by the dielectric layer thickness, for given mass, geometry, and bending stiffness of the tape.

2.4.1 Tape capacitance variation per unit length $\Delta\hat{c}$

This section shows how variations in the tape features affect the capacitance of the tape per unit length $\Delta\hat{c}$. The goal is to provide useful tools for the design of EA gripper fingers to maximize the electrostatic force produced and consequently improve the wrapping capabilities. We investigated the effects of the variation of the relative permittivity of the dielectric surrounding the electrodes ε_{TAPE} and of the object ε_{OBJECT} and of geometric features of the tape on the capacitance variation.

As we discussed in Section 2.2.4, we write $\Delta\hat{c} = \frac{C_c - C_\infty}{L}$, with C_c the capacitance of the tape in full contact and C_∞ the capacitance of the tape only surrounded by air. As showed, we used COMSOL Multiphysics to compute the tape capacitance, since the interdigitated configuration hinders a simple analytical calculation. We modeled the longitudinal section of a semi-electrode pair of the EA tape as done in [4] (see Section 2.2.4). Here we exclude for simplicity the case in which the object is conductive, limiting ourselves to the cases in which a relative permittivity ε_{OBJECT} can be defined. We also controlled for the distance w between the interdigitated electrodes in the tape. We expressed it as a nondimensional ratio with respect to the thickness d of the dielectric layer covering the electrodes.

Figure 2.17b-d shows the dependence of $\Delta\hat{c}$ on $\frac{w}{d}$, for various values of ε_{TAPE} and ε_{OBJECT}. We limited our analysis to values of $\frac{w}{d} > 2$. For lower values, the electrostatic attraction between the electrodes becomes stronger than between electrodes and object (even in the limit case of a conductive object). Not only the electric field between the electrodes does not contributes to EA, but also dielectric separating the electrodes becomes the tape region with the higher risk of dielectric breakdown. $\Delta\hat{c}$ always decreases with $\frac{w}{d}$. ε_{TAPE} being constant, the decrease is more marked if the permittivity of the object is larger (Figure 2.15b). Conversely, the decrease is less dependent on ε_{TAPE}, with ε_{OBJECT} constant (Figure 2.15c,d). For small relative permittivity of the object ($\varepsilon_{OBJECT} = 3$), $\Delta\hat{c}$ is slightly affected by the relative distance between the electrodes (Figure 2.15c). The negative trend becomes more pronounced with higher object permittivity ($\varepsilon_{OBJECT} = 10$) (Figure 2.15d). The trends are easily explained by considering that changes in ε_{TAPE} affect both C_c and C_∞, but ε_{OBJECT} only influences C_c.

2.4.2 Dependence of zipping on the features of the tape

In this last section, we want to provide graphical tools for the design of EA soft grippers. Our aim is to show how the tape features can influence the zipping phenomenon. We show the influence of the dielectric layer thickness d ($\frac{w}{d}$ kept constant and equal to 16, the same value of our tape, Section 2.3) on the two voltage thresholds $V_{NO\ ZIP}$ and $V_{FULL\ ZIP}$ for various values of the mass and the bending stiffness of the tape. We kept constant the relative permittivity of the tape and the object (both equal to 3), and the geometrical factor $\gamma = 311\ mm^2$, corresponding to an object radius of 30 mm and to a tape length of 48 mm.

The plots (Figure 2.17e, f) show that both $V_{NO\ ZIP}$ and $V_{FULL\ ZIP}$ increase with d, and that the trend is more marked with higher bending stiffness and mass, as expected. Heavier or stiffer tapes would require higher voltages to zip onto the object, but this becomes infeasible if the dielectric layer is too thin. The graphs also show the breakdown region of the tape, obtained by calculating the limit voltage applicable to the tape for given thickness of the dielectric layer, according to the dielectric breakdown strength of the dielectric (PDMS in this case, $E_{BD} = 100\frac{kV}{mm}$). The allowable voltage increases linearly with the dielectric layer thickness.

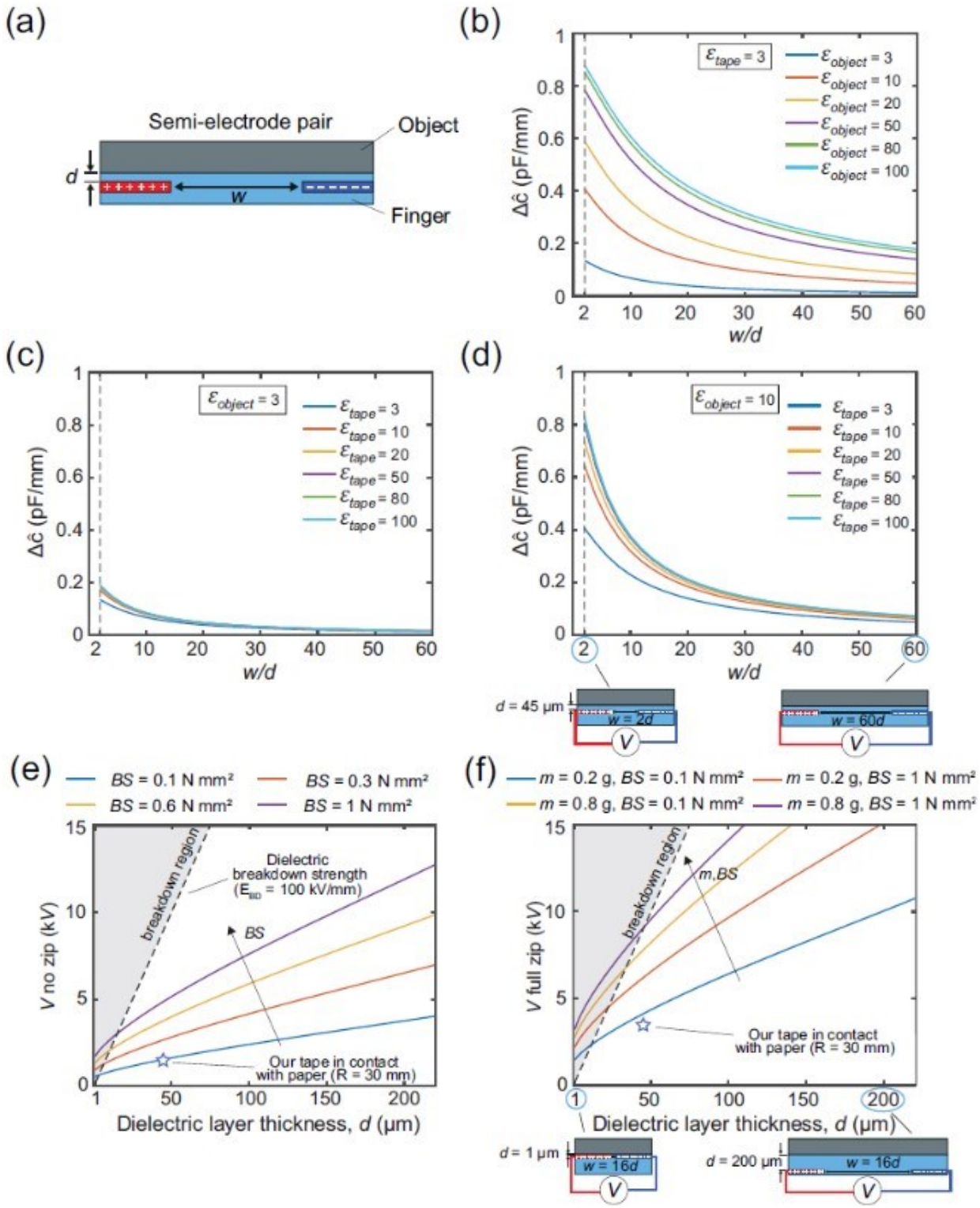

Figure 2.17 – (a) Sketch of the semi-electrode pair section. (b-d) Tape capacitance per unit length $\Delta\hat{c}$ as a function of $\frac{w}{d}$, plotted for various values of the dielectric constant of the tape and of the object. (e-f) $V_{NO\ ZIP}$ and $V_{FULL\ ZIP}$ increase with the dielectric layer thickness d ($\frac{w}{d}$ kept constant). The increase is more marked if the tape bending stiffness and mass are higher. With increasing d the maximum voltage that can be applied to the tape increases as well, delimiting the breakdown region where the tape would fail. Reproduced with permission from Mastrangelo et al. [1].

2.5 Conclusions

This chapter deals with the problem of EA soft grippers passively wrapping curved objects, leveraging zipping induced by electroadhesion forces.

We firstly presented an analytical model (two alternative approaches are included) to describe the wrapping process. The model results show that the dependence of the wrapping angle on the voltage applied to the gripper is characterized by two precise voltage thresholds, and that the whole process is influenced by the balance between the electrostatic and the mechanical forces acting on the system.

Then, we validated the model with experiments. Experimental results are in good agreement with model, even if some observed phenomena are still not explained and will be object of further work. The model does not account for the dynamics of the charges in the system or for the surface properties of the contact interface between the gripper and the object, yet these effects seem to have great influence on our experiments.

We finally provided design tools to improve the fabrication of passively wrapping EA soft grippers, highlighting the mutual relationship among the grasping system parameters, and showing how they influence the gripping performance.

We demonstrated that wrapping with EA soft grippers is possible even without added actuators and with demanding geometries such as the curved ones. The demonstrated wrapping capabilities provide very high holding forces, according to previous works [3,29] and to the results that will be presented in Chapter 3. However, current softness and compliance of passively wrapping EA soft grippers can still hinder their manipulation capabilities, limiting their ability to rotate the grasped object or to move payload fast. We will address this topic in future works.

This works broadens the knowledge about the performance of EA soft grippers. Moreover, we also believe that the outcomes of this work could also be adapted to various devices based on electroadhesion zipping, such as HASELs [57], HAXELs [58] and electro-ribbon and origami [56] actuators, constituting a tool for the design of soft actuators and machines.

3. Electroadhesion of soft tapes on curved objects[2]

3.1 Introduction

In the previous chapter we discussed the problem of EA soft grippers wrapping objects without the aid of any external actuator. Focusing on curved objects, we discovered the relationship between mechanical and electrical features of the system and the conditions allowing the gripper's finger to conform to a circular shape. In this chapter, we investigate the effect on the maximum holding force of the gripper produced by the posture assumed to adapt to the curved surface. In a broad sense, we will discuss the mechanics effect of the object's curvature on the detachment force of EA soft tapes adhered on it.

EA soft grippers leverage EA to grasp objects without squeezing them. The gripper's fingers embed interdigitated electrodes. When a voltage difference is applied between electrodes, they generate an electrostatic fringing field. The field penetrates the object producing an accumulation of charges on the object surface. The mutual electric attraction between the charges accumulated in the fingers and in the object leads to adhesion. The holding force of the gripper is indeed the maximum force that can be applied to the fingers without leading to their detachment from the object surface.

A lot of effort has been made for the modeling of EA detachment forces. However, most of work focused on the electrical and tribological aspects of the problem [33,52,72,73]. The mechanics of the EA has been mostly ignored in these studies, yet in the case of robotic devices that exploit EA as working principle, such as EA soft grippers, it becomes an important parameter as well, able to influence the performance of such machines.

In contrast to previous literature, recent works highlighted the role of the mechanics in EA of robotic devices. In particular, [4,29] show how the grasping posture of an EA soft gripper (dependent on both the gripper and the object) influences its maximum holding force. Authors from [29] produced a preliminary study of the influence of the gripper's posture on the holding force. The gripper involved in the study combines EA with dielectric elastomers actuators for bending the elastomeric fingers towards the objects. The authors tested the holding force on paper-covered both circular objects with increasing diameter and a flat object (Figure 3.1). Since the fingers are mounted on a fixed frame, the angle between the finger and the adhesion surface is forced to change to adapt to the different geometries. The holding force varies accordingly, from the highest value obtained with the smallest diameter (the finger experiences compression toward the object plus shear), to increasingly lower values with smaller diameters until the lowest holding force with the flat object (finger subject to peeling). However, due to the structure of the gripper, the reported experiments were unable to decouple the different effects of the peeling angle and of the shape of the grasped object on the measured holding force.

[2] Part of this chapter has been reproduced with permission from the article:
M. Mastrangelo and V. Cacucciolo, "High-Force Soft Grippers with Electroadhesion on Curved Objects", 2022 IEEE 5th International Conference on Soft Robotics (RoboSoft).

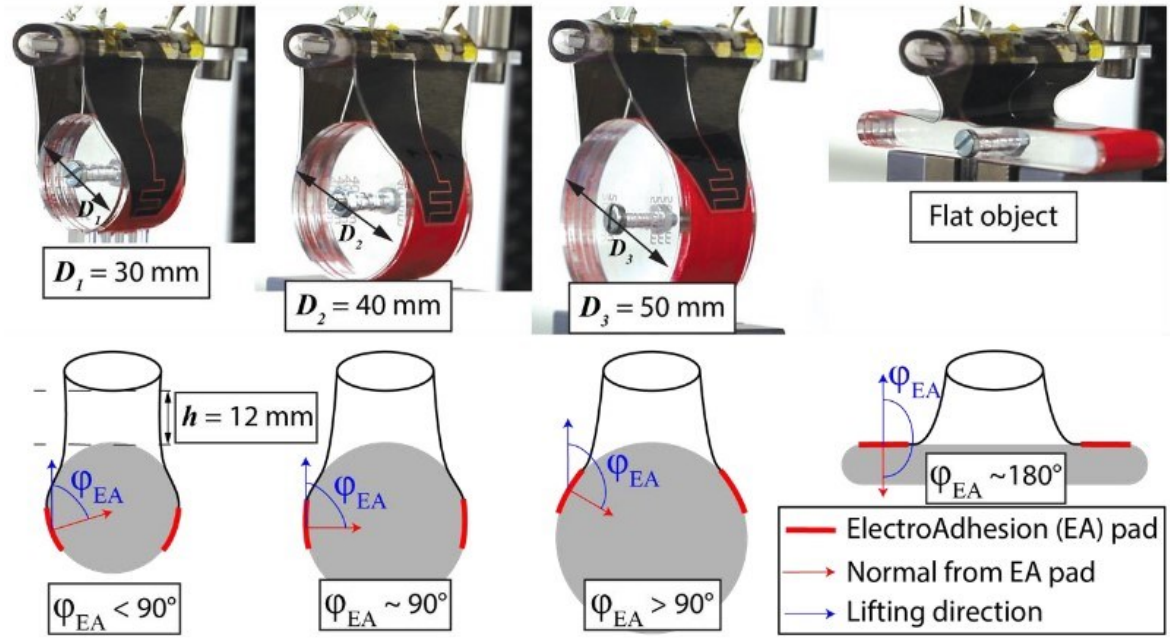

Figure 3.1 – The configurations tested in [29]. Due to the fixed structure of the gripper, different geometries of the grasped object forced the fingers to assume different angles with respect to the object's surface. The increase in the angle between the fingers and the surface negatively affect the maximum holding force. Reproduced with permission from Cacucciolo et al. [29].

The influence of the peeling angle between the finger and the object surface is systematically investigated in [4]. The study involved soft and thin elastomeric EA tapes with no rigid backing. The authors observed that when the peeling angle between the EA finger and the adhered substrate is > 0°, the maximum detachment force can be accurately described by adapting the classical Kendall's (based on Rivlin's) model [32,74] to the EA case. The detachment force is modeled as $F = \frac{bR_{EA}}{1-\cos\theta}$, where θ is the peeling angle, b is the tape width and R_{EA} is the surface energy required to create new surfaces from breaking the adhesive joint.

For $\theta = 0°$ (commonly defined "lap-shear configuration"), in the case of stretchable tapes with no rigid backing and if the frictional stresses dominate over adhesion energy, as in [4], the force can be expressed (neglecting the adhesion term) as $F = \tau_{EA} ab$, with a the length of the area where friction forces are exchanged and τ_{EA} the frictional stress. When the tape is pulled, part of the previously adhered area starts to slide over the substrate, and the sliding area increases proportionally to the pulled force until the whole contact area is involved and the tape reaches the maximum applicable force, as already observed for generic elastomeric tapes [75]. The maximum holding force is then given by the product of the shear stresses (assumed constant and uniform) times the initial adhesion area. The same approach is widely used for the calculation of the maximum holding force of electrostatic clutches [30,39,40], soft wearable devices used to produce on-demand mechanical impedance in applications such as rehabilitation or teleoperation [76,77]. Conversely, when the adhesion energy prevails over the frictional stress, the failure mechanism involves the propagation of a crack front, with the detachment force steady and proportional to the tape width [75]. Finally, for the case of soft tapes with a stiff backing pulled in lap-shear mode, a recent work [28] proposes a model based on a fracture mechanics physical framework: according to the authors, the pulling force depends not only on the surface energy of the adhesive interface and on the initial contact area, but also on the total stiffness of the adhesive joint.

The effect of the shape of the grasped object is also reported as an impacting parameter in [4]. Due to the improved architecture of the soft gripper frame with respect to previous work [29], the described manipulator was able to control for the peeling angle of each finger, isolating its

influence from other effects. The authors observed that, when their EA soft gripper is used to grasp curved objects with peeling angle = 0°, higher forces than those predicted by their model for lap-shear configuration are measured. They attribute the discrepancy to the increase in frictional stress due to the curvature of the substrate, but do not propose any contribute to explain the phenomenon.

The goal of the work presented in this chapter is to disclose the reason behind the increase in the maximum holding force of a soft gripper when it wraps curved objects. The outcomes of the investigation are of great interest for EA soft grippers, since they motivate the fabrication of improved grippers able to wrap objects and exploit the full potential of the technology in terms of higher holding forces. Moreover, our results could be effective even for renewing the design of other EA-based robotic devices such as, for example, electrostatic clutches [30,40,73]. The augmentation of the transmitted force due to the mechanic effects introduced by the curvature of the adhering surfaces can indeed lead to clutches with higher force output at the same footprint, or similar outputs with smaller devices (critical for wearable applications) or lower requirements in terms of voltage supply.

We propose an analytical model for the detachment force of EA soft tapes with no backing adhering on curved surfaces, extending the work from [4], valid for cases in which friction dominates. As for the case of lap-shear configuration with adhesion on flat substrates, the model predicts the appearance of a sliding zone with the tape being pulled. Our hypothesis is that normal components of the longitudinal tension in the tape lead to increased normal pressure exchanged between the tape and substrate, and accordingly to increased frictional stresses. The model predicts a holding force exponentially depending on the friction coefficient between the tape and the object and on the initial wrapping angle of the tape, and linearly depending on the radius of the grasped object. Similar and well-known force enhancement is observed and leveraged in various mechanisms such as capstans [78], belt transmissions [79] and force amplifiers [80], but never investigated in the case of adhesion.

We compared the results of our model with the preliminary data from [40], finding very good agreement with the data [3]. Then, we also tested the validity of the model by conducting pulling test of EA soft and stretchable tapes electro-adhered on curved substrates. We report the materials and methods of our experiments, and the results of our preliminary experiments that confirm the goodness of our hypotheses.

The chapter is organized as follows. Section 3.2 presents the model for the maximum holding force of EA stretchable (no backing) soft tapes wrapped around curved objects. We also include the results of this model in this section. Section 3.3 includes the validation of the model. We include the description of the experimental set-up and the results of our experiments.

Nomenclature

F = external pulling force applied to the tape

σ = longitudinal tension in the tape

τ = frictional stress exchanged between tape and substrate

p_N = normal pressure exchanged between the tape and the substrate

p_{EA} = Maxwell stress generated by the electrostatic attraction produced between the charges on the tape and on the object

R = radius of the object

t = tape thickness

b = tape width

Φ = initial wrapping angle

L = length of the initial wrapping zone

φ^* = sliding angle

l^* = length of the sliding zone

φ = angle coordinate in the sliding zone

l = longitudinal coordinate in the sliding zone

σ^* = longitudinal tension at the end of the sliding zone

$\Delta\sigma$ = longitudinal tension jump due to the creation of new surface at the end of the wrapping zone

R_{EA} = electroadhesion surface energy

σ^+ = longitudinal tension in the free zone

3.2 Theoretical model for the detachment force of electroadhesion stretchable tapes wrapping curved objects

The model presented in this section predicts the maximum detachment force of an EA soft tape adhering on a curved object. The model assumes stretchable tapes with no stiff backing. We also assume that frictional stresses dominate over adhesion energy in the contact between tape and object. We hypothesize that, when a pulling force is applied to the tape, a sliding area appears, and that this area increases with the force, as already observed for EA tapes adhered on flat surfaces [4]. The difference with respect to the flat case is the increase of the frictional stresses in the sliding zone due to the curvature of the substrate. Normal components of the longitudinal tension in the tape increase the normal reaction exchanged between the object and the tape in the sliding zone. This in turn causes an increase of the frictional stresses exchanged at the sliding interface, and finally in augmented longitudinal tension in the tape, resulting in the exponential dependence of the holding force on the length of the adhesion zone and on the friction coefficient between tape and substrate. The predicted holding force remains proportional to the width of the tape and to the radius of the object, as well as the to the normal pressure (Maxwell stress) coming from the electrostatic attraction between the tape and the substrate, as in the flat case.

3.2.1 Model formulation

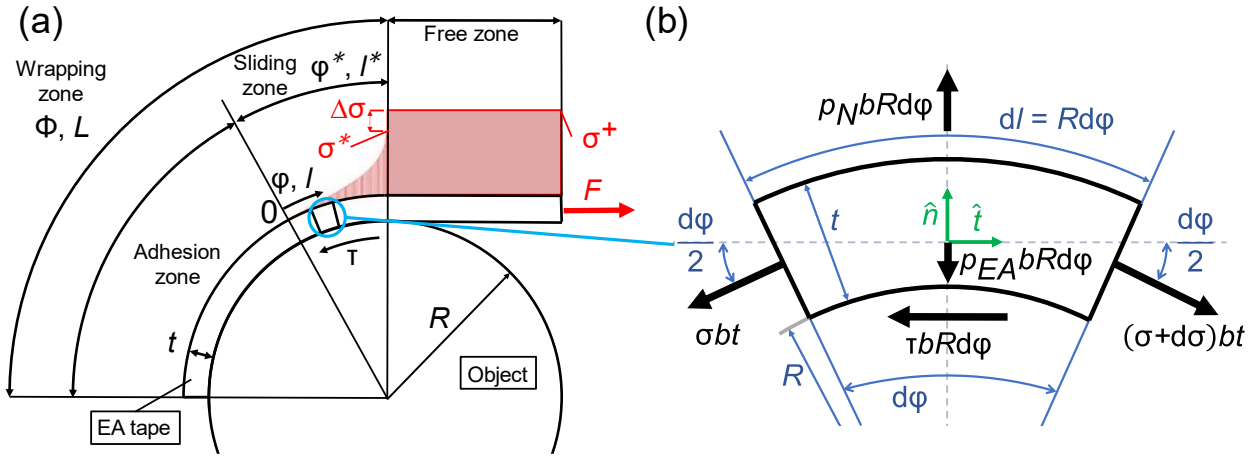

Figure 3.2 – (a) An EA tape wrapping a curved surface for a total wrapping length L. When a pulling force F is applied at the tape tip, according to our hypothesis three zones can be distinguished: (1) adhesion zone, no shear stress exchanged between tape and surface, longitudinal tension in the tape equal to 0; (2) sliding zone, shear stress exchanged between tape and substrate, longitudinal tension exponentially increasing along the zone; (3) free zone, the tape is not in contact with the object, the longitudinal tension in the tape is constant and equal to $\frac{F}{bt}$, where F is the applied force, b is the tape width and t is the tape thickness. The sliding zone increases with the applied force until the adhesion zone totally disappears and the tape detaches from the substrate. (b) Force balance on an infinitesimal element of the tape in the sliding zone. According to our hypothesis, the exponential growth of the longitudinal tension σ in the sliding zone is due to normal components of the longitudinal tension generated by the curvature of the substrate. These components add to the normal load exchanged between tape and substrate. Being valid the Amonton-Coulomb law of dry friction [2], friction stress in turn increases as well producing a growth of the longitudinal tension in the tape along the sliding zone. Reproduced with permission from Mastrangelo et al. [3].

Consider a soft tape adhered by EA to a circular substrate for a total wrapping angle Φ (Figure 3.2a). We consider only the case in which the dry adhesion is negligible with respect to EA. An external force is applied to the tape tip. We only consider quasistatic loads, then neglecting dynamics or viscous effects.

As the pulling force F is applied, we hypothesize that three zones appear: (1) *adhesion zone*: the tape remains adhered to the substrate and is subject to no stress (both the longitudinal stress σ and

the frictional stresses τ are equal to 0); (2) *sliding zone*: in this area frictional stresses τ are exchanged between the tape and the object and the longitudinal tension in the tape is $\sigma > 0$. We further hypothesize that the length of the sliding zone increases with the applied force F; (3) *free zone*: here the tape is not in contact with the substrate, the strain of the tape is uniform, and the longitudinal stress is constant and equal to $\sigma = \sigma^+ = \frac{F}{bt}$, with b = tape width and t = tape thickness.

Consider the force balance on an infinitesimal tape section in the sliding zone (Figure 3.2b) on the normal and tangential direction of the tape, indicated by the unit vectors $\hat{n}$ and $\hat{t}$, respectively:

$$\hat{t}) \qquad [\sigma(\varphi) + d\sigma(\varphi)]bt\cos\frac{d\varphi}{2} - \sigma(\varphi)bt\cos\frac{d\varphi}{2} - \tau(\varphi)bRd\varphi = 0 \qquad (3.1)$$

$$\hat{n}) \qquad p_N(\varphi)bRd\varphi = p_{EA}bRd\varphi + [\sigma(\varphi) + d\sigma(\varphi)]bt\sin\frac{d\varphi}{2} + \sigma(\varphi)bt\sin\frac{d\varphi}{2} \qquad (3.2)$$

φ is the angle coordinate in the sliding zone (Figure 3.2a), p_N is the normal reaction exchanged between the tape section and the substrate, p_{EA} is the Maxwell's stress resulting from the electrostatic attraction between the charges on the two surfaces [33] (assumed constant along the wrapping length).

By assuming the condition of infinitesimal small angles, the approximation $d\varphi \cong 0$ holds. This implies that $\cos\frac{d\varphi}{2} \cong 1, \sin\frac{d\varphi}{2} \cong \frac{d\varphi}{2}$. By neglecting higher-order terms, eqn. (3.1, 3.2) can be written as:

$$\hat{t}) \qquad td\sigma(\varphi) = \tau(\varphi)Rd\varphi \quad \rightarrow \quad \frac{d\sigma(\varphi)}{d\varphi} = \sigma'(\varphi) = \frac{R}{t}\tau(\varphi) \qquad (3.3)$$

$$\hat{n}) \qquad p_N(\varphi)Rd\varphi = p_{EA}Rd\varphi + \sigma(\varphi)td\varphi \quad \rightarrow \quad p_N(\varphi) = p_{EA} + \frac{t\sigma(\varphi)}{R} \qquad (3.4)$$

Eqn. (3.3) indicates that the variation of the longitudinal tension in the tape along φ is proportional to the frictional stress. The system composed by eqn. (3.3, 3.4) contains three unknown variables: $\tau(\varphi)$, $\sigma(\varphi)$, $p_N(\varphi)$. The solution is undetermined.

We further hypothesize that the frictional stress $\tau(\varphi)$ depends on the normal reaction $p_N(\varphi)$. This statement is supported by literature for elastomers in contact with rough substrates [81]. Our hypothesis is that the frictional stresses can be captured by the Amonton-Coulomb law of dry friction [2] in our case: $\tau(\varphi) = \mu\, p_N(\varphi)$, where μ is the friction coefficient between tape and substrate (assumed independent from the normal load and constant along the wrapping zone). The equilibrium is now close and by substituting eqn. (3.4) in (3.3) one gets $\frac{d\sigma(\varphi)}{d\varphi} = \mu\sigma(\varphi) + \mu p_{EA}\frac{R}{t}$. By integrating and by recalling that the longitudinal tension is $\sigma = 0$ in the adhesion zone (boundary condition: $\sigma(\varphi = 0) = 0$):

$$\sigma(\varphi) = \frac{p_{EA}R}{t}(e^{\mu\varphi} - 1) \qquad (3.5)$$

for $0 \leq \varphi \leq \varphi^*$, φ^* length of the sliding zone (Figure 3.2a). Eqn. (3.5) expresses the variation of the longitudinal tension in the tape along the sliding zone. An alternative formulation is obtained by recalling that the angle coordinate can be written as $\varphi = \frac{l}{R}$, with l the longitudinal coordinate in the sliding zone (Figure 3.2a). The longitudinal tension becomes: $\sigma(l) = \frac{p_{EA}R}{t}\left(e^{\mu\frac{l}{R}} - 1\right)$. By deriving the longitudinal tension in this form with respect to l and by letting $R \to \infty$ one obtains $\lim_{R\to\infty} \sigma'(l) = \frac{\mu p_{EA}}{t}$ meaning that for very large angles the variation of the longitudinal tension along the wrapping zone is constant, as already obtained for flat substrates in [4].

By combining eqn. (3.4) and (3.5) one also gets the variation of the normal pressure along the sliding zone: $p_N(\varphi) = p_{EA}\, e^{\mu\varphi}$. The normal pressure is constant and equal to the Maxwell stress in the adhesion zone, but exponentially increases along the sliding zone.

At the detachment point ($\varphi = \varphi^*$) (Figure 2a) the longitudinal tension reaches its maximum in the sliding zone: $\sigma(\varphi = \varphi^*) = \sigma^* = \frac{p_{EA}R}{t}\left(e^{\mu\varphi^*} - 1\right)$. At $\varphi = \varphi^*$, the longitudinal tension is characterized by a jump, due to the additional tension component required to the creation of new surface from the detachment of the tape from the substrate. This contribute can be accounted for as $\Delta\sigma = \frac{R_{EA}}{t}$, where R_{EA} is the surface adhesion energy [4]. One can then write $\sigma^+ = \frac{p_{EA}R}{t}\left(e^{\mu\varphi^*} - 1\right) + \frac{R_{EA}}{t}$.

The external force is directly balanced by the longitudinal stress in the free zone, multiplied by the cross-section area of the tape. One gets:

$$F = \sigma^+ bt = bp_{EA}R\left(e^{\mu\varphi^*} - 1\right) + R_{EA}b \qquad (3.6)$$

By increasing the applied force F, the sliding angle increases until the sliding zone covers the wrapping zone ($\varphi^* = \Phi$). The maximum force that can be applied to the tape to avoid slippage then becomes:

$$F_{MAX} = bp_{EA}R(e^{\mu\Phi} - 1) + R_{EA}b \qquad (3.7)$$

3.2.2 Model results

Eqn. (3.7) expresses the linear dependence of the maximum holding force of an EA tape on the tape width b, on the radius of the substrate R and on the Maxwell stress p_{EA} produced by the electrostatic attraction between the contacting surfaces. The difference introduced by the substrate curvature with respect to the flat case [4] consists in the exponential dependence of the force on the frictional coefficient between substrate and tape and on the length of the contact area (the wrapping arc Φ). The force is further dependent on the surface adhesion energy R_{EA}, but its contribute is negligible [4]. The exponential trend of the holding force comes from the increase of the longitudinal force in the tape along the sliding zone, expressed by eqn. (3.5). Due to the curvature of the substrate, longitudinal stress σ acquires a normal component, increasing the normal reaction exchanged at the contact interface (Figure 3.2b). In turn, the increase in the normal reaction leads to enlarged frictional stresses, according to the Amonton-Coulomb law of dry friction [2]. Since the variation σ' of the tension along the tape is proportional to the frictional stresses (tangential equilibrium, eqn. 3.3), the longitudinal stress is exponential rather than linear as reported for flat substrates.

Figure 3.3a reports the trend of the longitudinal stress in the tape along the sliding zone (eqn. (3.5)), for different values of R. We referred to the case in which the tape adheres on a curved object covered by paper (same substrate of [4]). The exponential trend of σ is more marked for smaller radii, since the normal components of the longitudinal tension are higher in the balance along $\hat{n}$. With increasing radii, the trend approximates the one obtained for flat substrates.

Figure 3.3b represents the normal pressure $p_N(\varphi) = p_{EA}\, e^{\mu\varphi}$ in the sliding zone. We plotted again the model results for paper-covered substrate (Fig. 3.3a). The trend of the normal pressure is exponential as well since $p_N(\varphi)$ is proportional to the longitudinal tension in the tape (eqn. 3.4). Figure 3.5b reports $p_N(\varphi) = p_{EA}\, e^{\mu\varphi}$ for different values of the voltage applied to the tape. The voltage influences the value of the Maxwell stress p_{EA} due to the electrostatic effects. Since the tape and the substrate are the same described in [4], we resorted to the same empirical law reported

in that work to calculate $p_{EA}(V)$: $p_{EA} = \frac{260V^2}{\mu}$ (Pa), with V expressed in kV, assuming valid the proportionality between frictional and normal stresses as expressed by the Amonton-Coulomb law of friction [2]. At $\varphi = 0$, $p_N(\varphi) = p_{EA}$.

Figure 3.3c reports on a colormap the dependence of the maximum holding force of an EA tape on the radius of the object and on the wrapping angle, as expressed by eqn. (3.7). The figure clearly shows that the holding force increases with the wrapping angle and the radius of the substrate, being constant other parameters. Continuous lines represent constant force lines. In the depicted range, the force is slightly influenced by the radius (lines are almost horizontal) and highly dependent on the wrapping angle. We also reported dotted lines indicating constant tape lengths. If the length of the tape is fixed, an increase in the radius of the object results in a decrease in the maximum wrapping angle. This is particularly interesting for EA soft grippers since it represents the allowable wrapping configurations for a certain gripper's finger length. The holding force scales with the dimensions of the gripper and the object: being the wrapping angle the same, our model predicts higher holding forces with a larger gripper holding a larger cylindrical object.

Based on the results on the zipping of an EA tape on a curved object (Chapter 2), here we also report theoretical predictions of the holding force of an EA tape wrapping curved objects in response to the applied voltage. In a typical configuration of EA soft gripper (Figure 2.2), the gripper fingers hang straight down when the voltage is off. As we demonstrated in the previous chapter, with curved objects the wrapping angle of the gripper fingers around the tape increases with the applied voltage. The wrapping behavior is characterized by two voltage thresholds. No wrapping is expected until the voltage reaches the $V_{NO\ ZIP}$ value (eqn. 2.9), and full wrapping is reached when $V = V_{FULL\ ZIP}$ (eqn. 2.13). The holding force is then affected by this behavior. Figure 3.3d illustrates the dependence of the holding force on the applied voltage with EA soft grippers grasping curved objects. When $V < V_{NO\ ZIP}$, the gripper exerts no holding force on the object. Between $V_{NO\ ZIP}$ and $V_{FULL\ ZIP}$, the wrapping angle increases with the voltage. Consequently, the holding force is expected to increase for two reasons. One, increasing voltage means increasing Maxwell stress p_{EA} exchanged between object and gripper fingers (according to [33]). This dependence is expected to be quadratic [4,33]. Moreover, the wrapping angle increases, so the friction force exponentially increases with it (eqn. 3.7). At $V = V_{FULL\ ZIP}$, the wrapping angle suddenly jumps from the critical value α^* to the full value α_F (eqn. 2.12). Consequently, the force is subjected to a sudden increase. Finally, for $V > V_{FULL\ ZIP}$, the holding force increases with the applied voltage, due to the dependence of the Maxwell stress on V.

The curved shape of the grasping object then strongly characterizes the dependence of the holding force on the applied voltage. Figure 3.3e illustrates the comparison, in terms of maximum holding force, between a soft EA gripper grasping a curved object and the same gripper grasping a flat object. In the latter case, gripper fingers fully contact the object for any voltage. This means that the (apparent) adhesion area is not affected by the voltage. The friction force then increases with the voltage since the Maxwell stress depends on it. In the case of a curved object, the force remains equal to 0 until $V_{NO\ ZIP}$ is reached, then increases for $V > V_{NO\ ZIP}$ and is subject to a jump at $V = V_{FULL\ ZIP}$, reaching very high values if compared to the flat object case.

Soft EA grippers grasp object with tangential forces resulting by the electrostatic attraction generated with the object and consequent adhesion (astrictive prehension [19]). The normal forces are kept very low. On the contrary, impactive prehension is not based on adhesion. Normal forces are much higher than in the astrictive case to generate adequate friction between gripper and object. However, when an EA soft gripper grasps a curved object, normal pressure dramatically increases, and, in some cases, they surpass the values reached for grasping of flat objects and becoming comparable to the one obtained with impactive grippers.

Refer to the grasping of a curved object. The maximum holding force of an impactive gripper would be:

$$F_{imp} = \mu A p_{N,imp} \qquad (3.8)$$

while the maximum holding force for an EA soft gripper would be the one expressed by eqn. (3.7). By imposing $F_{imp} = F_{MAX}$ and by neglecting the term due to the adhesion energy one obtains $b p_{EA} R(e^{\mu\Phi} - 1) = \mu A p_{N,imp}$. By remembering $p_N(\varphi) = p_{EA}\, e^{\mu\varphi}$, the maximum normal pressure exerted by an EA soft gripper would be in this case $p_{N,MAX} = p_{EA}\, e^{\mu\Phi}$($\Phi$ is the total wrapping length). If the contact area and the friction coefficient are the same for both grippers, by rearranging one finally obtains:

$$\frac{(p_{N,MAX} - p_{EA})}{p_{N,imp}} = \mu\Phi. \qquad (3.9)$$

The product $\mu\Phi$ expresses a comparison between the normal pressures exerted by the two grippers holding the same weight. When $\mu\Phi > 1$, the increase in the normal pressure (with respect to the flat case) of the EA soft gripper introduced by the curvature of the object is higher than the normal pressure exerted by the impactive gripper. This happens for smaller wrapping angles if the friction coefficient increases.

Figure 3.3 – (a) The longitudinal tension in the sliding zone of an EA soft tape adhered on a curved object (radius R) (eqn. 3.5). The tension exponentially increases along the sliding zone. The exponential increase is more marked with smaller radius. With increasing radii the trend approximates the one for flat substrates [4]. Data: $\mu = 3$, $t = 290$ μm, $b = 20$ mm, $p_{EA} = 1$ kPa (obtained for 3.5 kV according to the dependence on the voltage of the frictional stresses reported in [4] and by supposing a linear relationship between frictional stresses and normal pressure [2]). (b) Normal pressure exchanged between tape and substrate in the sliding zone. For $\varphi = 0$, p_N equals the Maxwell stress due to the electrostatic attraction between tape and substrate, dependent on the applied voltage. We hypothesize a quadratic dependence of the Maxwell stress on the applied voltage, as commonly reported in literature [4,5]. The normal pressure increases exponentially along the sliding zone. Data: $\mu = 3$, $t = 290$ μm, $b = 20$ mm. (c) Colormap of the maximum force F_{MAX} as predicted by eqn. (3.7). Continuous lines are constant force lines. Dotted lines are constant wrapping length L lines. Data: $\mu = 3$, $t = 290$ μm, $b = 20$ mm, $V = 3$ kV. (d) Influenced by the dependence of the wrapping angle on the applied voltage, the maximum holding force of an EA soft gripper grasping curved object is subjected to an irregular increase with the voltage, characterized by two jumps at two voltage thresholds. (e) The comparison between the maximum holding force of an EA soft gripper grasping a curved object and a flat one.

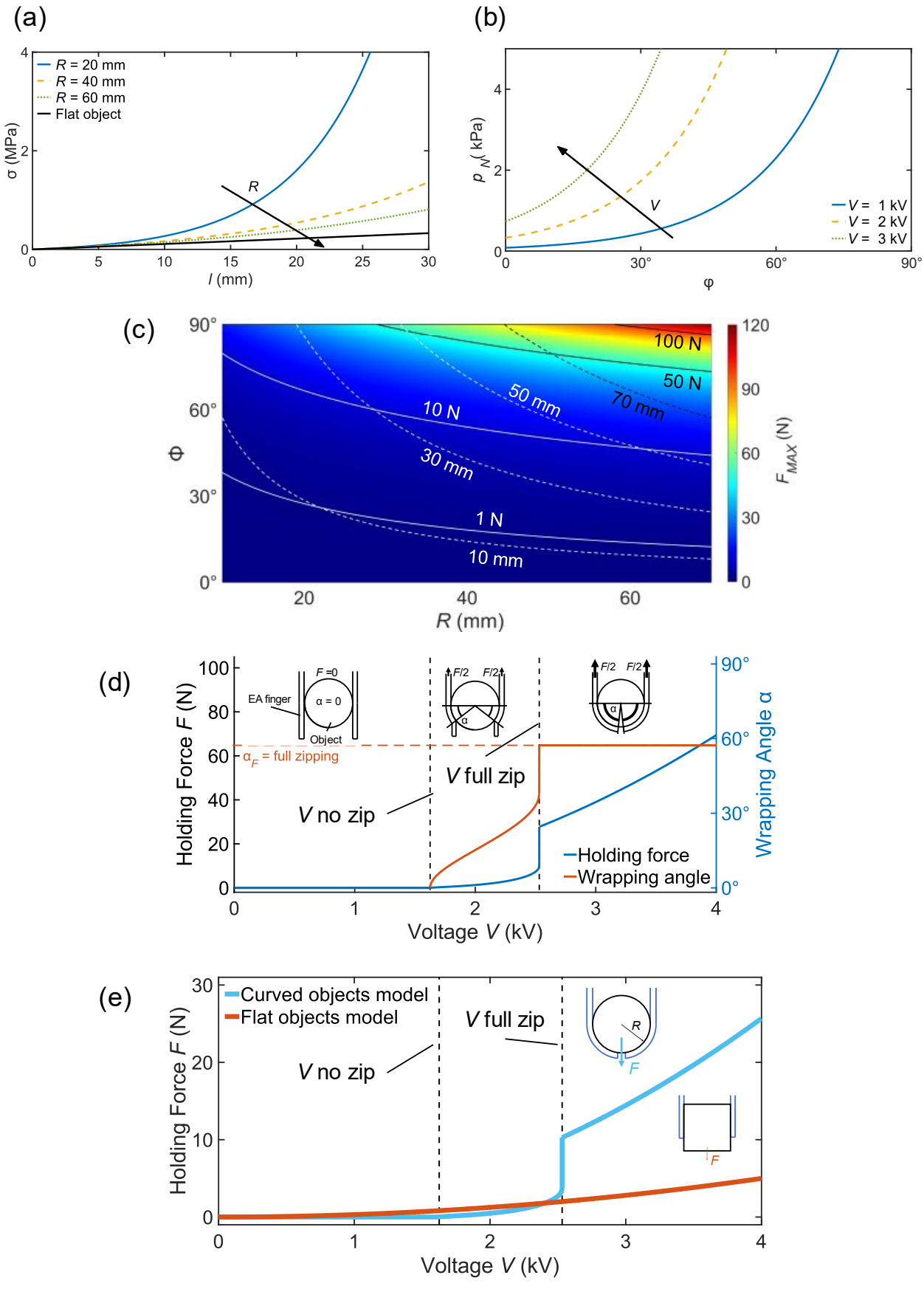
(a)
R = 20 mm
R = 40 mm
R = 60 mm
Flat object
σ (MPa)
l (mm)
R
(b)
p_N (kPa)
φ
V
V = 1 kV
V = 2 kV
V = 3 kV
(c)
100 N
50 N
10 N
1 N
50 mm
70 mm
30 mm
10 mm
θ
R (mm)
F_MAX (N)
(d)
Holding Force F (N)
Wrapping Angle α
EA finger
Object
α = 0
F =0
F/2
α_F = full zipping
V no zip
V full zip
Holding force
Wrapping angle
Voltage V (kV)
(e)
Curved objects model
Flat objects model
V no zip
V full zip
Holding Force F (N)
Voltage V (kV)
R
F

3.3 Validation of the model for electroadhesion stretchable tapes

This section reports the validation of the model for EA on curved objects we presented in Section 3.2. First, we present the comparison between the predictions of our model with experimental data reported in literature [29]. The comparison shows good agreement and improvements in prediction accuracy with respect to previous models [4] that didn't account for the curvature of the substrate. Then, we report the results of the preliminary experiments we performed to validate the theoretical model. We tested the model outcomes by comparing them to the measured maximum pulling force of EA tapes adhered on curved substrates in various conditions. We include the description of the experimental set-up and of the testing methods.

3.3.1 Comparison with data from literature

Figure 3.4 compares the experimental results from [29] to the predictions coming from our model (eqn. 3.7) and model for flat objects [4], about the maximum holding force of EA soft grippers grasping curved objects. The gripper from the experiments is depicted in Figure 3.1. The predictions from the two models have been calculated using the following data: friction coefficient $\mu = 2.7$ (extracted from data reported in [24]), wrapping length $L = 20$ mm, substrate radius $R = 20$ mm. Since the gripper's fingers from [29] has a trapezoidal shape, we estimated a medium width b of the fingers equal to 15 mm in the adhesion zone. EA parameters have the value: $V = 3.5$ kV, $\tau_{EA} = 3.2$ kPa (EA shear stress, calculated with the empirical relationship reported in [4]), $p_{EA} = \frac{\tau_{EA}}{\mu} = 1.2$ kPa [4] (Maxwell stress). R_{EA} is negligible with respect to other force components, so we did not include it in the calculation. F_{MAX} (eqn. 3.7) is doubled to account for two gripper fingers.

The graph shows a very good agreement between the experimental data (measured force = 10 N) and the prediction from our model ($F_{MAX} = 9.8$ N). Previous model not accounting for the curvature of the substrate predicts a detachment force $F_{MAX} = 1.9$ N. Our model reduced the error from 81% to 2%.

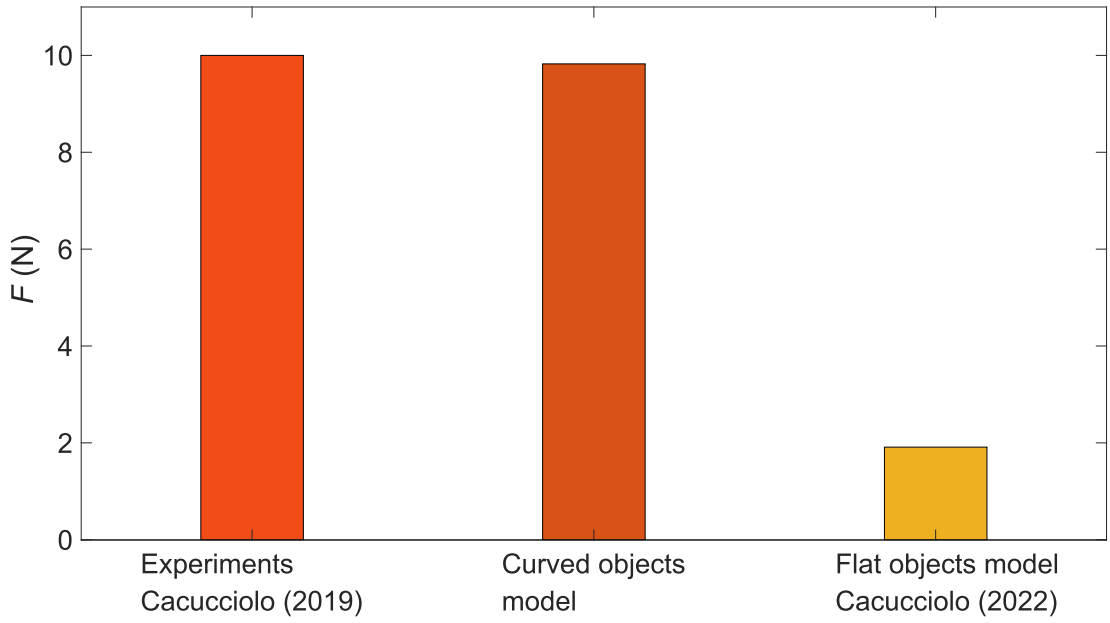

Figure 3.4 – Comparison between experimental data from [29] and model predictions for the maximum holding force of an EA soft gripper grasping curved objects. Our model (eqn. 3.7) shows a strong reduction in the prediction error compared with previous models [4] not accounting for the curvature of the object. Reproduced with permission from Mastrangelo et al. [3].

3.3.2 Experiments on the maximum pulling force of EA tapes wrapping curved surfaces

In this section we report the preliminary results coming from experiments of the detachement force measured by pulling EA tape wrapped on curved objects. We include the details about our set-up and the results of the tests.

3.3.2.1 *Experimental set-up*

The experimental set-up used in our experiments enumerates several components (Figure 3.5a,b). A linear actuator (Igus) is used to provide the pulling force, measured by a load cell (Applied Measurements Ltd) mounted on it. An amplifier receives the signal from the load cell and sends it to the PC by means of an I/O device (National Instruments). Two voltage suppliers feed the load cell amplifier and the linear stage, respectively. An Arduino board connected to the PC controls the actuator with a motor driver (Elprico). Signal coming from the load cell is recorded with a homemade Matlab code.

We conducted three typologies of test. Our set-up has been conceived to be able to perform all the tests with minimal adaptations. Detachment tests of EA tapes are conducted by pulling EA tapes electroadhered on curved substrates (Figure 3.5b and Figure 3.6a). The high voltage is provided by a DC-HVDC (Direct Current to High Voltage Direct Current) converter (XP Power A series), and high-voltage optocouplers (VMI OC 100G) for the AC voltage. The goal of the pulling experiments is to measure the detachment force of EA tapes on curved objects and to compare the results with the model predictions. Since we didn't know the value of the friction coefficient between the tested tapes and the substrates, we adapted the same set-up for the measure of the friction coefficient. We also measured the value of the Maxwell stress by conducting pulling tests in lap-shear configuration. We estimated the value of the Maxwell stress by dividing the measured force by the initial adhesion area and by the friction coefficient previously obtained. By doing so, we avoided simulations to obtain the value of the Maxwell stress. We modified the setup to perform complementary experiments. Lap-shear experiments have been conducted by removing the curved substrates and by directly adhering the tape to the flat substrate (Figure 3.6b). In the case of the friction tests, we pulled a mass coated by PDMS over the flat substrate (Figure 3.6c).

The EA tapes are custom-made rectangular stripes (50 mm-long, 30 mm-wide, 29 μm-thick) made by PDMS (Polydimethylsiloxane, Sylgard 184 produced by Dow Corning, $\varepsilon_{PDMS} = 2.7$) (Figure 3.7a, b). The tape embeds interdigitated electrodes made by carbon loaded PDMS. The electrode width is 0.5 mm, and the pitch between the electrodes is 0.7 mm. The EA surface containing the interdigitated electrodes is 30 mm-long and 20 mm-wide. The electrodes are separated from the substrate by a 70 μm-thick PDMS layer. The tapes are fabricated with the same process described in Section 2.3.1.1: blade casting and curing in the oven at 80 °C of the PDMS backing and the PDMS-carbon composite for the electrodes, followed by laser ablation to shape the electrodes and blade casting and curing of the covering PDMS insulating layer. The volume fraction of the electrodes with respect to the whole tape is small, so we assumed homogeneous material properties equal to that of the PDMS: Young's modulus E = 3.9 MPa [69] and density ρ = 1030 kg/m^3 [70].

We performed adhesion tests on curved objects by pulling EA tapes wrapped around cylindrical substrates (Figure 3.7c). The tested substrates are custom-made 3D-printed PLA (Polylactic Acid) cylindrical objects. We used object of 30, 40, and 50 mm. We coated the substrates only with paper since our goal is to detect the influence of the curved substrate on the tape detachment, compared to the experiments performed in [4] on flat substrates. The object is coated by a 0.1 mm-thick paper layer, bonded to it using a 3M VHB 4910 adhesive (1 mm-thick).

3.3.2.2 *Experimental methods*

We performed pulling tests of EA tapes adhered on curved substrates (Figure 3.6a). The tape is at first laid onto the substrate. Then, the voltage is applied inducing the zipping of the tape onto the substrate, producing adhesion at the interface. After 10 seconds, the pulling starts by moving the linear actuator. We chose a speed of 0.1 mm/s to exclude the influence of dynamical effects on the measured load. Every time the measured force reached the maximum value of around 15 N, we stopped the experiment to preserve the tape. We only applied AC voltage (in the form of a 10 Hz bipolar square wave) to avoid the influence of space charges on the tests [30]. We repeated the test three times for each configuration.

According to eqn. (3.7), being equal other features such as tape characteristics, the detachment force of an EA tape from a curved object depends on: the radius of the object, the electrostatic pressure (Maxwell stress, dependent on the applied voltage) and the wrapping angle. We then repeated the experiments with different radii of the substrate (30, 40, 50 mm), voltages (1500 and 2500 V), and wrapping lengths L (10, 20 and 30 mm) with constant radius, to inspect the influence of these parameters. The choice of the wrapping length values is motivated by the length of the tape (30 mm). We also chose those values since the predicted forces (eqn. 3.7) for smaller radii and higher voltages are well beyond the limit imposed to preserve the tape (never over 15 N). Also, voltage lower than 1.5 kV didn't produce adequate adhesion in our experiments.

We applied the same procedure to perform pulling tests of EA tapes adhered on flat substrates (lap-shear configuration, Figure 3.6b). We performed these tests to obtain the value of the Maxwell stress generated by the EA tape adhered on a paper-covered PLA substrate (Figure 3.6b) rather than by performing simulations. The value of the Maxwell stress is needed to compare the experimental results from pulling tests on curved objects with the force value as expressed by the model (eqn. 3.7). The Maxwell stress is extracted by measuring the peak force and by dividing its value by the initial adhered contact area and the friction coefficient, under the hypothesis of constant Maxwell stress along the adhesion zone. As for pulling tests on curved objects, we applied the voltage for 10 seconds before moving the linear stage. We pulled the tape with a speed of 0.1 mm/s and repeated the test three times.

To obtain the value of friction coefficient between the PDMS tape and paper, we pulled a mass (placed on a support) over a paper-covered flat substrate (Figure 3.6c). The mass support was coated by PDMS to reproduce the conditions of the pulling experiments. Even in this case, the linear speed of the actuator was 0.1 mm/s. The mass was 562 g.

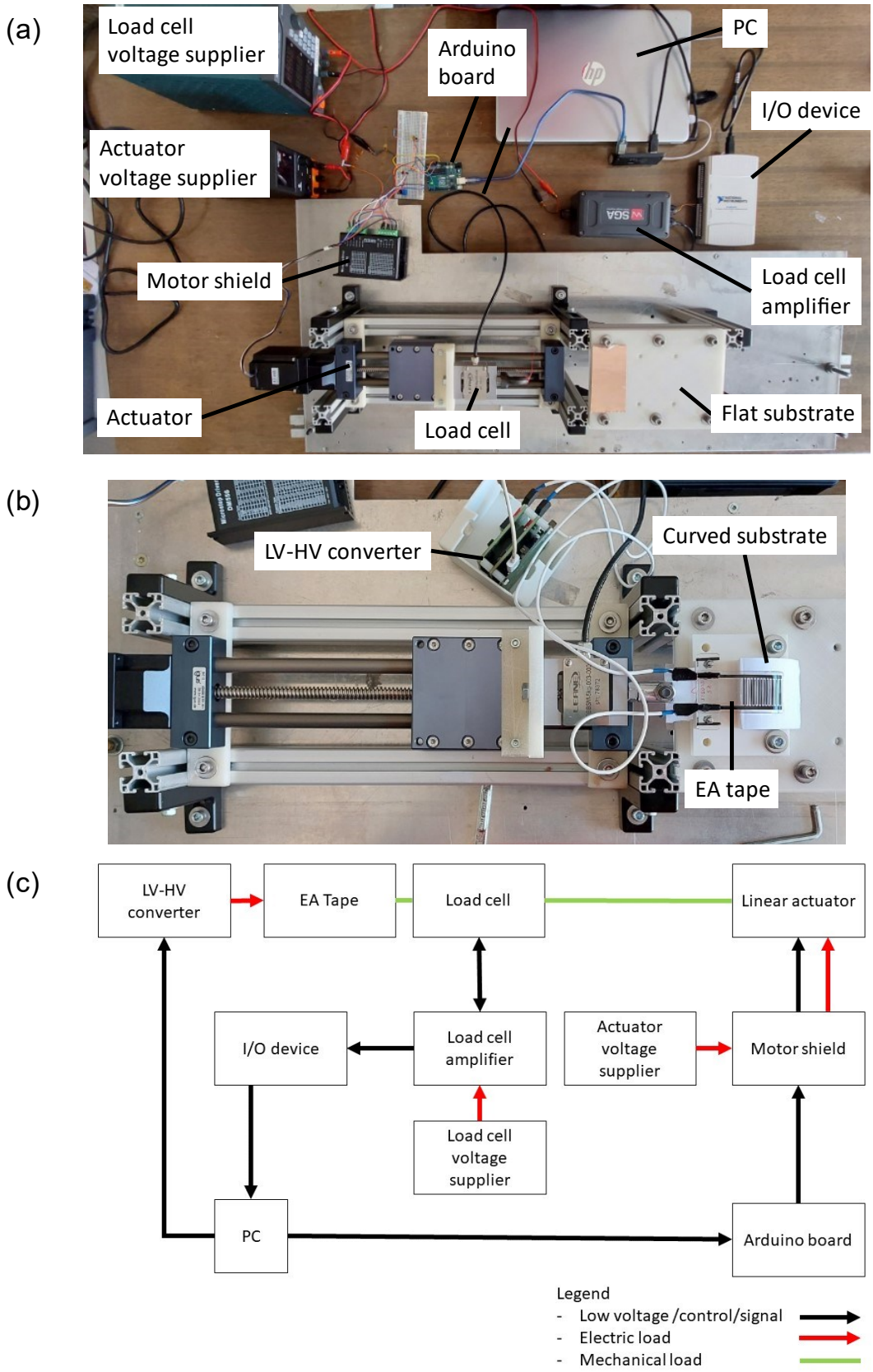

Figure 3.5 – The experimental set-up components. (a) The set-up includes a linear actuator that provides the pulling displacement, controlled by an Arduino board and a motor driver; the force is measured with a load cell: the load cell amplifier sends the force signal to an I/O device. The Arduino board and the load cell are driven with homemade Arduino and MATLAB codes, respectively. Two voltage suppliers provide the supply for the actuator and amplifier. (b) Details of the set-up adapted for pulling test on curved substrate. An additional curved substrate is fixed onto the flat one and a LV-HV converter is utilized to supply the EA tape. (c) Flow diagram of the set-up.

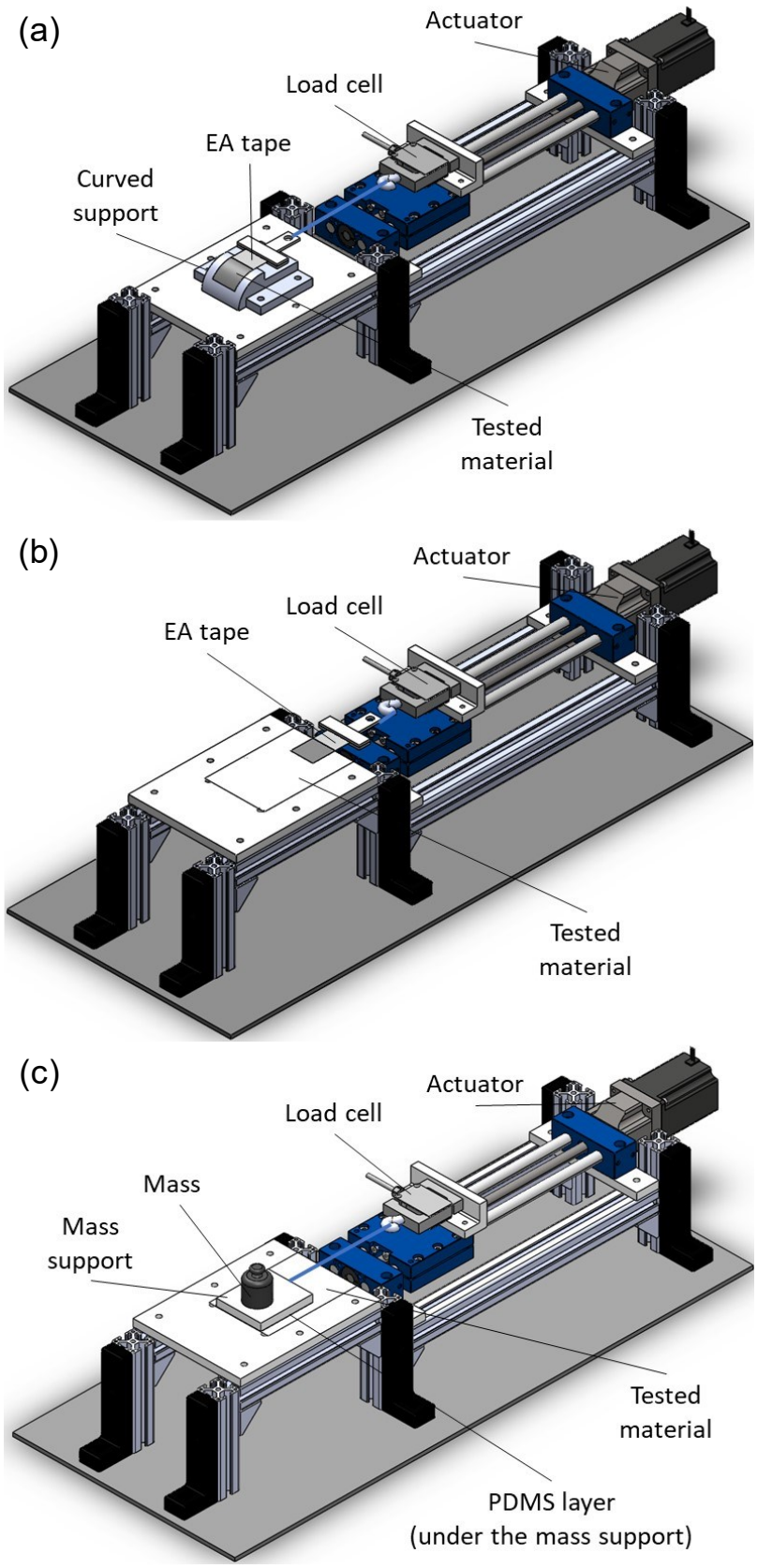

Figure 3.6 – The three configurations of the set-up. (a) Set-up for pulling tests from curved substrates. (b) Set-up for pulling tests in lap-shear configuration. These tests are required to get the value of the Maxwell stress produced by the tape. (c) Set-up for friction tests. A PDMS-coated mass is pulled over a substrate.

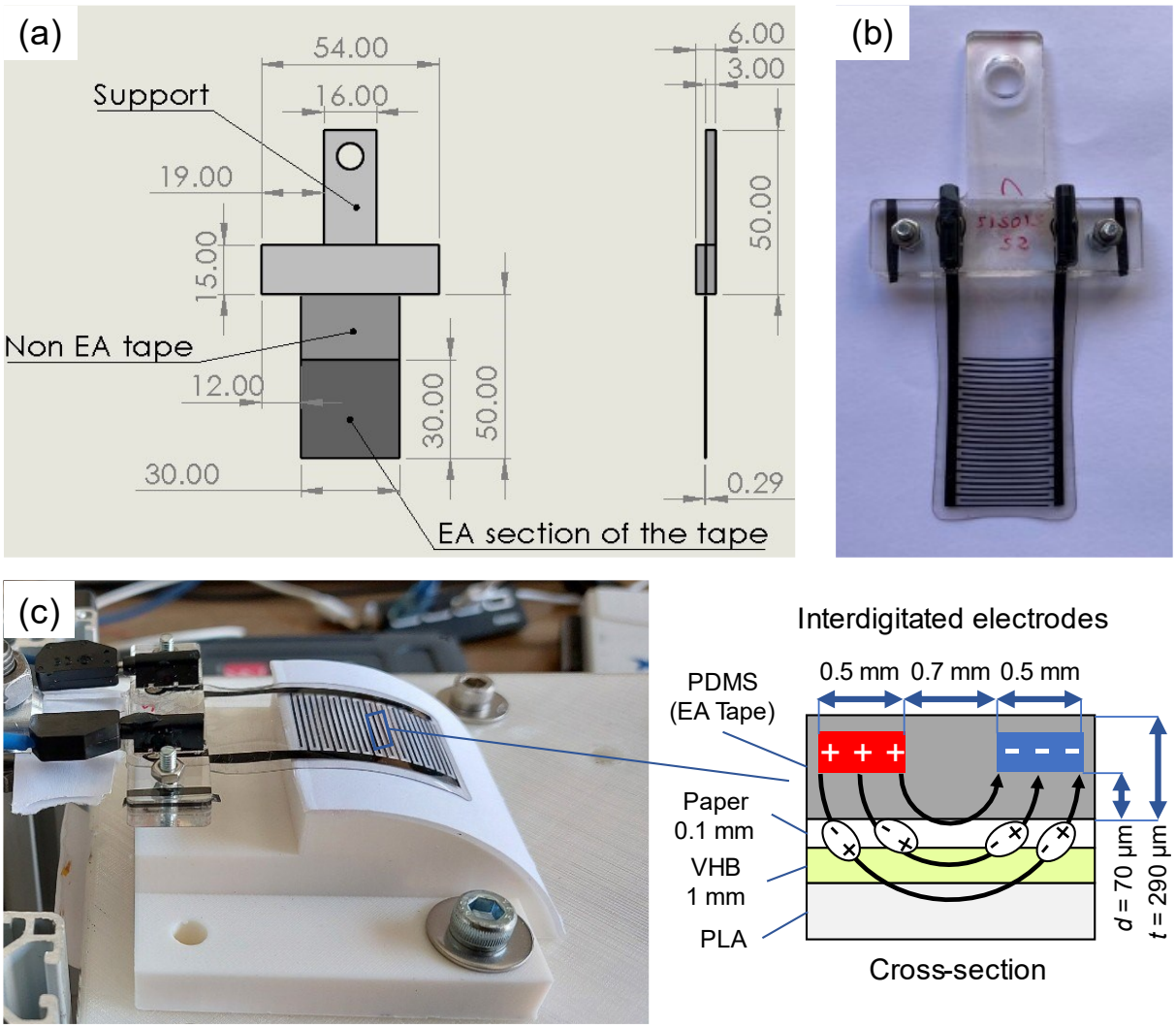

Figure 3.7 – The EA tape utilized in the pulling experiments. (a) Dimensions of the EA tape. (b) Front view of the tape. (c) EA tape wrapped on the curved substrate (radius = 50 mm) before the pulling experiment. The adhesion to the curved substrate is generated by electrostatic effects inducing the deposition of charges in the substrate layer components.

3.3.2.3 *Experimental results*

Figure 3.8a reports the results of the friction test we performed to measure the value of friction coefficient between PDMS Sylgard 184 and paper. We performed the tests with the same specimen. To obtain the value of the friction coefficient from the raw data reported in the picture, we averaged the value of the measured force for each test over time for a specific time interval. The time interval is a window in which the value of the force appears to be stable. Then, we furtherly averaged the results of the tests and divided the global average force for the weight of the pulled mass (562 g). We report a friction coefficient value of 3.19.

Figures 3.8b,c,d report raw data of the pulling force of EA tapes adhered on curved substrates coated with paper. The radius of the substrate was 50, 40 and 30 mm, respectively. Applied voltage was 1500 V, and the length of the initial wrapping zone was 30 mm. Graphs show the dependence of the maximum measured force on the substrate radius. Smaller radius produces an increase in the peak pulling force, being equal the applied voltage and the wrapping length, as expected (eqn. 3.7). We also observed good repeatability of tests of the tests with radius = 50 mm, with decreasing repeatability in the 40- and 30-mm cases.

Figures 3.8e,f show a bar graph comparison between the measured maximum force and model prediction for detachment tests of EA tapes on curved objects. In Figure 3.8e, we compare model predictions and data for different values of the substrate radius (30, 40 and 50 mm). The applied voltage was 1.5 kV, the wrapping length was 30 mm. The substrate was covered by paper. To calculate model prediction, we firstly tested the pulling force of EA tapes on flat surfaces (lap shear configuration). We extracted the value of the averaged maximum force. According to [4], the maximum EA force in lap shear configuration is equal to the EA shear stress times the initial adhesion area. By estimating the Maxwell stress as $p_{EA} = \tau_{EA}/\mu$, with τ_{EA} the EA shear stress and μ the friction coefficient, we calculated the Maxwell stress as $p_{EA} = F_{lap-shear}/\mu A$, with $F_{lap-shear}$ the measured maximum force and A the initial contact area (20 x 30 mm^2) in our case. We then used the calculated p_{EA} and the friction coefficient μ obtained from friction tests (Figure 3.8a) to calculate model predictions (eqn. 3.7) for the maximum force of EA tapes on curved objects. The bar graph shows good agreement between model predictions and measured data.

We repeated the calculation of the Maxwell stress p_{EA} for $V = 2.5$ kV and compared model predictions (eqn. 3.7) with data (raw data not reported). Figure 3.8f compares model predictions and data for different values (10, 20, 30 mm) of the wrapping length. Radius of the object was 50 mm. We stopped tests with wrapping length equal to 30 mm to avoid tape breakage under forces higher than admittable (12 N). Even in this case, data and model predictions show very good agreement.

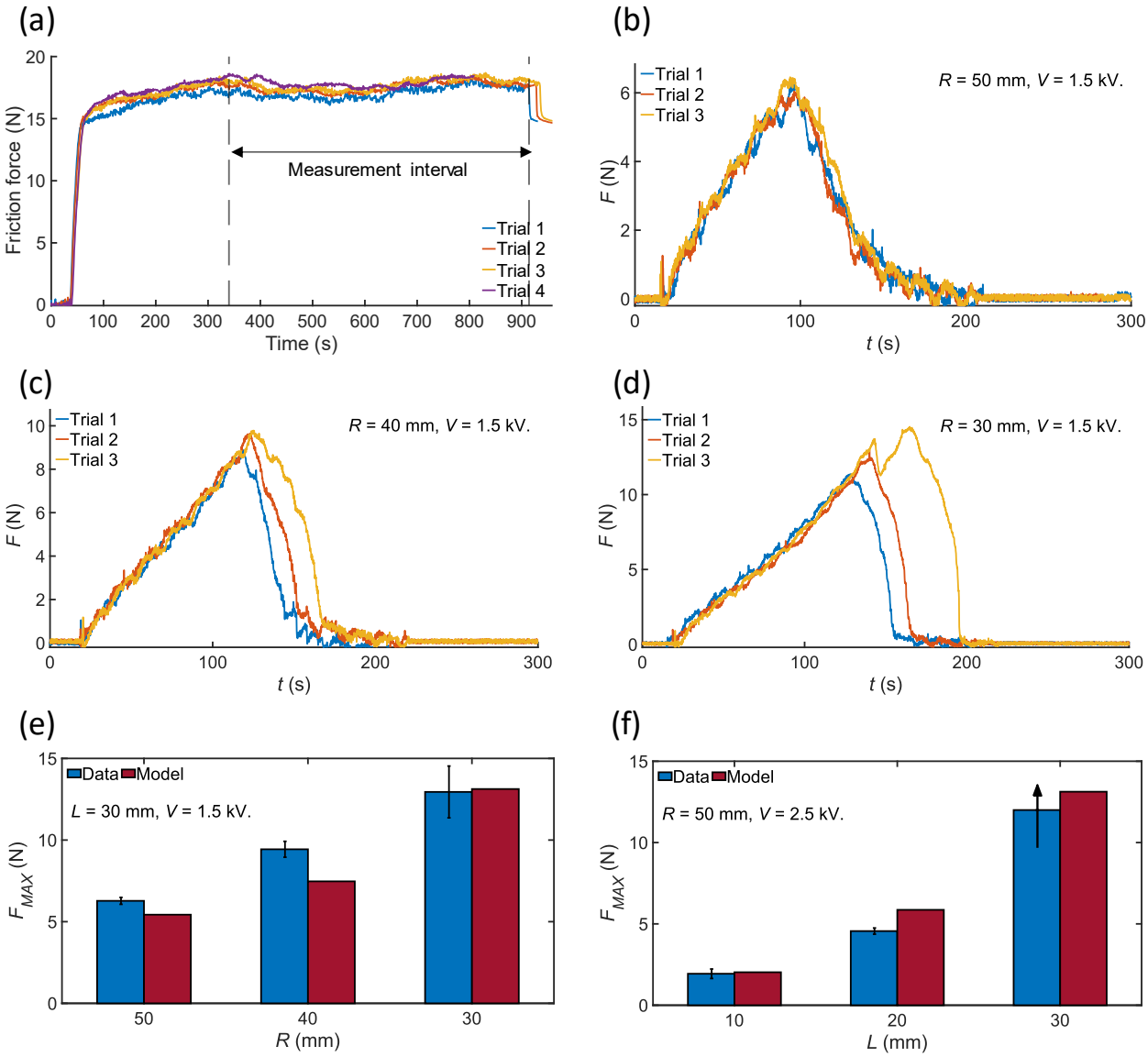

Figure 3.8 – (a) Raw data of PDMS-paper friction tests. We averaged the value of the friction force along an interval in which friction force appeared to be stable, then furtherly averaged the obtained values over the performed trials and divided the resulting average force for the weight of the pulled mass to obtain the friction coefficient. (b,c,d) Raw data of pulling test of EA tape adhered on curved objects. The radius of the object was 50, 40, 30 mm, respectively. The applied voltage was 1.5 kV. (e) Bar graph representing the comparison of measured data vs model predictions (eqn. 3.7) of the maximum pulling force of EA adhered on curved objects, for three (30, 40 and 50 mm) values of the substrate radius. Applied voltage was 1.5 kV. Wrapping length was 30 mm. We calculated model predictions by using the value of the Maxwell stress p_{EA} extracted from pulling tests in lap-shear configuration, and of the friction coefficient obtained from friction tests (a). Data and model show good agreement. (f) Bar graph showing the comparison of measured data vs model predictions (eqn. 3.7) of the maximum pulling force of EA adhered on curved objects, for three (10, 20 and 30 mm) values of the wrapping length. Applied voltage was 2.5 kV. Substrate radius was 50 mm. We reported the maximum force value (12 N) for test with a wrapping length of 30 mm. We decided to not pull the device further to prevent tape breakage. Model predictions capture well the experimental observation.

3.4 Conclusions

This chapter presented the results of our investigation about the role of the geometry of the involved surfaces on electroadhesion force, focusing on EA soft tapes wrapping curved surfaces.

Starting from experimental evidence from previous works, we produced a theoretical model that, accounting for the curvature of the substate, explains the motivation behind the high increments in the holding force observed for EA tapes adhered on curved surfaces compared to the same tapes adhering on flat ones. The model is able improve theoretical prediction and reduce discrepancies between theory and experimental data in literature with respect to models not accounting for the curvature of the substrate (error reduction from 81% to 2%).

We discussed the role of our investigation in the maximum holding force predictions for EA soft grippers grasping curved object. Our model predicts the expected maximum holding force in terms of the geometry of the tape and the curved object, as well as the voltage applied and the friction coefficient between gripper and object. Moreover, by referring to the results presented in Chapter 2, we also show how the zipping behavior of the gripper finger will influence the holding force, depending on the voltage applied.

We also conducted our own preliminary experimental tests to validate the model outcomes. Our preliminary data show good agreement with model predictions. However, further work is needed to fully validate the model.

Our work provides the starting point for a more in-depth study. Our first goal will be to produce a systematic investigation of EA tapes in contact with different substrates, in terms of curvature and surface and material properties.

The results in this Chapter are of high interest for the design of EA soft grippers, clutches, mobile robots that, leveraging the advantages (in terms of output force) coming from curved substrates, will be capable of outstanding the performances of current designs.

4. Electric modulation of hydrogel contact forces

4.1 Introduction

The last chapter of this thesis presents the results of the preliminary work conducted on the topic of the modulation of the friction of hydrogels sliding on an external surface by means of voltage difference applied to it. The final goal of the project would be realizing soft robots implementing hydrogel-made components that would take advantage from the effect. Possible devices that could benefit from modulating friction with electricity could be, for example, soft EA grippers or electrostatic clutches, that leverage friction between contacting surfaces and whose working principle is based on electric effects. Previous works [82–84] have shown that hydrogel friction can be controlled by electricity, by using both electric fields [82,83] or flowing current [84]. According to our hypothesis, the integration of the hydrogel as component of the soft robot, combined with the use of electricity, would enable the on-demand control of friction at the soft robot's interfaces, thanks to the electrical stimuli-responsive behavior of the hydrogel.

A hydrogel is a material composed by a three-dimensional network of hydrophilic polymers (natural or synthetic) solvated with water [85]. In recent years, hydrogels have gained attention in soft robotics thanks to their unique and suitable properties. In contrast to other soft materials, the structure of the hydrogels is composed by both water and polymers. Thus, hydrogels exhibit features of both liquids and solids. Their solid matrix allows them to sustain stress and recover their initial shape after the stimulus is removed. The liquid phase allows diffusion of solutes across the matrix and fluid convection [86].

Current EA soft grippers [4,50] and electrostatic clutches [30,40,87] modify the friction force $F_{friction}$ at the interface by regulating the voltage applied to the device. Normal force N exchanged between contacting surfaces depends on the electrostatic attraction of the charges deposited onto the surfaces in response to applied voltage. Normal attraction increases with the voltage. Being constant the friction coefficient μ at the interface, friction force varies with the normal force according to the Amonton-Coulomb law of dry friction [2]: $F_{friction} = \mu N = \mu\, f(V)$.

In contrast, in a hydrogel-based soft robotic device the friction would be modulated by controlling the properties of the sliding interface. For a generic hydrogel for example, the control could involve the movement of water from or to the interface. Our hypothesis is that the active control of water content at the sliding interface would allow the device to generate completely different contact interactions in a wide range of physical behaviors, going from lubrication to adhesion.

In general, friction of hydrogels exhibits unusual features [86]. For example, gel friction does not obeys Amonton-Coulomb law of dry friction [2], that implies that the friction force is proportional to the normal load applied to the interface. On the contrary, previous works demonstrated that the friction force F is proportional to a power of the normal load. For several hydrogels a decrease of the friction coefficient with the normal load has been observed [88]. Also, hydrogel friction is proportional to a power of the apparent contact area A. By mixing the aforementioned results, hydrogel friction can be expressed with the empirical law $F \propto AP^{a}$, with P the normal pressure (normal load over apparent area) and a a coefficient whose value empirically lies between 0 and 1. Hydrogel friction also depends on the properties of the substrate onto which the hydrogel slides, since the interfacial interaction between the gel and the underlying substrate plays a critical role [89]. The hydrophilicity of the surface on which the hydrogel has been polymerized is also important. When a gel is polymerized on a hydrophobic surface, branched dangling polymer

chains are formed. The presence of polymers chains reduces friction with respect to the same hydrogel with high cross-linking density at the surface. High cross-linking of the chains is instead obtained by polymerization on a hydrophilic surface [90]. Finally, friction of hydrogels strongly depends on the sliding velocity between the surfaces. Gong et al. [91] proposed a model for friction of gels sliding on a smooth substrate. According to their model, gel friction is ruled by the nature of the interaction between the gel and the substrate. If the interaction is repulsive, the polymer network of the gel is repelled from the substrate. In this case, friction force is only attributed to the lubrication due to the presence of water at the interface, and friction becomes proportional to the relative sliding velocity. On the contrary, in the attractive case the effect of the elastic deformation of polymer chains is added to that of water. Elastic contribute comes from the deformation of polymers chains that periodically adhere to and detach from the substrate. With low sliding speeds, contribution coming from viscous friction of water is low with respect to the elastic one, and friction increases with the velocity. With increasing velocity, at first friction decreases since polymer chains do not have enough time to be adsorbed again to the substrate after their detachment, and then increases again since the viscous contribute from lubrication becomes dominant.

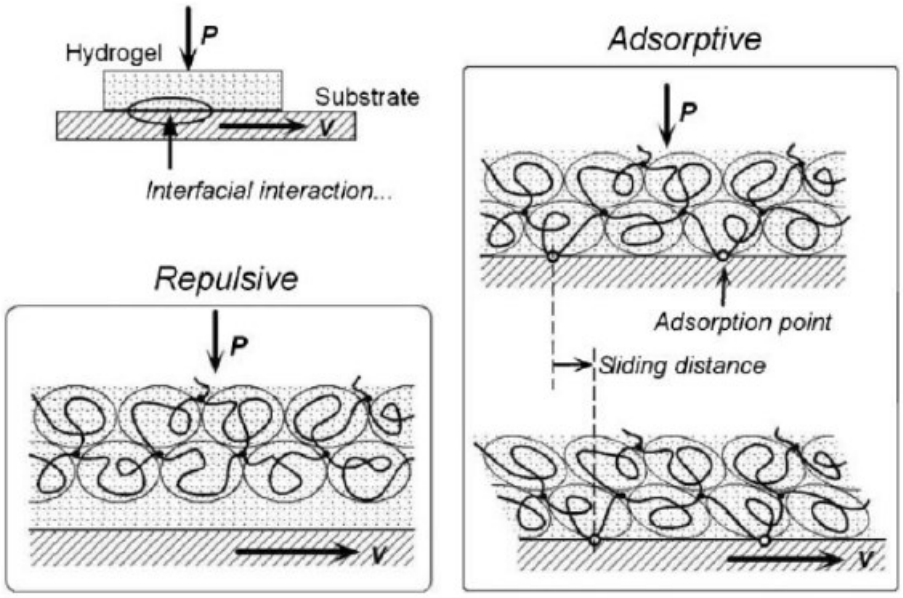

Figure 4.1: friction of hydrogels depends on the nature of the interaction between polymeric chains of the gel and the substrate [86]. If the polymers are repelled from the substrate, friction is only due to the water layer at the interface (lubrication). If the interaction is attractive, polymers adhere to the substrate and friction is due to both lubrication and elastic stretching of adsorbed chains. In the latter case, the prevalence of one of the two effects depends on the sliding velocity (Reproduced with permission from Gong et al. [86]).

Previous works have shown that the adhesion and friction of hydrogels can be controlled by electric effects. The authors from [92] demonstrate the ability to modulate the strength of adhesion between hydrogels. They use external electric fields to control the movement of hydrated ions that act as mediators for achieving adhesion. In [44] hydrogel adhesion programmable with electricity is leveraged to build a climbing robot, and in [93] electroadhesion of hydrogels to animal tissues is demonstrated.

For what concerns hydrogel friction, in [82] the authors tested the frictional response of a charged gel to the application of an external electric field. The gel was placed between two electrodes and connected to a rheometer. The lower electrode was covered by an insulator. When the voltage was applied, functional groups in the hydrogel were attracted toward the charged surface of the insulator and adhered to it. Authors observed increase in friction coefficient up to 10 times with

the voltage going from 0 V up to 70 V, even if with great variance in the response among different samples. The results were in agreement with the predictions of the model for gel friction presented in [91]. Moreover, the effect was reversible, and the initial frictional properties of the gel were recovered when the voltage was removed. In a subsequent work, authors also obtained a reduction in hydrogel friction under the application of voltage [83]. In this work, they added a charged surfactant to the gel. Friction control was reached by moving the surfactant to the sliding interface under the application of the electric field. In both works, authors were unable to measure the friction response under inversed polarity. All the tests were performed with the insulated electrode as the positive pole. With polarity inversion electrolysis of water was observed at the sliding interface that influenced the measure.

Wada et al. [84] were able to obtain control of hydrogel friction under the application of voltages up to 5 V across the gel and with polarity inversion. The authors used a double-network (DN) hydrogel. Friction was measured with a ball-on-disk test. The gel was positioned onto a metal plate (lower electrode) and a metal ball (upper electrode) was moved onto its surface. The gel and the electrodes were not insulated. The authors observed a decrease in friction with the ball connected to the cathode (negative pole), and the opposite behavior when the polarity was inverted. The authors attribute the observed modulation of friction to the movement of water molecules to the anode when the voltage was on. Moreover, above 3.5 V authors observed a variation in the trend, arguably due to electrolysis detected by nonzero measured current across the gel.

However, none of the work conducted on the modulation of hydrogel contact forces with electricity have been never applied to create soft robots. On the contrary, the final goal of the investigation presented in this chapter is to exploit the already demonstrated principle in a practical soft robotics application. Here, we present the preliminary findings of this investigation. The work has been mainly focused on creating a soft robotic gripper finger made by hydrogel. At first, we aimed at replicating the results obtained in previous works. This part of the work included the formulation of the hydrogel recipe, the characterization of the hydrogel, the assembly of a setup for friction tests and the identification of a method for bonding the hydrogel to a surface. Then, we will present the results of the friction tests conducted on the hydrogel. Finally, we will include the results of the preliminary tests conducted on various archaic prototypes of a soft gripper finger and we will highlight the next steps toward the goal of a hydrogel based, friction modulating soft robotic gripper.

4.2 Experimental set-up

This section illustrates the components and the features of the experimental set-up assembled for friction tests of hydrogels. Our goal was to measure the friction force of a hydrogel sliding on a surface. We also wanted to apply voltage to the hydrogel during pulling and investigate the influence of the voltage on the measured friction force.

4.2.1 Components of the experimental set-up

The components of the set-up for friction tests are illustrated in Figure 4.2. The hydrogel (8) is bonded to a mass (6) and slides over a substrate (7). The mass is pulled by a wire (cotton) directly connected to a load cell (Uxcell, 5) mounted on a linear stage (OSMS-26-300ZSGSP, Optosigma, 2). The linear stage controller (SHOT-702, Optosigma, not in the picture) is operated with a dedicated software interface (BIOSControl). The load cell amplifier (HX711, 4) is connected to an Arduino Uno board (3) and operated with a Python GUI interface, similarly to the set-up described in [94].

The set-up measures the friction force between the hydrogel and the substrate. The hydrogel is bonded to the lower surface of the sliding mass. Both this surface and the substrate on which the hydrogel slides vary according to the conducted test, as we will show in the following. In the picture, both the bonding and the sliding surfaces are constituted by an aluminium tape (3M) and connected to a voltage supplier (PMX18-5A, KIKUSUI, 1) that produces the voltage difference between the two electrodes.

4.2.2 Validation of the set-up

We validated the friction set-up before using it for hydrogel friction tests. We assessed the reliability of the friction set-up by testing a material with known friction coefficient. Our choice was the Polytetrafluoroethylene (PTFE), commercially known as Teflon. Literature reports very low friction coefficient for dynamic friction of Teflon sliding on Teflon, usually in the interval 0.05-0.1 [95]. Also, [96] reports that the static coefficient of friction for Teflon on Teflon contact usually lies between 0.1 and 0.16, and that the sliding friction coefficient for a sliding speed of 1 mm/s lies in the range 0.07-0.09.

We performed Teflon on Teflon sliding tests by pulling a mass covered by a 1-mm Teflon layer (1) on a substrate covered with the same material (2) (Figure 4.3). We applied Teflon on acrylic plates by using VHB tape. We performed tests at three different sliding speeds (0.01, 0.1 and 1 mm/s) and repeated the test three times for each sliding speed. Results are reported in Figure 4.4.

Figure 4.4a, c, e reports the measured friction force for sliding speeds of 0.01, 0.1, 1 mm/s, respectively, for three consecutive trials. Friction behavior exhibits a peak force corresponding to the value of the static friction, and a sudden decrease of the measured value corresponding to the transition towards the dynamic friction phase. The relatively slow increase in the measured value before the peak force is due to the tensioning of cotton wire connecting the mass to the load cell, deforming due to the movement of the linear stage until the static friction force is reached. We observe a similar behavior for the three tested speeds, except force the measured static friction force for 1 mm/s of sliding speed, higher than those reported for 0.01 and 0.1 mm/s (0.24 N on average vs 0.19 N for both 0.01 and 0.1 mm/s).

Figure 4.4b, d, f compares the measured friction force coefficient (static and dynamic) with the values reported in literature [95,96]. Dark-colored bars report the value of the dynamic friction coefficient for the three trials conducted. We averaged the dynamic friction force value over the displacement and divided the averaged value by the normal force exerted by the weight of the pulled mass (164 g). Error bars indicate standard deviations of data. Light-colored bars indicate static friction coefficient, obtained by dividing the measured peak force by the normal load.

Horizontal grey and pink bars show the intervals of variability for Teflon friction coefficients as reported by [96] for static friction and by [95] for dynamic friction. Our data are consistent with values reported in literature, so we considered the set-up validated.

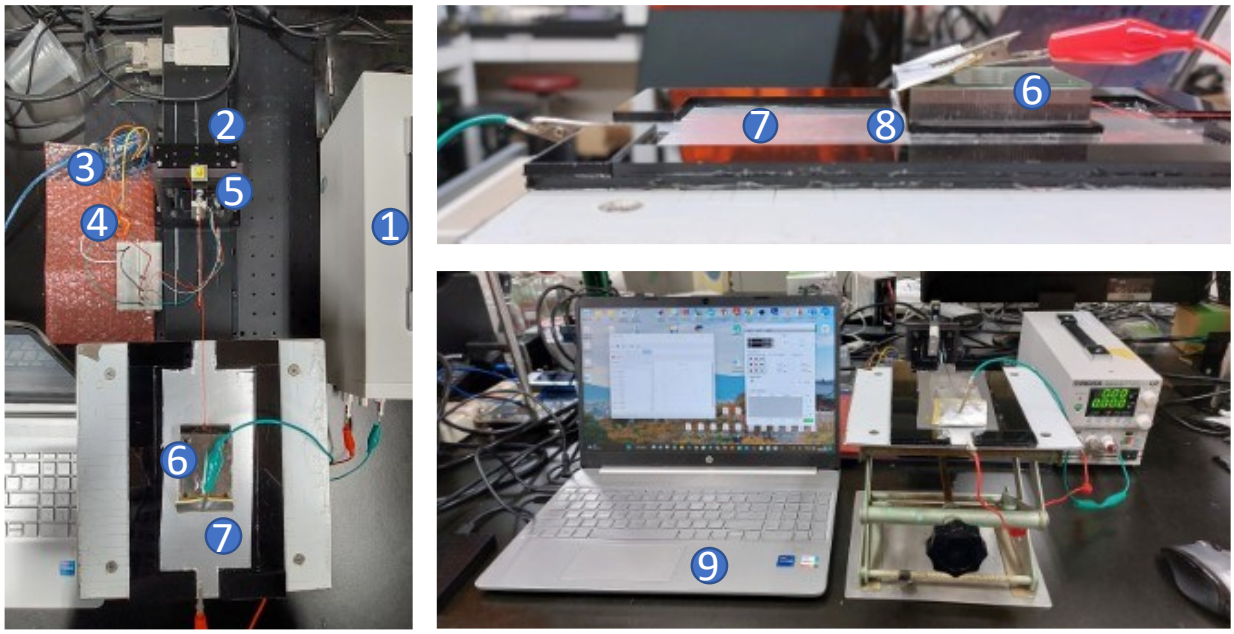

Figure 4.2 Views of the experimental set-up used for friction tests of hydrogels. The set-up is composed by: (1) voltage supplier, (2) linear stage, (3) Arduino board, (4) load cell amplifier, (5) load cell, (6) sliding mass, (7) substrate, (8) hydrogel, (9) pc, and a linear stage controller (not in the picture).

Figure 4.3 The pulled mass (1) and the substrate (2) covered by Teflon to perform validation tests of the friction set-up.

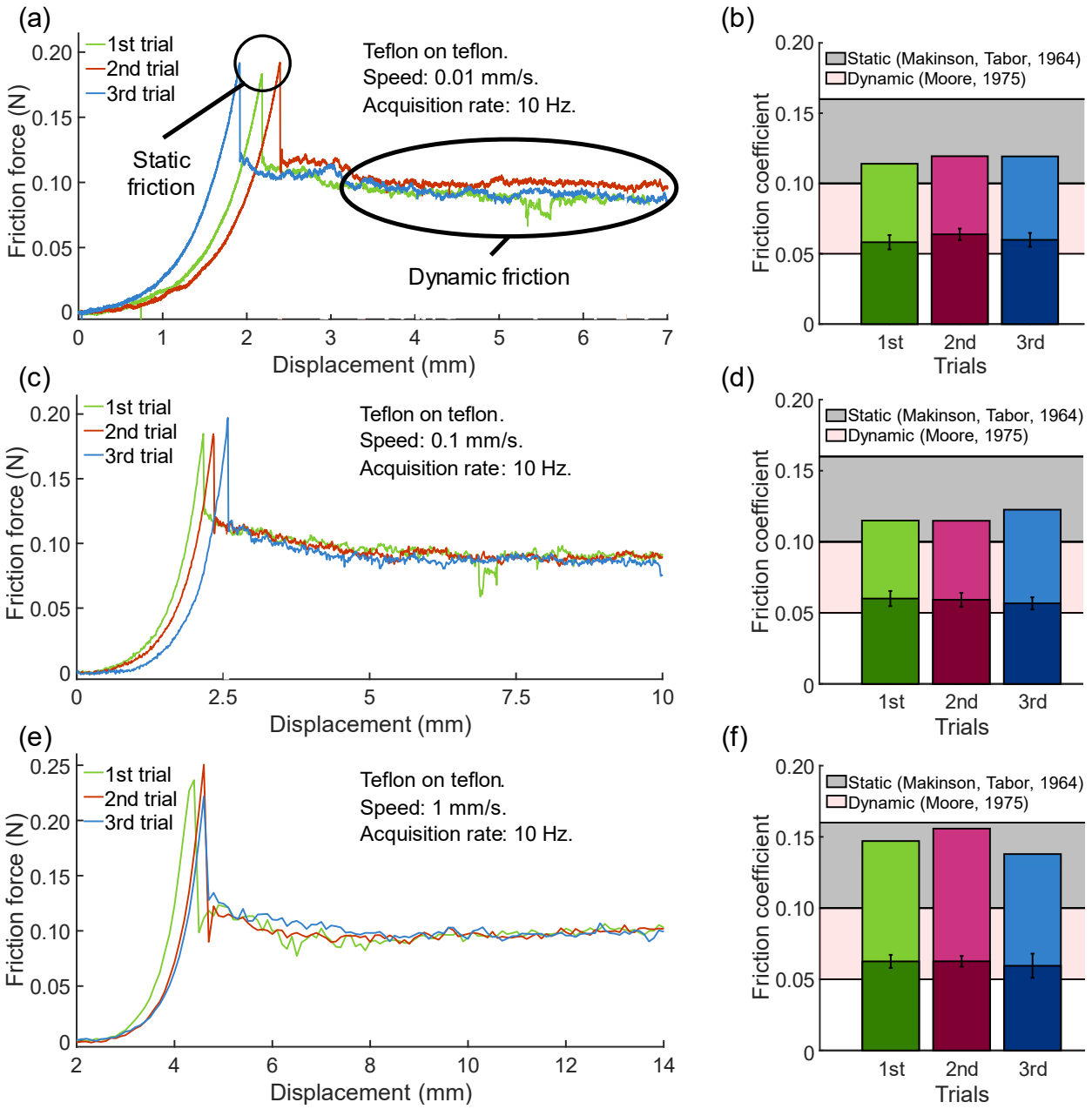

Figure 4.4 The results of the validation test of the set-up for friction characterization. (a, c, e) Friction force as a function of the displacement imposed on the pulled mass for sliding speeds of 0.01, 0.1 and 1 mm/s, respectively. (b, d, f) Comparison of the friction coefficient measured during the experiments with the values reported in [95,96]. The dark-colored bars indicate the value of the measured dynamic friction coefficient: we averaged the value of the friction force measured during the experiments (a) and divided the value by the applied normal force (sliding mass = 164 g). Light-colored bars indicate the value of the static friction coefficient obtained by dividing the peaks of the friction force (a) by the normal force. Horizontal grey and pink bars graphically indicates the values of the static and dynamic friction coefficient intervals as reported by [96] and [95], respectively. Measured data are consistent with literature.

4.3 Hydrogel fabrication and characterization

This section contains information about the fabrication process of the hydrogels tested in friction experiments. We report: the fabrication recipes and methods we followed to fabricate hydrogel specimens and characterization of hydrogel water retention capabilities.

4.3.1 Hydrogel fabrication

We decided to perform friction tests on simple polyacrylamide hydrogels to test the validity of our hypotheses. We hypothesized that applying voltage to the gel would have caused the movement of water inside the gel, and that this effect alone could have influenced the friction force.

The Polyacrylamide (PAAm) is a highly water-absorbent polymer ($-CH_2CHCONH_2-$). When hydrated, PAAm is easily solvated and forms a hydrogel [97]. The subunit of the PAAm macromolecule is the acrylamide (AAm) ($CH_2=CHC(O)NH_2$). Other chemical species can be included into the hydrogel composition to obtain different chemical and physical features. In this case, we decided to only include AAm in the composition (apart from the crosslinker and the initiator, whose roles will be explained in the following), obtaining a nonionic (neutral) PAAm hydrogel [98]. This allowed to keep the fabrication method easy and fast. Moreover, as already discussed in the Introduction, the sliding friction of a hydrogel can be modulated by applying a voltage difference to the gel. According to our hypothesis, the modulation of the hydrogel friction could be reached by controlling the amount of water at the sliding interface. Molecules of water would move from or towards the sliding surface in response to the applied voltage, even without the involvement of other chemical species.

4.3.1.1 Recipes formulation

Hydrogel fabrication requires the polymerization of the monomer molecules and the solvation of water to the polymeric chains. Usually, the process of fabrication of PAAm hydrogels involves the free radical crosslinking copolymerization of acrylamide with *N,N'* – Methylenebisacrylamide (MBAA) [99]. The MBAA has the role of crosslinker among polymer chains. Cross linking stabilize the mutual position of polymeric chains and affects hydrogel properties as elasticity, strength and solubility [100]. Free-radical polymerization is a polymerization method in which a polymeric chain is created by concatenating free-radical units. A specific molecule, called initiator, produces free radicals by decomposition. The high chemical reactivity of radicals let them link to the monomer molecules and create the polymeric chain. According to the polymerization method, different types of initiators can be used. We fabricated and tested hydrogels made with both photo- and thermopolymerization. In the first case, the molecules of the initiator are broken down by photons [101]. In the second case, the decomposition of the molecules is obtained by heating them. Accordingly, we chosen two different types of initiators. We used α-ketoglutaric acid as photo initiator and 2,2'-Azobis(isobutyronitrile) (AIBN) as thermo initiator. Moreover, we also fabricated a third typology of PAAm hydrogel, whose polymerization can be triggered by both light and heat. The initiator in this case was 2,2'-Azobis(2-methylpropionamidine) dihydrochloride, also known as V50. The recipes of the fabricated hydrogels, reporting the ingredients and their quantities, are included in Table 4.1.

Recipe	Monomer	Crosslinker	Initiator	Solvent	Polymerization method
1	AAm, 14.627 g	MBAA, 0.3728 g	α-keto, 0.304 g	Pure water, 75.15 ml	Photopolymerization
2	AAm, 12.651 g	MBAA, 0.3234 g	AIBN, 0.296 g	Pure water, 65 ml	Thermopolymerization
3	AAm, 12.861 g	MBAA, 0.1132 g	V50, 0.246 g	Pure water, 65 ml	Photopolymerization or thermopolymerization

Table 4.1 – The recipes of the fabricated hydrogels. Although the AAm has been used as the main component for all the recipes, different initiators have been used according to the chosen polymerization process.

4.3.1.2 Fabrication process

The fabrication process of the hydrogels in Table 4.1 started with the preparation of the monomeric solution. AAm monomer, crosslinker and initiator were dissolved into pure water. The solution was then stirred for at least 30 minutes to obtain dissolution of the solutes into water. The solution was then inserted with a tuberculin into a homemade mold formed by two glass plates (74 x 55 mm^2) divided by a 1-mm thick rubber frame.

Hydrogel photopolymerization (recipes 1 and 3, Table 4.1) was then attained by placing the samples into an ultraviolet curer for 12 minutes. Thermopolymerization (recipes 2 and 3, Table 4.1) was attained by heating the samples in an oven at 60° (recipe 2) or 56° (recipe 3) for 8-12 hours.

4.3.2 Improvement of water retention capabilities of hydrogel

As discussed in the Introduction, the goal of the work presented in this chapter would be the fabrication of a soft robotic device containing hydrogel. One of the obstacles along the way is the inability of the hydrogel to retain its water content for a long operation time [85,102]. Water loss causes the hydrogel to shrink and deform. Conversely, high water retention capabilities allow the hydrogel not only to retain its shape, but also its friction modulation capabilities over time when voltage is applied. Current methods to prevent water loss can include, for example, the encapsulation of the hydrogel between coating layers to physically prevent the dehydration of the gel [103]. Alternatively, improved water retention capabilities have been demonstrated by introducing highly hydratable salts into the monomeric solution of the hydrogel [104]. Salts in hydrogels are used for various applications. For example they are the conductive medium in ionotronics applications [103,105]. When it is utilized for water retention purposes, the dissolved salt ionizes into water and the ions hydrate with water molecules, preventing their evaporation. We aimed at obtaining water retention improvement by including salt in the hydrogel. Here we report the experimental methods and the results of the tests.

4.3.2.1 Method for water retention improvement

We decided to perform water retention tests on PAAm hydrogel (recipe 1, Table 4.1) with different concentrations of LiCl. Authors from [104] reported that LiCl had the best water retention capabilities among the tested salts. Rather than inserting the salt into the monomer solution as done in [104], we followed a different procedure. We prepared circular samples of already polymerized hydrogel (42 mm diameter x 1 mm thickness), and we dipped them into water solutions of LiCl at

different concentrations. Then, we left the hydrogels into the LiCl solution for at least 12 h to reach osmotic equilibrium. We prepared hydrogels samples dipped into LiCl chloride solutions at 0%, 3%, 6%, 12% LiCl concentrations. We prepared 3 samples for each LiCl concentration.

We then placed the samples over a plastic substrate and recorded the evaporation process of water with a camera. Before the test, we cleaned up the samples with drying paper to remove water excess and measured the weight of each sample. We repeated the measurement at the end of the test to determine the water loss of the samples.

4.3.2.2 Results of water retention tests

Results of the weight measurements are reported in Figure 4.5. The weights of the hydrogels are reported as averages (with standard deviations) over the three tested samples. We measured hydrogel mass at the beginning and at the end (after 22 h) of the water retention experiment. Hydrogel mass increases with the LiCl concentration. Samples weight increases with LiCl concentration at the beginning of the experiment. Moreover, increasing LiCl concentration positively influences water retention capabilities. We defined the quantity "mass loss" *m.l.* as the relative mass loss of the gel during the process:

$$m.l. = -(\text{mass}_{\text{end}} - \text{mass}_{\text{start}}) / \text{mass}_{\text{start}} \qquad (4.1)$$

Table 4.2 summarizes the results of the mass loss of the samples. We observed an increased mass loss with lower concentrations of LiCl in the gel. With 12% LiCl, samples exhibited even negative mass loss, indicating that the hydrogels adsorbed water from the environment. This behavior is not surprising and has been already reported for high salt concentrations [104].

Figure 4.6 shows the timelapse of the water retention experiment. We captured the hydrogel samples at different times during the experiments. Samples that were dipped into LiCl 12% solution exhibited no shrinking or shape variations. Conversely, water loss in the samples with less LiCl showed size reduction. 0% LiCl hydrogels showed a dramatic decrease in diameter and even out-of-plane bending.

In conclusion, we demonstrated water retention improvement of hydrogels by dipping them into LiCl water solutions. Water retention is a critical feature for hydrogels in soft robotics, and the result demonstrate that it can be improved without physical modifications of the devices. Further steps of our works will include the investigation of the effect of the ions of LiCl on the behavior of the gel when a voltage is applied to it.

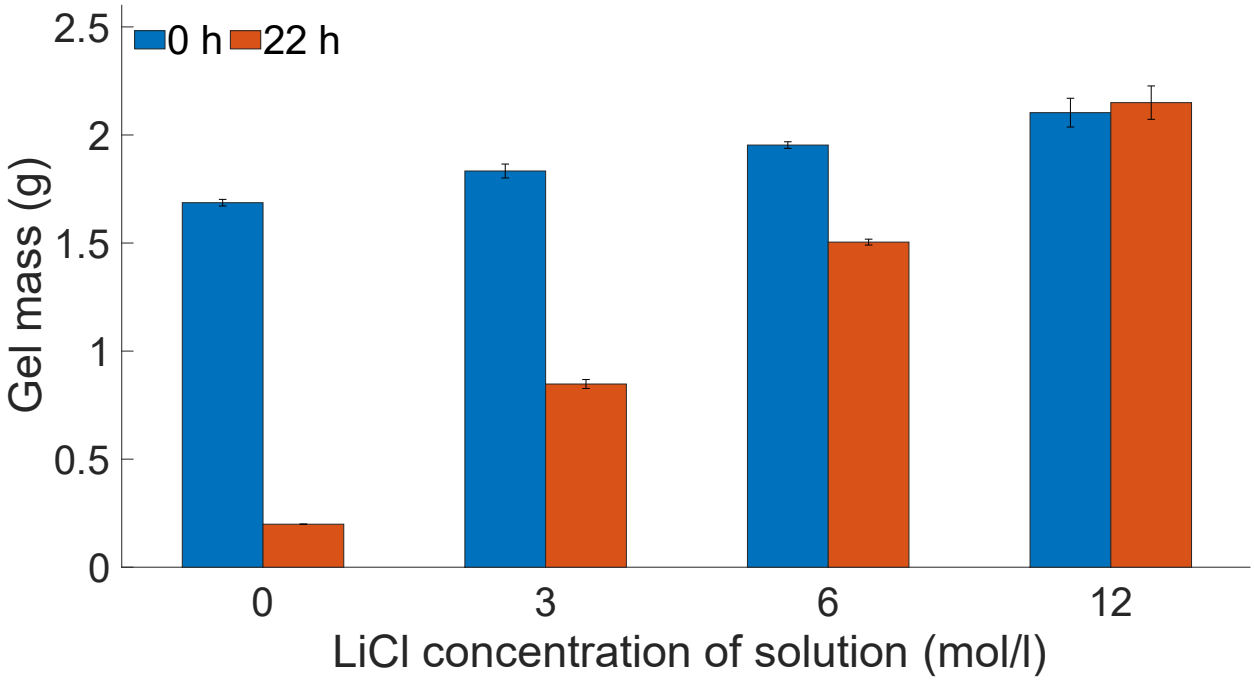

Figure 4.5 – Results of hydrogel mass measurements before and after water retention tests, for hydrogel dipped in different LiCl concentration solutions. The weight of the hydrogel increases with the concentration of LiCl in the solution. We observed an increase in water retention capabilities with the salt concentration. After 22 h, hydrogel with 12% LiCl even exhibited an increase in their mass, since water contained in air humidity was absorbed by the gel. Other gels exhibited water loss decreasing with LiCl concentration.

Solution LiCl concentration	12%	6%	3%	0%
Mass loss	-2.20 %	22.99 %	53.76 %	88.20 %

Table 4.2 – Mass loss (eqn. 4.1) of hydrogel samples reported as a function of the LiCl concentration.

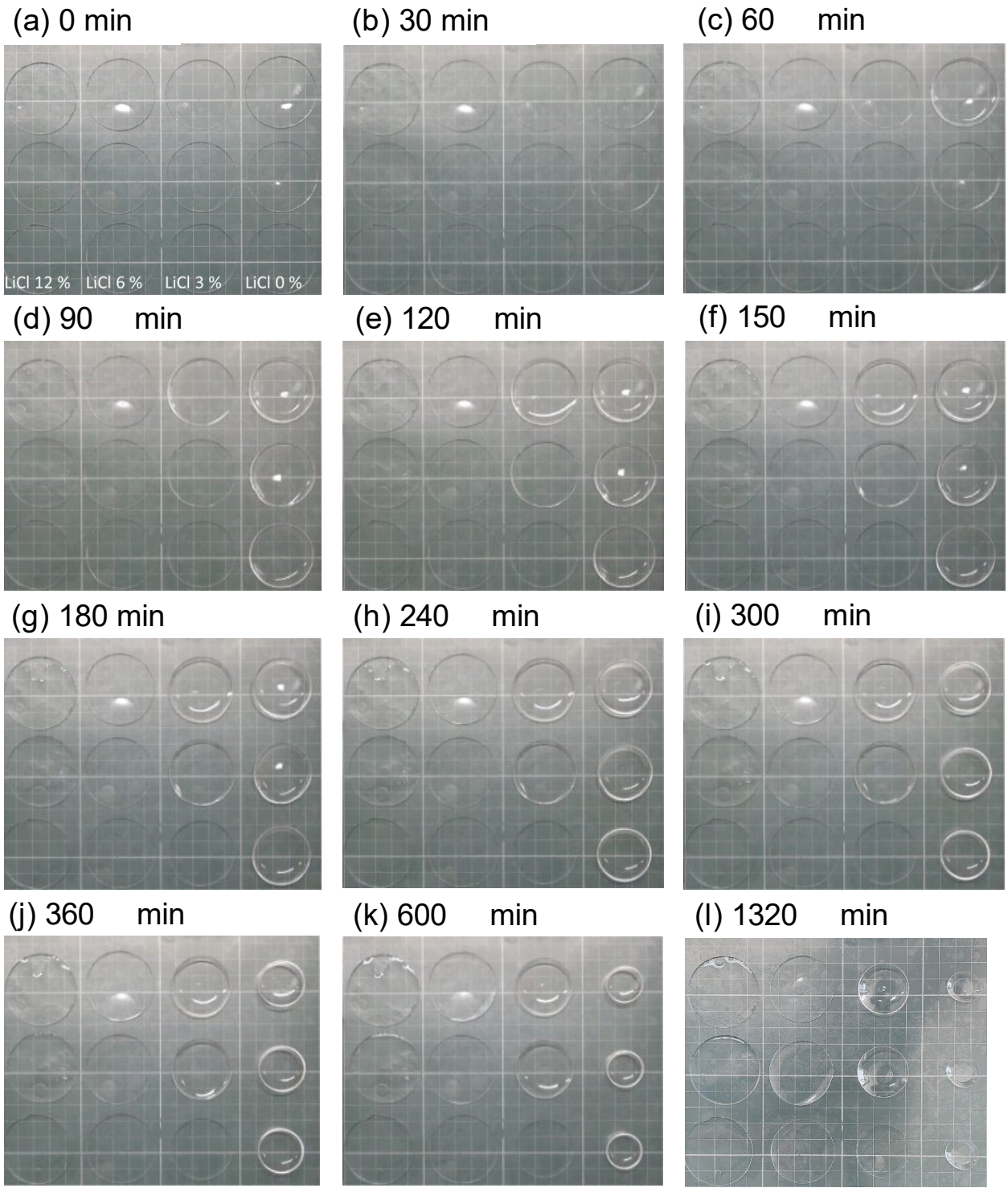

Figure 4.6 – Timelapse of the water retention test experiment. 12% LiCl gels exhibits no variation in their shape or size. Increasingly marked deformations (shrinking and bending) are observed for samples with lower salt content.

4.4 Bonding of hydrogel to solid surfaces

Testing hydrogel friction with the set-up described in Section 4.2 required reliable bonding of the hydrogel to the pulled mass. Hydrogel bonding to surfaces is in general a complex task, due to high content of water that hinders adhesion of polymeric chains to the target surface [106]. Water in the hydrogel is in the liquid state. Even if the external materials bonds to a layer of water molecules, adhesion forces are weakly transmitted to the other molecules of water or to the polymeric chains. Strong bonding between hydrogel and external materials then can be obtained if the polymeric chains forming the hydrogel network are involved and bond to the external surface.

Strong hydrogel adhesion (adhesion energy > 1000 J m^{-2}) has been reported for the first time in [107]. The novelty of this work consists in the use of silanes. Silanes are a type of adhesion promoters. They act at the interface between two dissimilar adherends to stimulate adhesion [108]. When dissolved in water, silane is subject to hydrolysis and forms silanol groups (Si-O-H). If the surface of the solid adherend has been pre-treated (for example, by oxygen plasma to add hydroxyl groups -OH on it), the silane links to the surface and works as attachment for the polymeric chains of the hydrogel.

We performed hydrogel bonding to various substrates by silane-based surface adhesion. We tested different methods and qualitatively determine the goodness of each procedure. We improved the method by subsequent tests on different hydrogels, surface treatments, curing methods. Here we report the results of our investigation.

4.4.1 Materials and Methods

We performed bonding tests of hydrogels fabricated according to the recipes and fabrication methods presented in Table 4.1. The aim of our investigation is to test the friction behavior of hydrogel under an applied voltage in different conditions. So, the target adherend surfaces in our bonding experiments were aluminium (conductor) and Kapton (insulator). We tested different methods and checked which one produced the best qualitative outputs.

In a preliminary investigation, we tried to adhere prefabricated hydrogel over an acrylic plate covered by aluminium tape. The aluminium cover had been manually cleaned with ethanol and pretreated with oxygen plasma (for 3 minutes) to bond silane molecules to the surface. We then dipped the plate into a water-silane solution (2:1 volume proportion) for 30 minutes or 12 hours according to the experiment. Finally, we manually applied the preformed hydrogel (1 mm thick) over the aluminium surface. We tested both hydrogel with and without water retention improvement treatment. Moreover, in some cases also the hydrogel had been dipped into the silane coupler solution.

In subsequent investigations, we only tested bonding of the hydrogel precursor (the solution of water, monomer, cross-linker, and initiator). We aimed at obtaining hydrogel bonding during its polymerization. We expected that during hydrogel gelation the silane on the surface would have grafted the PAAm polymeric chains [106]. The resulting adhesion force was expected to be stronger than that obtained by bonding an already polymerized gel. As in the preliminary tests with preformed gels, the adherend surface was cleaned with ethanol and treated with plasma oxygen for 3 minutes. In a first set of experiments, the surface was dipped into a water – silane solution (2:1 volume proportion) for times variable from 30 minutes to 12 hours. In a second set of experiments, the water in the silane solution was substituted with ethanol and dipping time was 30 minutes. The plate was then retrieved from the ethanol – silane solution and heated in an oven for 1 hour at 50°. The plate was then covered with a mold in which the hydrogel precursor was cured, according to one of the processes described in Table 4.1. The mold was composed by a rubber

frame inserted between a glass plate or a PET sheet and the bonding surface. At the end of the curing time, the hydrogel was removed from the mold and the bonding was qualitatively tested.

4.4.2 Experimental results

Figure 4.7 reports some of the results from bonding tests. Figures 4.7a, b show a water droplet on an aluminium-covered plate before and after an oxygen plasma treatment for 3 minutes. Oxygen plasma increases the wettability of the surface by promoting the creation of hydroxyl groups on the treated surface. The change in wettability is reflected by the different contact angle produced by the droplet on the same surface: around 90° in case (a) and nearly 0° in case (b).

Figures 4.7c, d show the results of preliminary bonding tests conducted on preformed hydrogels (recipe 1, Table 4.1). In both cases, we tested bonding between hydrogel and aluminium. Aluminum surface had been cleaned with ethanol, treated with oxygen plasma, and dipped into the water-silane solution (2:1 volume ratio). In (c), dipping time was 30 minutes. In (d), it was 12 hours. Moreover, in the second case the hydrogel had been dipped into the silane solution before bonding. We let the hydrogel dry to test the goodness of the bonding under bending stresses generated by water loss (Section 4.3). Figures show that in both cases hydrogel bonding was incomplete and insufficient. We repeated the tests with hydrogels treated with water retention improvement method (Section 4.3) and at least three times for each parameter combination, but all the tests exhibited unsuccessful bonding. Unreliable bonding of preformed hydrogel was not so unexpected since the polymeric chains in the hydrogel are already formed and their bonding to silane molecules is limited in this case [106]. We concluded that bonding of already formed gels does not produce good results and went on with different methods.

We then performed bonding tests of hydrogel precursor, as discussed in Section 4.4.1. After pretreatment based on cleaning up with ethanol, oxygen plasma, and silane solution dipping, the adherend surface was included into the hydrogel mold, also composed by a glass plate (or PET sheet) and a rubber frame. The hydrogel was then cured and removed from the mold. Figure 4.7e shows the cured hydrogel incapsulated into its mold. The adherend surface was aluminium in this case and the cover was a PET sheet.

Figure 4.7f shows the outcome of one of the bonding tests performed of the hydrogel precursor (recipe 2, Table 4.1) on aluminium. The mold included a glass tape in this case and the aluminium surface had been dipped into a water – silane solution for 12 hours. Qualitatively, the bonding method seemed successful and reliable. We performed various tests, changing dipping time (from 30 minutes to 12 hours), the silane solution composition (ethanol or water as solvent, same 2:1 solvent:solute proportion), the mold (glass plate vs. PET sheet), and the adherend surface (aluminium, Kapton, or mixed). We also tested the effect of heating the silane – treated surface for 1 hour at 50° to ease the elimination of superfluous solute from the adherend surface before the curing.

We found that hydrogel prepared according to recipe 3 (Table 4.1), cured over a surface dipped into an ethanol – silane solution produced the best outcomes in terms of bonding outcome and repeatability of the process, being equal other parameters. Moreover, the use of PET sheets as mold components eased the detachment of the hydrogel from the mold. One should keep in mind that the polymerization surface affect the frictional properties of the hydrogel [86]. Furtherly, we observed that in general using water instead of ethanol as solvent for silane prolongs needed dipping time (up to 12 hours vs up to 30 minutes), and both photo and thermopolymerization worked produced good bonding outcomes. As we will show in the following Sections, however, bonding failed in some friction tests. The origin of these failures is still not clarified and further investigations are required.

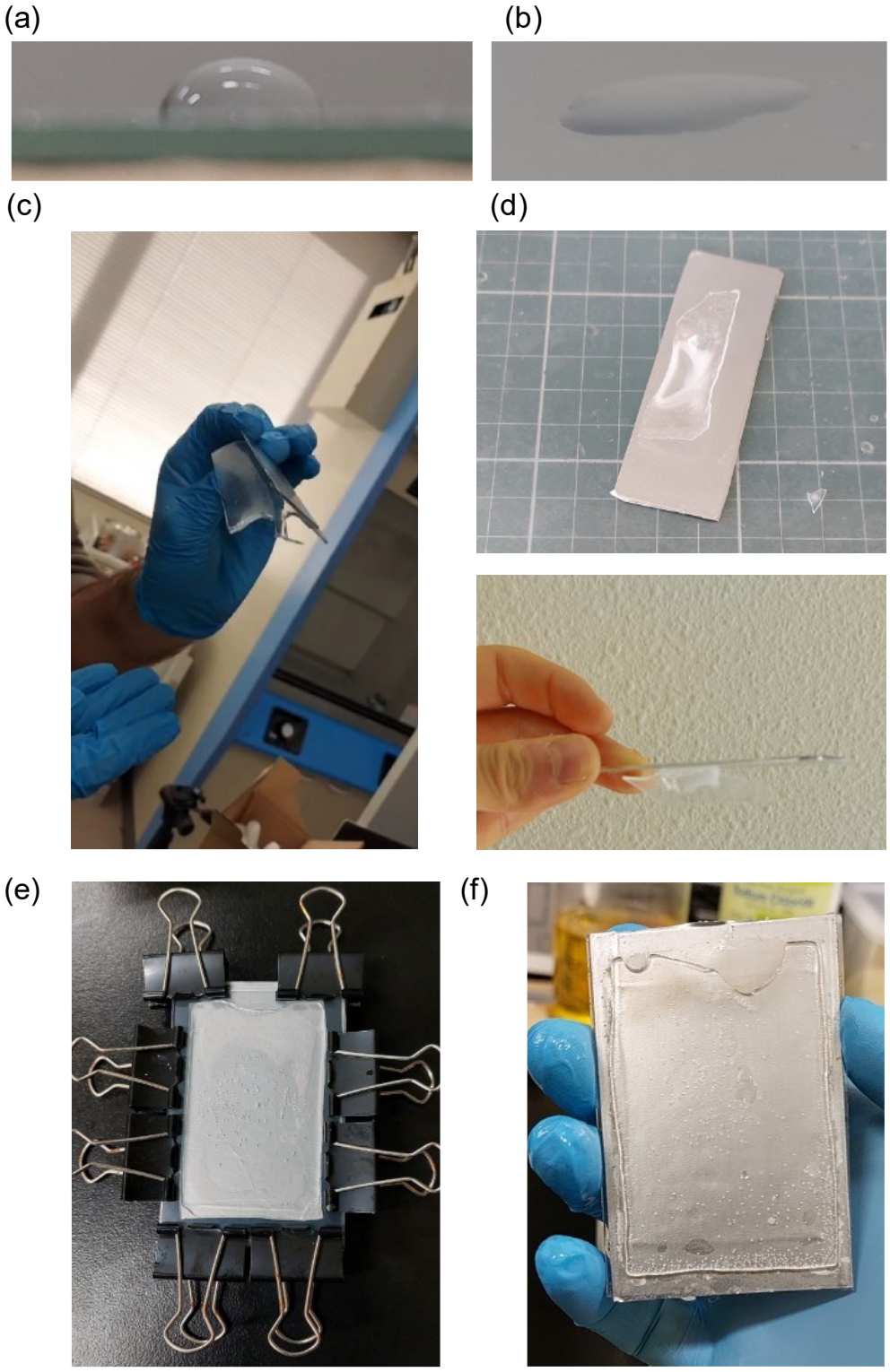

Figure 4.7 – A water droplet on the adherend surface of an aluminium-covered plate before (a) and after (b) the oxygen plasma treatment. Oxygen plasma promotes the wettability of the surface. (c, d) Results of preliminary bonding tests with preformed hydrogels: (c) hydrogel (recipe 1, Table 4.1) manually bonded on silane-treated aluminium: partial and ineffective bonding; (d) both hydrogel (recipe 1, Table 4.1) and aluminium plate were dipped into silane solution before manual bonding: partial and not reliable bonding. (e) curing mold for hydrogel. The hydrogel precursor is inserted into a mold formed by a silane-treated surface (aluminium in this case) and glass plate (or PET in other experiments) separated by a rubber frame. The hydrogel is then cured according to one of the processes described in Table 4.1. (f) Successful bonding on a hydrogel onto an aluminium substrate. The aluminium was pretreated with oxygen plasma and inserted into a water-silane solution. The hydrogel was then thermopolymerized in the mold showed in Figure 4.7 (a glass plate was used for the mold).

4.5 Friction tests of hydrogel

This section reports the results of the friction tests performed on PAAm described in Section 4.3. Our goal was to investigate the modulation of the sliding friction force of hydrogels under the application of an external voltage. Here we present the outcomes of our first exploratory study. The results reported, although preliminary, offer important indications that help in the understanding of the phenomenon and offer valuable hints towards its implementation into a soft robotic system.

4.5.1 Materials and Methods

We performed friction tests on hydrogel with the set-up described in Section 4.2. In each experiment, we pulled an object (160 g, 10 x 40 x 50 mm^3) over a flat and planar substrate. The pulled object was a metal parallelepiped whose lower surface was coated by a bonding layer onto which the hydrogel was bonded (Figure 4.8a). The object was manually attached to the load cell (Figure 4.2) with a cotton wire. The sliding speed imposed by the linear stage was 0.1 mm/s in all the experiments, to minimize the influence of dynamic effects on the measurements. The voltage was applied to the hydrogel by connecting the bonding surface and the substrate to a DC voltage supplier (Section 4.2).

We prepared hydrogel specimens according to the fabrication process described in Section 4.3. The specimen was bonded to the lower surface of the pulled mass by the bonding methods for hydrogel precursors described in Section 4.4. We performed different experiments by changing the nature of the substrate and of the bonding surface. In a first set of experiments, the hydrogel was bonded to aluminium tape, that was also used as lower electrode (Figure 4.8b, and Figure 4.9a, b). By doing so, we replicated the configuration of [84], in which voltage was applied to the hydrogel by electrodes in direct contact with the hydrogel surface. We further tested two configurations in which one of the electrodes was covered by insulator. We manually covered aluminium tape with Kapton tape (30 μm thick) in these configurations (Figure 4.8c). Figure 4.8c,1 and Figure 4.9c show the first configuration: the upper electrode is covered by the insulator, and the hydrogel is bonded to the insulator. The lower electrode is uncovered, and the hydrogel slides over it. In the second configuration (Figure 4.8c,2 and Figure 4.9d) the hydrogel is bonded to the upper electrode. The lower electrode is covered by Kapton, and the hydrogel slides over it.

4.5.2 Experimental results

Figure 4.10a shows the result of one of the friction tests performed over a hydrogel specimen (recipe 2, Table 4.1) in the conductor-conductor configuration (Figure 4.8b and Figure 4.9a). The hydrogel had been cured on a pretreated aluminium surface (see Section 4.4) with a PET sheet mold. We applied 10 V across the hydrogel in this experiment. Upper electrode was the positive one. The application of the voltage is indicated by colored bars. Although the friction force profile appears to be generically irregular, the effect of voltage application is clearly visible. In this configuration, voltage produces a drop (1-2 N) in the measured friction force. The results are in accordance with [84]. We attribute the drop in the friction force to the movement of water molecules to the sliding interface with positive voltage applied to the upper electrode. We repeated the tests several times over the same specimen and found that the friction force decreases with the amount of performed tests, but the voltage still influences the friction response. Figure 4.10b shows the result of the third experiment performed on the same sample.

We repeated the tests with different hydrogel recipes and fabrications methods, finding similar results. Figure 4.10c presents the result of the first test performed on a different sample, produced according to the same fabrication process, except for the mold (glass in this case). Friction force graph appears to be smoother than before, arguably due to the glass mold on the hydrogel sliding

surface. The polymerization on glass rather than on PET could be also the reason for increased peak friction force with respect to the case of Figure 4.10a (nearly 6 N vs around 3 N), since the polymerization mold has great effect on frictional properties [86]. Moreover, in this case the applied voltage (10 V) was not sustained during the test. This phenomenon could be attributed to nonuniform distribution of the silane over the bonding surface. We observed that the silane layer works as insulator on the coated substrate. The insulation effect is not guaranteed if some of the spots of the substrate are not covered by the silane. Another reason could be a different value of the hydrogel bulk electrical resistance with respect to the case in Figure 4.10a.

When we inverted polarity (lower electrode as the positive one) we observed the detachment of the specimen form the bonding surface, and adhesion to the lower surface (Figure 4.9b). We hypothesized that with inverted polarity, water molecules moved toward the bonding interface between hydrogel and aluminium. This could have produced the degradation of the silane-based bonding and the consequent detachment. Alternatively, movement of water could have produced adhesion force with the substrate higher than the bonding force between the gel and the upper electrode, resulting in failure of the silane bonding under the application of an external load. Electrical-induced adhesion of hydrogel have been already demonstrated in previous works [93]. Further investigations are needed to clarify the causes of the observed phenomenon.

Finally, we tested friction modulation of hydrogel in conductor-insulator configurations (Figure 4.8c and Figure 4.9c, d). In these trials, the insulator layer is Kapton tape. We tested both configurations and both polarities, with voltages up to 18 V, but we found that friction force resulted not affected (Figure 4.10d).

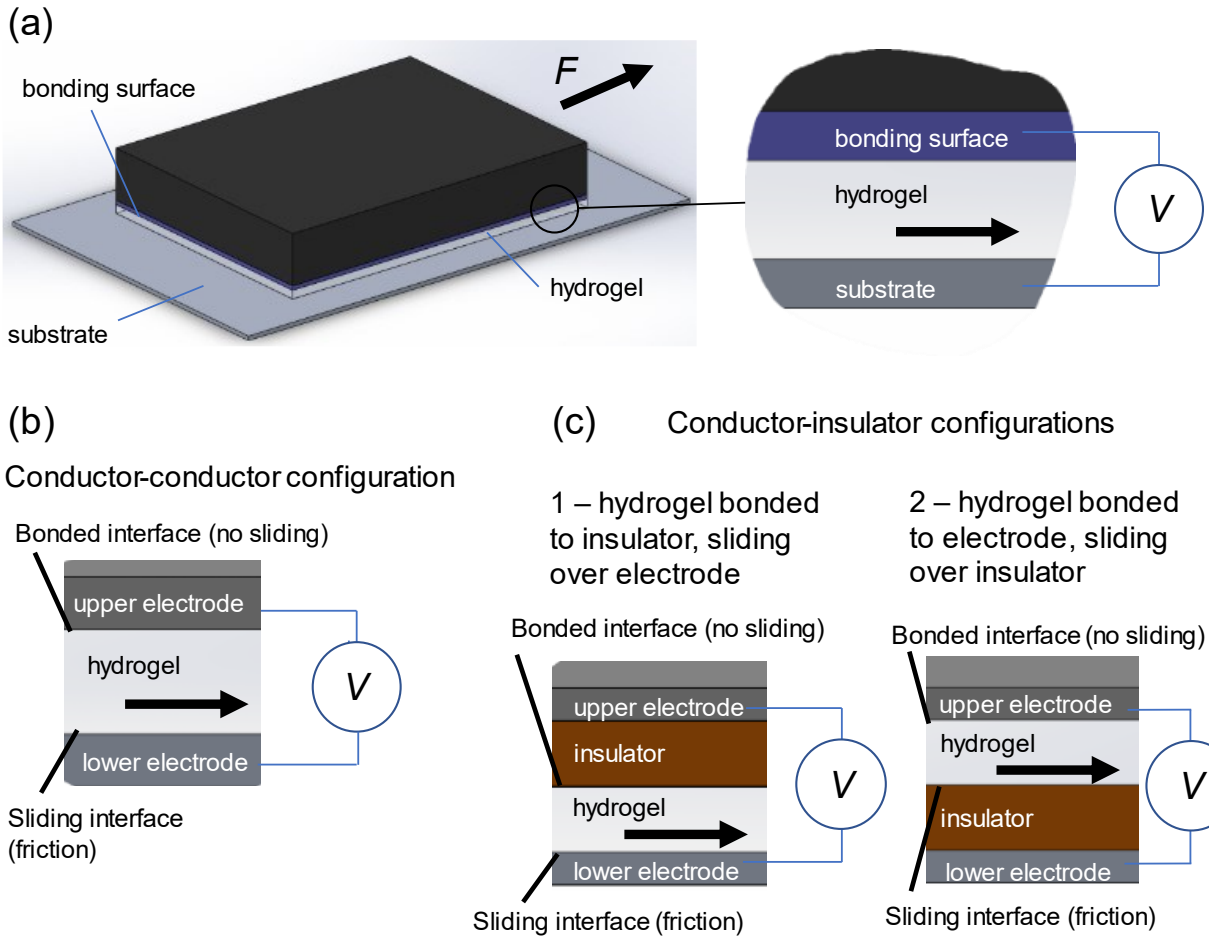

Figure 4.8 – Friction tests configurations. (a) We pulled a parallelepiped metal mass (black) over a substrate. We attached a bonding layer on the lower surface of the mass, onto which the hydrogel was bonded. The nature of the bonding surface and of the substrate changed according to the performed experiment. During the test, we applied a voltage across the hydrogel by attaching both the bonding surface and the hydrogel to a voltage supplier. (b) Conductor-conductor configuration. The bonding surface is aluminium (upper electrode). The hydrogel is attached to it. The sliding surface is aluminium (lower electrode) as well and the hydrogel slides over it. (c) Conductor-insulator configurations. (1) The bonding surface is insulator (Kapton) attached to the upper electrode (aluminium). The hydrogel is bonded to Kapton and slides over the lower electrode (aluminium). (2) The hydrogel is attached to the upper electrode (aluminium) and slides over the lower electrode covered by Kapton.

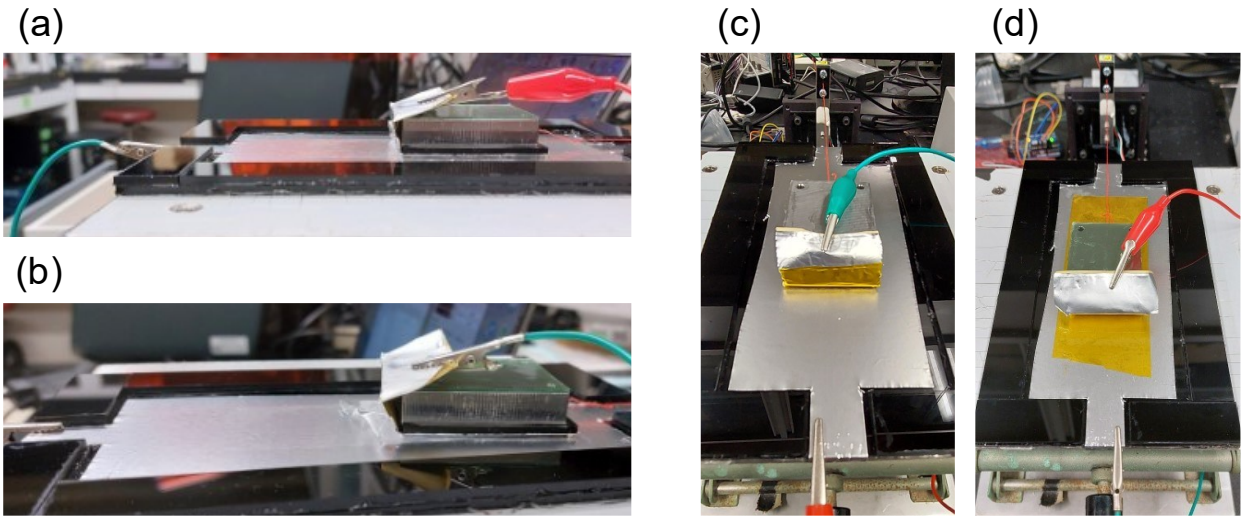

Figure 4.9 – (a) Conductor-conductor configuration. The hydrogel is directly bonded on the upper electrode and slides over the lower electrode. (b) Conductor-conductor configuration with detail of the hydrogel detached from the lower electrode. This happened when the lower electrode was positive and the upper was negative. (c) Conductor-insulator configuration 1. The upper electrode is covered with Kapton tape. (d) Conductor-insulator configuration 2. The lower electrode is covered with Kapton tape.

Figure 4.10 – (a) Friction test performed in conductor-conductor configuration. Hydrogel friction is modulated by the applied voltage. (b) Friction force measured during the third test performed on the same specimen. Friction force decreased with respect to the first attempt (a), but the modulating effect of voltage is still visible. (c) Friction test in conductor-conductor configuration with a new sample. Friction modulation is still visible even if the applied voltage (10 V) is not sustained across the hydrogel. (d) Friction tests of hydrogels in conductor-insulator configuration. Voltage has no impact on friction in this configuration.

(a)

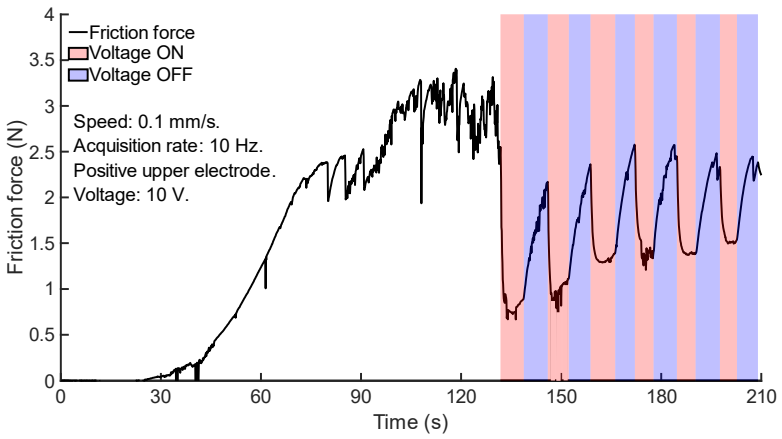
Friction force
Voltage ON
Voltage OFF
Speed: 0.1 mm/s.
Acquisition rate: 10 Hz.
Positive upper electrode.
Voltage: 10 V.
Friction force (N)
Time (s)

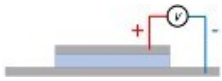

(b)

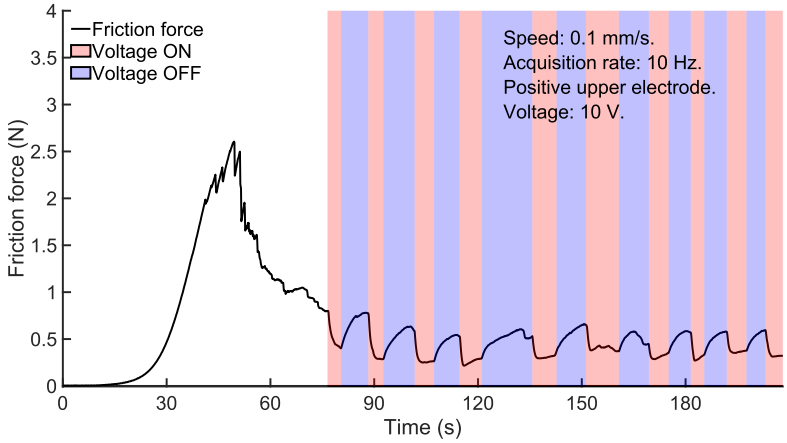
Friction force
Voltage ON
Voltage OFF
Speed: 0.1 mm/s.
Acquisition rate: 10 Hz.
Positive upper electrode.
Voltage: 10 V.
Friction force (N)
Time (s)

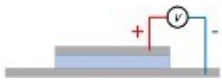

(c)

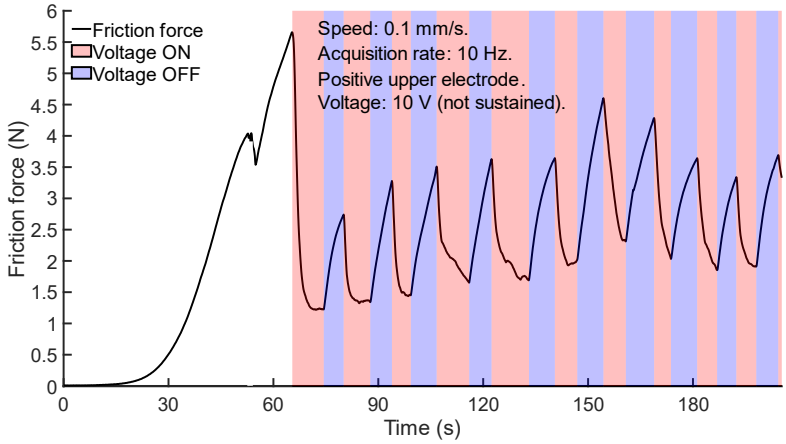
Friction force
Voltage ON
Voltage OFF
Speed: 0.1 mm/s.
Acquisition rate: 10 Hz.
Positive upper electrode.
Voltage: 10 V (not sustained).
Friction force (N)
Time (s)

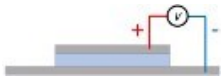

(d)

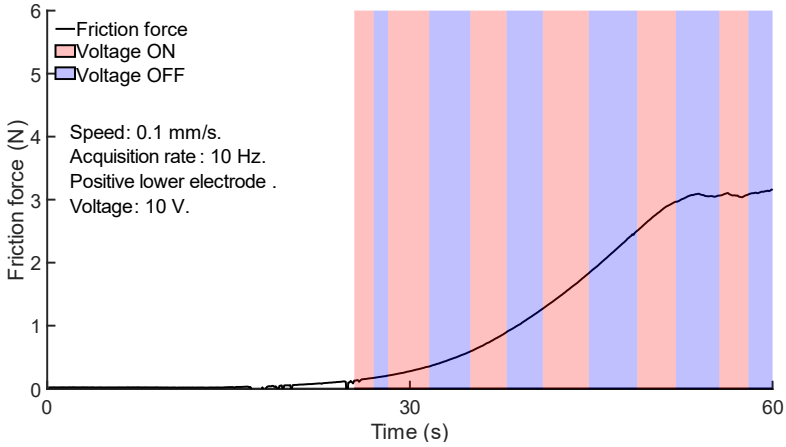
Friction force
Voltage ON
Voltage OFF
Speed: 0.1 mm/s.
Acquisition rate: 10 Hz.
Positive lower electrode .
Voltage: 10 V.
Friction force (N)
Time (s)

4.6 Preliminary design of a soft robotic application: a gripper's finger made by hydrogel

The final goal of our investigation is to create a soft robotic finger containing hydrogel, able to modify its friction behavior in response to an electrical stimulus. One of the main obstacles toward this goal is to embed the modulating ability in one single body. In Section 4.5, we demonstrated modulation of hydrogel friction under the application of a moderate voltage (10V) when the hydrogel is directly bonded on the electrode and slides over the other electrode. When the electrode bonded to the hydrogel (upper electrode) is connected to positive voltage, we observed decrease in the measured friction force. We attribute this phenomenon to the movement of water molecules toward the negative electrode, lubricating the sliding interface. When we switch the polarity, water goes toward the upper electrode, causing the degradation of the bonding and/or adhesion to the lower substrate. In any case, we demonstrated friction modulation at the sliding interface between two different bodies, with each of the electrodes placed in one of the two bodies involved in the sliding contact. No study has been conducted until now about the integration of the friction modulation properties into a single device.

In this section, we present the results of the preliminary tests conducted on the first prototypes of a self-contained, hydrogel-based device able to modify the frictional properties of its surface with voltage applied to it. We produced four different prototypes and tested each one in friction tests. The geometric design of the prototypes is freely inspired to that of an interdigitated EA tape, as the one described in Chapters 3 and 4. In an EA tape, two interdigitated electrodes generate an electric field, sustained thanks to the insulating effect produced by the dielectric layer separating them. The device is self-contained since it produces electrostatic adhesion to the body without needing that the external body works as one of the electrodes. In the following subsection, we present the results of our preliminary investigation.

4.6.1 Design 1: hydrogel on aluminium electrodes

The first tested design consists of two interdigitated aluminium electrodes and a hydrogel bonded over them. We cut aluminium sheets and placed them onto an acrylic plate. Then, we treated the surface with silane and cured hydrogel onto it (Figure 4.11a, b). Each of the teeth of the electrodes was 2 mm wide, and the distance among them was 1 mm. The hydrogel was 1 mm thick.

We tested design 1 with our friction set-up. Sliding voltage was 0.1 mm/s, voltage was 18 V. Under the application of the voltage, no clear influence on the friction force was detected, apart from a small variation in the slope of the graph in the increasing friction zone (before peak). Figure 4.11c shows this effect. The almost unperceivable variation in the measured friction force is arguably due to the movement of water molecules toward the negative electrode from the positive one. We suppose that this effect only influenced a limited area around the electrodes, so the resulting effect at the sliding interface is limited. Further investigation is needed to detect the influence of the hydrogel thickness on this configuration, limited in our current investigation by not suitable fabrication equipment. We suppose that decreasing the hydrogel thickness could positively affect the desired outcome.

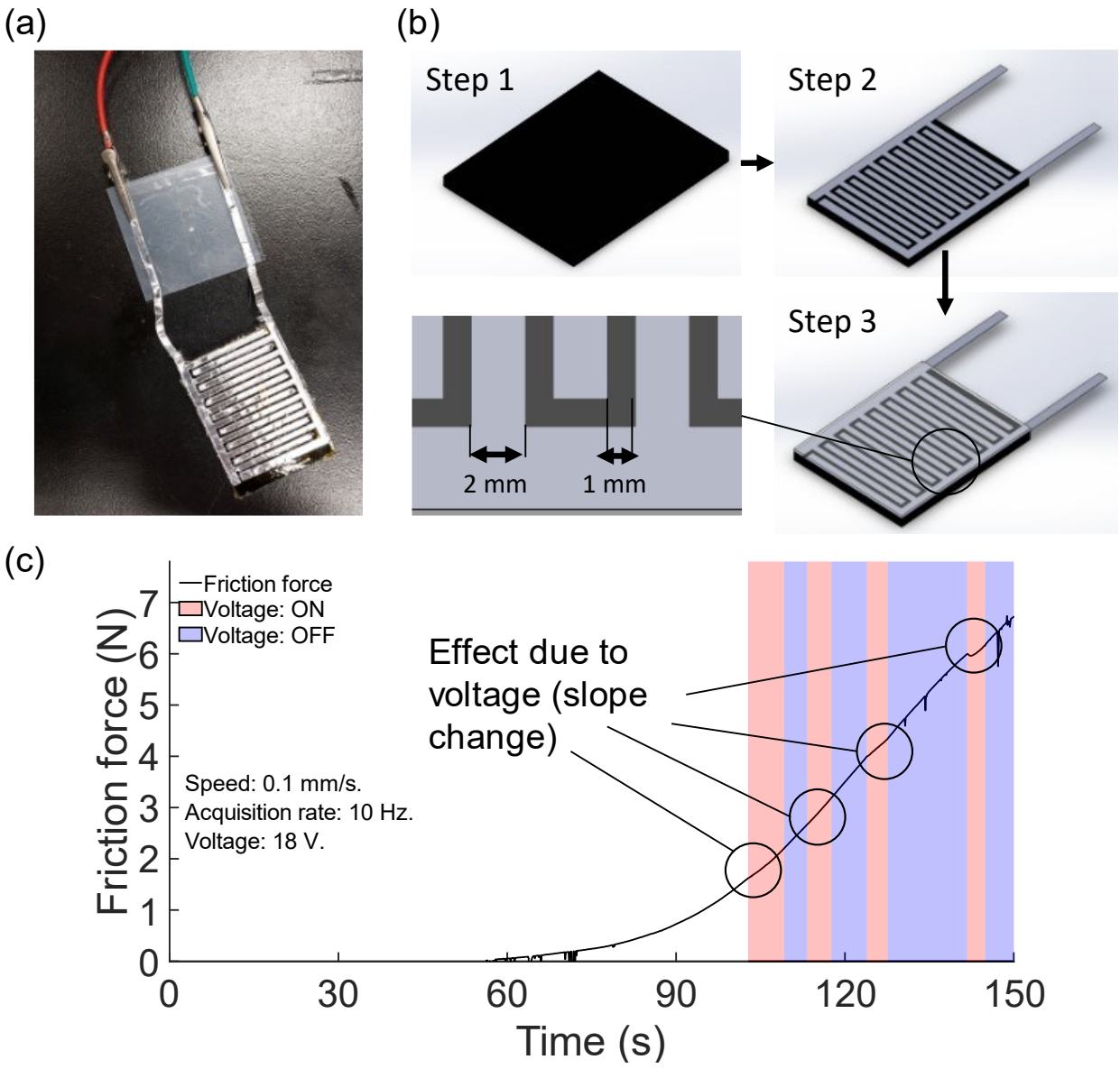

Figure 4.11 – (a) the prototype of the design 1. (b) Fabrication steps of design 1. Aluminium interdigitated electrodes are placed over an acrylic plate, the surface is silane-treated and then a hydrogel is cured onto it. (c) No clear effect due to applied voltage can be detected from the graph, apart from a slight decrease in the slope of the graph.

4.6.2 Design 2: hydrogel on aluminium electrodes, placed on different surfaces

Design 1 showed little friction modulation capabilities. We attributed this to the fact that the electrodes lie on the same plane and that the electrode plane is quite far from the sliding interface. Movement of water molecules happens between electrodes and the interface is not affected by it. To partially resolve the problem, we proposed an alternative design, in which the two electrodes lie on two different planes (Figure 4.12). The hydrogel is then cured over them. Due to limitations in the fabrication process, however, we couldn't fabricate a hydrogel thinner than 1 mm. This limitation was reflected in the results of our tests since we did observe only a slight influence of the applied voltage on the friction force (same experimental conditions of Section 4.6.1). We can then conclude that current design didn't show any improvement with respect to design 1. However, we believe that repeating the tests with decreased hydrogel thickness would improve the outcome of the experiments. Moreover, design 2 seems better than 1 since it requires less strong bonding between hydrogel and the bonding surface. The gel is partially embedded into the structure of the bonding surface, and this allows to make the attachment stronger.

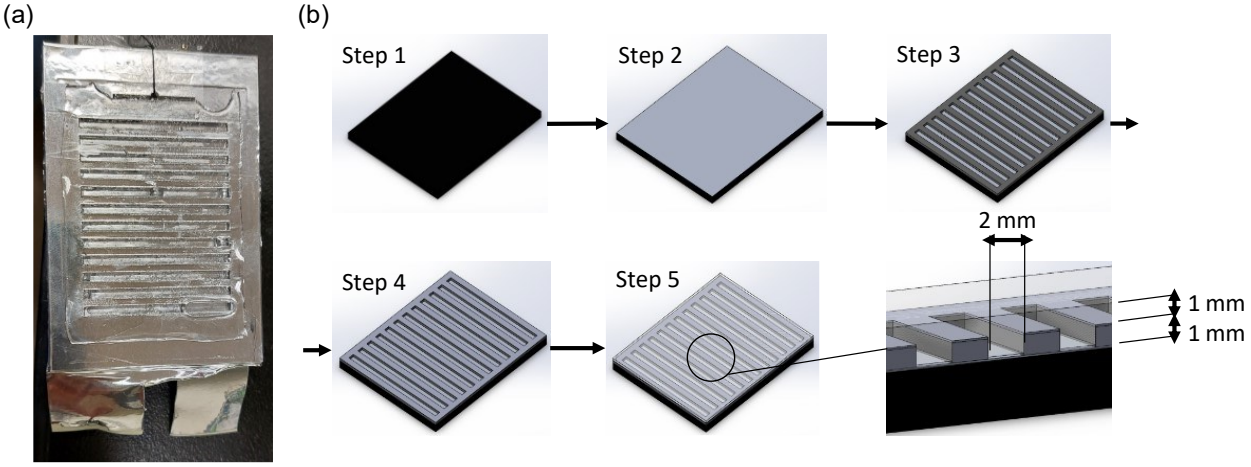

Figure 4.12 – (a) the prototype of design number 2. The two electrodes lie onto two different planes. (b) Fabrication process of design 2. The first electrode is placed over an acrylic plate. We then place an acrylic pre-cut plate over aluminium and shape the second electrode over its profile. The hydrogel is cured over them. The resulting hydrogel has a thickness of two millimeters from the lower electrode and 1 mm from the upper electrode. Holes in the mask are 2 mm wide.

4.6.3 Designs 3 and 4: hydrogel on insulated electrodes for high voltage application

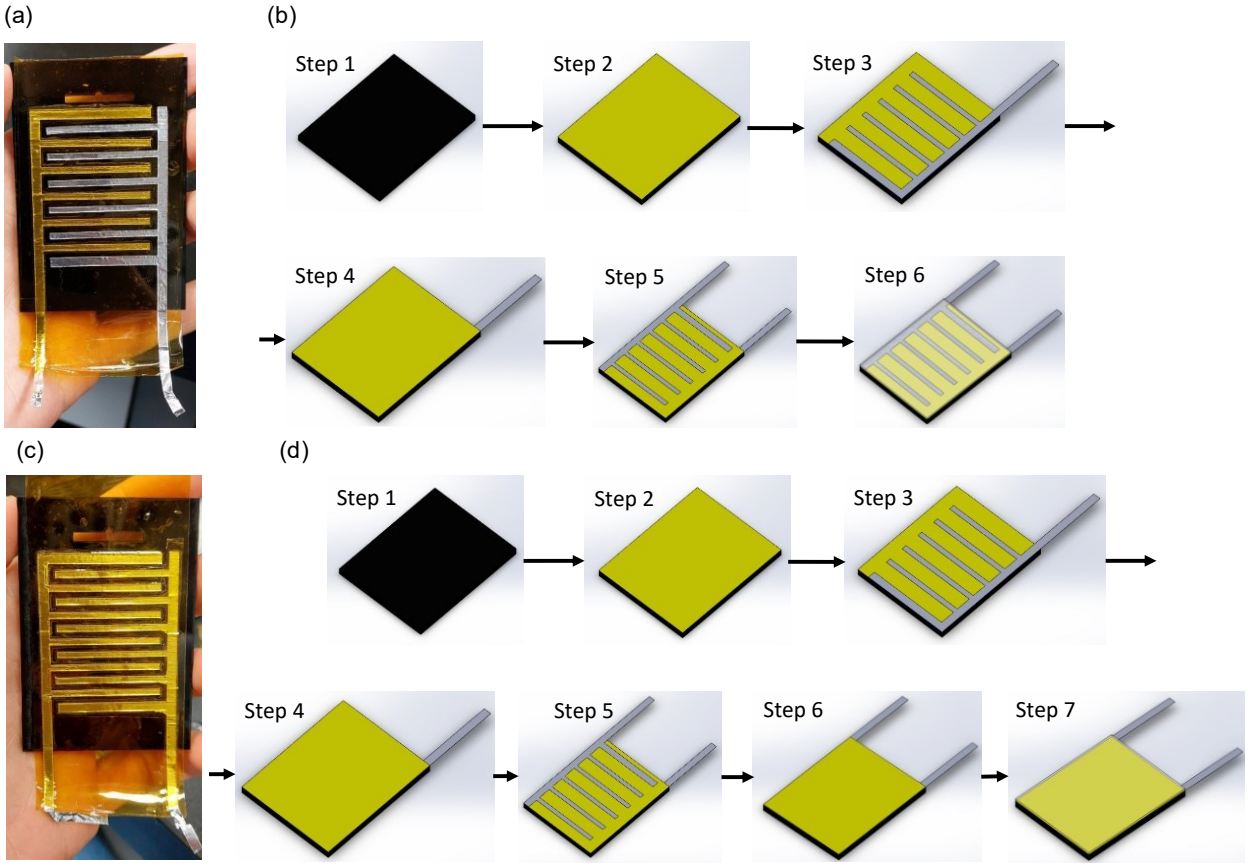

Figure 4.13 – (a, b) Design 3. (c, d) Design 4. Both designs are realized to test high voltage applications. However, none of them showed the capability to allow the control of hydrogel friction.

Finally, we decided to test two similar prototypes designed for high voltage testing. The fabrication process is nearly the same. Kapton tape is attached to an acrylic plate. One of the two electrodes is then manually placed over the first Kapton layer, and a second layer is used to coat the first electrode. Then the other electrode is applied. The electrodes are separated by Kapton to allow the application of relatively high voltage across them. The only difference between the two designs is that in design 4, the second electrode too is covered by Kapton, to avoid direct contact between gel and electrode at high voltage. The final surface is then silane-treated, and hydrogel is cured over it.

We first tested the breakdown resistance of the device, discovering that the maximum sustainable voltage is around 3 kV. So, we limited our investigation to an applied voltage of 3 kV. Then we tested the effect on the application of the voltage on hydrogel friction. We hypothesized that the fringing electric field coming out from the electrodes would cause the movement of water into the electrodes and generate variation in observed friction. However, we didn't observe any effect related to the application of the voltage, with hydrogel thickness equal to 1 mm and voltage limited to 3 kV. Further investigations are needed to test the influence of higher voltage values and thinner hydrogel but would require an improved fabrication process of both the hydrogel and the bonding surface.

4.7 Conclusions

In this chapter we presented the results of the preliminary work conducted toward the fabrication of the first soft robotic finger made by hydrogel, whose friction response could be changed according to electric effects generated by voltage applied to it.

We presented a method for improving water retention of hydrogel, one of the main problems hindering the use of hydrogels in soft robotics. We furtherly demonstrated hydrogel bonding to various substrate, paving the way toward the creation of multi-material devices partially composed by hydrogels. Further investigation will regard the demonstration of the compatibility between the water retention method and the hydrogel bonding technique.

Modulation of hydrogel friction has been demonstrated, for the case in which two electrodes are placed at the two sides of the hydrogel and hydrogel (simple PAAm hydrogel) is attached to one of them. We demonstrated decrease in hydrogel friction due to movement of water molecules toward the sliding interface and lubrification. Increase in friction due to adhesion of hydrogel to substrate has not been fully demonstrated due to failure of bonding. Improvement of hydrogel bonding method is needed. Further study will also investigate the effect on friction modulation of the dissolution of salts into the hydrogel (ionic conduction).

Finally, we produced the first prototypes of novel types of soft robotic fingers grippers made by gel. Performed tests gave important insights toward the realization of this novel kind of devices. Improvement of fabrication method is needed to obtain thinner hydrogel. Use of charged gels will be also tested to investigate its behavior.

5. Conclusions and future work

In this thesis I presented advancements about applications of EA in soft robotics, focusing in particular on EA soft robotic grippers. In the first two Chapters, I investigated the role of mechanics in EA, that only recently has gained importance in the research field. The first Chapter dealt with the interplay between mechanics and electrical features of an EA grasping system that influences the grasping task. I have shown the conditions in which an EA gripper is able to wrap an object under the only action of electrostatic forces, without the use of external actuators. The phenomenon of electrostatic zipping is responsible for the passive wrapping. The phenomenon is widely employed in electrostatic and electro-hydraulical actuators, making the outcomes of the investigation extremely valuable not only for soft grippers, but also for this kind of devices.

In the second Chapter I investigated how the shape of the grasped object influences the holding force of an EA soft gripper. Even in this case the mechanics of the system plays an important role in determining the electroadhesion strength. The theoretical model produced to account for the shape of the object is in accordance with previous observations. My preliminary experimental investigation confirms the model outcomes. The results of this Chapter are of great interest for devices such as electrostatic clutches having the task of transmitting force between two parts adhered by EA. New geometries of the clutch could lead to devices with augmented force transmission capabilities or with less requirements in terms of electrical equipment or footprint, being equal the output force.

Finally, in the third Chapter I presented my preliminary investigation about the possibility of realizing the first EA soft gripper made with hydrogels. Hydrogel exhibit modulation of adhesion and friction if a relatively low voltage is applied to them. Embedding hydrogel into a soft gripper's finger will allow to have control of friction properties of the gripper, switching from adhesion to lubrication at very low voltages if compared with current EA soft grippers designs.

Future work will be aimed at fabricating EA soft grippers leveraging the interplay between mechanics and electroadhesion to obtain improved performances and more dexterous manipulation. Attention will be paid to extend the result of the investigation of the wrapping capabilities of EA soft grippers to more complicated geometries, such as spheres. Moreover, further investigation is needed to understand the role of the dynamics of charges in the zipping phenomenon, that appears to be still unclear but influencing the voltage thresholds and the time needed to complete the wrapping.

Further investigation on the influence of the shape of the object on the maximum EA force of a soft tape adhered to it is needed to fully determine the capabilities of current gripper's designs. The validated model will be then exploited to guide the fabrication on novel clutches with improved performances.

Finally, the preliminary work conducted on hydrogel will be completed with the refinement of methods for improving water retention and bonding to external surfaces. Novel designs for the bonding interface will be produced to reach control of hydrogel friction in a single body and push the work toward the realization of an EA soft robotic gripper embedding hydrogel in its fingers.

Bibliography

[1] M. Mastrangelo, F. Caruso, G. Carbone, V. Cacucciolo, Electroadhesion zipping with soft grippers on curved objects, Extreme Mechanics Letters. 61 (2023) 101999. https://doi.org/10.1016/j.eml.2023.101999.
[2] I.M. Hutchings, P. Shipway, Tribology: friction and wear of engineering materials, 2nd ed, Elsevier, Oxford, 2017.
[3] M. Mastrangelo, V. Cacucciolo, High-Force Soft Grippers with Electroadhesion on Curved Objects, in: 2022 IEEE 5th International Conference on Soft Robotics (RoboSoft), IEEE, Edinburgh, United Kingdom, 2022: pp. 384–389. https://doi.org/10.1109/RoboSoft54090.2022.9762116.
[4] V. Cacucciolo, H. Shea, G. Carbone, Peeling in electroadhesion soft grippers, Extreme Mechanics Letters. 50 (2022) 101529. https://doi.org/10.1016/j.eml.2021.101529.
[5] N. Berdozzi, Y. Chen, L. Luzi, M. Fontana, I. Fassi, L. Molinari Tosatti, R. Vertechy, Rapid Fabrication of Electro-Adhesive Devices With Inkjet Printed Electrodes, IEEE Robot. Autom. Lett. 5 (2020) 2770–2776. https://doi.org/10.1109/LRA.2020.2972838.
[6] G.M. Whitesides, Soft Robotics, Angew. Chem. Int. Ed. 57 (2018) 4258–4273. https://doi.org/10.1002/anie.201800907.
[7] C. Majidi, Soft Robotics: A Perspective—Current Trends and Prospects for the Future, Soft Robotics. 1 (2014) 5–11. https://doi.org/10.1089/soro.2013.0001.
[8] D. Rus, M.T. Tolley, Design, fabrication and control of soft robots, Nature. 521 (2015) 467–475. https://doi.org/10.1038/nature14543.
[9] Helmut Hauser, Rudolf M. Fuchslin, Kohei Nakajima, Opinions and Outlooks on Morphological Computation, in: Morphological Computation - The Physical Body as a Computational Resource, n.d.
[10] N. Li, T. Yang, P. Yu, J. Chang, L. Zhao, X. Zhao, I.H. Elhajj, N. Xi, L. Liu, Bio-inspired upper limb soft exoskeleton to reduce stroke-induced complications, Bioinspiration & Biomimetics. 13 (2018) 066001. https://doi.org/10.1088/1748-3190/aad8d4.
[11] C. Di Natali, T. Poliero, M. Sposito, E. Graf, C. Bauer, C. Pauli, E. Bottenberg, A. De Eyto, L. O'Sullivan, A.F. Hidalgo, D. Scherly, K.S. Stadler, D.G. Caldwell, J. Ortiz, Design and Evaluation of a Soft Assistive Lower Limb Exoskeleton, Robotica. 37 (2019) 2014–2034. https://doi.org/10.1017/S0263574719000067.
[12] C. Rognon, S. Mintchev, F. DellAgnola, A. Cherpillod, D. Atienza, D. Floreano, FlyJacket: An Upper Body Soft Exoskeleton for Immersive Drone Control, IEEE Robot. Autom. Lett. 3 (2018) 2362–2369. https://doi.org/10.1109/LRA.2018.2810955.
[13] T. Ranzani, G. Gerboni, M. Cianchetti, A. Menciassi, A bioinspired soft manipulator for minimally invasive surgery., Bioinspir Biomim. 10 (2015) 035008. https://doi.org/10.1088/1748-3190/10/3/035008.
[14] R.F. Shepherd, F. Ilievski, W. Choi, S.A. Morin, A.A. Stokes, A.D. Mazzeo, X. Chen, M. Wang, G.M. Whitesides, Multigait soft robot, Proc. Natl. Acad. Sci. U.S.A. 108 (2011) 20400–20403. https://doi.org/10.1073/pnas.1116564108.
[15] M.T. Tolley, R.F. Shepherd, B. Mosadegh, K.C. Galloway, M. Wehner, M. Karpelson, R.J. Wood, G.M. Whitesides, A Resilient, Untethered Soft Robot, Soft Robotics. 1 (2014) 213–223.
[16] G. Li, X. Chen, F. Zhou, Y. Liang, Y. Xiao, X. Cao, Z. Zhang, M. Zhang, B. Wu, S. Yin, Y. Xu, H. Fan, Z. Chen, W. Song, W. Yang, B. Pan, J. Hou, W. Zou, S. He, X. Yang, G. Mao, Z. Jia, H. Zhou, T. Li, S. Qu, Z. Xu, Z. Huang, Y. Luo, T. Xie, J. Gu, S. Zhu, W. Yang, Self-powered soft robot in the Mariana Trench, Nature. 591 (2021) 66–71. https://doi.org/10.1038/s41586-020-03153-z.
[17] Y. Chen, H. Zhao, J. Mao, P. Chirarattananon, E.F. Helbling, N.P. Hyun, D.R. Clarke, R.J. Wood, Controlled flight of a microrobot powered by soft artificial muscles, Nature. 575 (2019) 324–329. https://doi.org/10.1038/s41586-019-1737-7.
[18] S. Palagi, A.G. Mark, S.Y. Reigh, K. Melde, T. Qiu, H. Zeng, C. Parmeggiani, D. Martella, A. Sanchez-Castillo, N. Kapernaum, F. Giesselmann, D.S. Wiersma, E. Lauga, P. Fischer, Structured light enables biomimetic swimming and versatile locomotion of photoresponsive soft microrobots., Nat Mater. 15 (2016) 647–653. https://doi.org/10.1038/nmat4569.
[19] J. Shintake, V. Cacucciolo, D. Floreano, H. Shea, Soft Robotic Grippers, Adv. Mater. 30 (2018) 1707035. https://doi.org/10.1002/adma.201707035.

[20] J. Hughes, U. Culha, F. Giardina, F. Guenther, A. Rosendo, F. Iida, Soft Manipulators and Grippers: A Review, Frontiers in Robotics and AI. 3 (2016). https://doi.org/10.3389/frobt.2016.00069.
[21] C.-H. Liu, T.-L. Chen, C.-H. Chiu, M.-C. Hsu, Y. Chen, T.-Y. Pai, W.-G. Peng, Y.-P. Chiang, Optimal Design of a Soft Robotic Gripper for Grasping Unknown Objects, Soft Robotics. 5 (2018) 452–465. https://doi.org/10.1089/soro.2017.0121.
[22] F. Ilievski, A.D. Mazzeo, R.F. Shepherd, X. Chen, G.M. Whitesides, Soft Robotics for Chemists, Angew. Chem. 50 (2011) 1890–1895.
[23] E. Brown, N. Rodenberg, J. Amend, A. Mozeika, E. Steltz, M.R. Zakin, H. Lipson, H.M. Jaeger, Universal robotic gripper based on the jamming of granular material, Proc. Natl. Acad. Sci. U.S.A. 107 (2010) 18809–18814. https://doi.org/10.1073/pnas.1003250107.
[24] J. Shintake, S. Rosset, B. Schubert, D. Floreano, H. Shea, Versatile Soft Grippers with Intrinsic Electroadhesion Based on Multifunctional Polymer Actuators, Adv. Mater. 28 (2016) 231–238. https://doi.org/10.1002/adma.201504264.
[25] K.M. Digumarti, V. Cacucciolo, H. Shea, Dexterous textile manipulation using electroadhesive fingers, in: 2021 IEEE/RSJ International Conference on Intelligent Robots and Systems (IROS), IEEE, Prague, Czech Republic, 2021: pp. 6104–6109. https://doi.org/10.1109/IROS51168.2021.9636095.
[26] E.W. Schaler, D. Ruffatto, P. Glick, V. White, A. Parness, An electrostatic gripper for flexible objects, in: 2017 IEEE/RSJ International Conference on Intelligent Robots and Systems (IROS), IEEE, Vancouver, BC, 2017: pp. 1172–1179. https://doi.org/10.1109/IROS.2017.8202289.
[27] I.-D. Sîrbu, M. Bolignari, S. D'Avella, F. Damiani, L. Agostini, P. Tripicchio, R. Vertechy, L. Pancheri, M. Fontana, Adhesion State Estimation for Electrostatic Gripper Based on Online Capacitance Measure, Actuators. 11 (2022) 283. https://doi.org/10.3390/act11100283.
[28] D.J. Levine, G.M. Iyer, R. Daelan Roosa, K.T. Turner, J.H. Pikul, A mechanics-based approach to realize high–force capacity electroadhesives for robots, Sci. Robot. 7 (2022) eabo2179. https://doi.org/10.1126/scirobotics.abo2179.
[29] V. Cacucciolo, J. Shintake, H. Shea, Delicate yet strong: Characterizing the electro-adhesion lifting force with a soft gripper, in: 2019 2nd IEEE International Conference on Soft Robotics (RoboSoft), IEEE, Seoul, Korea (South), 2019: pp. 108–113. https://doi.org/10.1109/ROBOSOFT.2019.8722706.
[30] R. Hinchet, H. Shea, High Force Density Textile Electrostatic Clutch, Adv. Mater. Technol. 5 (2020) 1900895. https://doi.org/10.1002/admt.201900895.
[31] P. Rajagopalan, M. Muthu, Y. Liu, J. Luo, X. Wang, C. Wan, Advancement of Electroadhesion Technology for Intelligent and Self-Reliant Robotic Applications, Advanced Intelligent Systems. 4 (2022) 2200064. https://doi.org/10.1002/aisy.202200064.
[32] K. Kendall, The adhesion and surface energy of elastic solids, J. Phys. D: Appl. Phys. 4 (1971) 1186–1195. https://doi.org/10.1088/0022-3727/4/8/320.
[33] B.N.J. Persson, General theory of electroadhesion, J. Phys.: Condens. Matter. 33 (2021) 435001. https://doi.org/10.1088/1361-648X/abe797.
[34] A. Johnsen, K. Rahbek, A physical phenomenon and its applications to telegraphy, telephony, etc., Journal of the Institution of Electrical Engineers. 61 (1923) 713–725. https://doi.org/10.1049/jiee-1.1923.0092.
[35] A.B. Croll, N. Hosseini, M.D. Bartlett, Switchable Adhesives for Multifunctional Interfaces, Adv. Mater. Technol. 4 (2019) 1900193. https://doi.org/10.1002/admt.201900193.
[36] Y. Vardar, B. Güçlü, C. Basdogan, Effect of Waveform on Tactile Perception by Electrovibration Displayed on Touch Screens, IEEE Transactions on Haptics. 10 (2017) 488–499. https://doi.org/10.1109/TOH.2017.2704603.
[37] R.H. Osgouei, J.R. Kim, S. Choi, Improving 3D Shape Recognition withElectrostatic Friction Display, IEEE Trans. Haptics. 10 (2017) 533–544. https://doi.org/10.1109/TOH.2017.2710314.
[38] O. Sirin, M. Ayyildiz, B.N.J. Persson, C. Basdogan, Electroadhesion with application to touchscreens, Soft Matter. 15 (2019) 1758–1775. https://doi.org/10.1039/C8SM02420K.
[39] S.B. Diller, Design, characterization, and implementation of lightwieght and energy-efficient electroadhesive clutches for robotics, Carnegie Mellon, 2018.
[40] V. Ramachandran, J. Shintake, D. Floreano, All-Fabric Wearable Electroadhesive Clutch, Adv. Mater. Technol. 4 (2019) 1800313. https://doi.org/10.1002/admt.201800313.

[41] A. Detailleur, S. Umans, H. Van Even, A. Pennycott, H. Vallery, Feasibility Analysis of a Self-Reinforcing Electroadhesive Rotational Clutch, in: 2021 IEEE/ASME International Conference on Advanced Intelligent Mechatronics (AIM), IEEE, Delft, Netherlands, 2021: pp. 478–483. https://doi.org/10.1109/AIM46487.2021.9517370.
[42] J. Li, Y. Xiong, B. Yang, K. Ma, X. Tao, Asymmetric Flexible Electroadhesive Clutches, SSRN Journal. (2021). https://doi.org/10.2139/ssrn.3931629.
[43] J. Germann, M. Dommer, R. Pericet-Camara, D. Floreano, Active Connection Mechanism for Soft Modular Robots, Advanced Robotics. 26 (2012) 785–798. https://doi.org/10.1163/156855312X626325.
[44] J. Huang, Y. Liu, Y. Yang, Z. Zhou, J. Mao, T. Wu, J. Liu, Q. Cai, C. Peng, Y. Xu, B. Zeng, W. Luo, G. Chen, C. Yuan, L. Dai, Electrically programmable adhesive hydrogels for climbing robots, Sci. Robot. 6 (2021) eabe1858. https://doi.org/10.1126/scirobotics.abe1858.
[45] R. Chen, A Gecko-Inspired Electroadhesive Wall-Climbing Robot, IEEE Potentials. 34 (2015) 15–19. https://doi.org/10.1109/MPOT.2014.2360020.
[46] G. Gu, J. Zou, R. Zhao, X. Zhao, X. Zhu, Soft wall-climbing robots, SCIENCE ROBOTICS. 3 (2018) 13. https://doi.org/DOI: 10.1126/scirobotics.aat2874.
[47] H. Wang, A. Yamamoto, Peel Force of Electrostatic Adhesion in Crawler-type Electrostatic Climbing Robots, Journal of the Japan Society of Applied Electromagnetics and Mechanics. 23 (2015) 498–503. https://doi.org/10.14243/jsaem.23.498.
[48] M.A. Graule, P. Chirarattananon, S.B. Fuller, N.T. Jafferis, K.Y. Ma, M. Spenko, R. Kornbluh, R.J. Wood, Perching and takeoff of a robotic insect on overhangs using switchable electrostatic adhesion, Science. 352 (2016) 978–982. https://doi.org/10.1126/science.aaf1092.
[49] R. Chen, Z. Zhang, J. Guo, F. Liu, J. Leng, J. Rossiter, Variable Stiffness Electroadhesion and Compliant Electroadhesive Grippers, Soft Robotics. (2021) soro.2021.0083. https://doi.org/10.1089/soro.2021.0083.
[50] G. Hwang, J. Park, D.S.D. Cortes, K. Hyeon, K.-U. Kyung, Electroadhesion-Based High-Payload Soft Gripper With Mechanically Strengthened Structure, IEEE Trans. Ind. Electron. 69 (2022) 642–651. https://doi.org/10.1109/TIE.2021.3053887.
[51] V. Alizadehyazdi, M. Bonthron, M. Spenko, An Electrostatic/Gecko-Inspired Adhesives Soft Robotic Gripper, IEEE Robot. Autom. Lett. 5 (2020) 4679–4686. https://doi.org/10.1109/LRA.2020.3003773.
[52] J. Guo, T. Bamber, M. Chamberlain, L. Justham, M. Jackson, Optimization and experimental verification of coplanar interdigital electroadhesives, J. Phys. D: Appl. Phys. 49 (2016) 415304. https://doi.org/10.1088/0022-3727/49/41/415304.
[53] J. Guo, J. Leng, J. Rossiter, Electroadhesion Technologies for Robotics: A Comprehensive Review, IEEE Trans. Robot. 36 (2020) 313–327. https://doi.org/10.1109/TRO.2019.2956869.
[54] R. Chen, R. Song, Z. Zhang, L. Bai, F. Liu, P. Jiang, D. Sindersberger, G.J. Monkman, J. Guo, Bio-Inspired Shape-Adaptive Soft Robotic Grippers Augmented with Electroadhesion Functionality, Soft Robotics. 6 (2019) 701–712. https://doi.org/10.1089/soro.2018.0120.
[55] J. Guo, K. Elgeneidy, C. Xiang, N. Lohse, L. Justham, J. Rossiter, Soft pneumatic grippers embedded with stretchable electroadhesion, Smart Mater. Struct. 27 (2018) 055006. https://doi.org/10.1088/1361-665X/aab579.
[56] M. Taghavi, T. Helps, J. Rossiter, Electro-ribbon actuators and electro-origami robots, Sci. Robot. 3 (2018) eaau9795. https://doi.org/10.1126/scirobotics.aau9795.
[57] P. Rothemund, N. Kellaris, S.K. Mitchell, E. Acome, C. Keplinger, HASEL Artificial Muscles for a New Generation of Lifelike Robots—Recent Progress and Future Opportunities, Adv. Mater. 33 (2021) 2003375. https://doi.org/10.1002/adma.202003375.
[58] E. Leroy, R. Hinchet, H. Shea, Multimode Hydraulically Amplified Electrostatic Actuators for Wearable Haptics, Adv. Mater. (2020) 2002564. https://doi.org/10.1002/adma.202002564.
[59] C. Keplinger, T. Li, R. Baumgartner, Z. Suo, S. Bauer, Harnessing snap-through instability in soft dielectrics to achieve giant voltage-triggered deformation, Soft Matter. 8 (2012) 285–288. https://doi.org/10.1039/C1SM06736B.
[60] Z. Suo, THEORY OF DIELECTRIC ELASTOMERS, ACTA MECHANICA SOLIDA SINICA. 23 (2010) 30. https://doi.org/10.1016/S0894-9166(11)60004-9.

[61] M. Righi, M. Fontana, R. Vertechy, M. Duranti, G. Moretti, Analysis of dielectric fluid transducers, in: Y. Bar-Cohen (Ed.), Electroactive Polymer Actuators and Devices (EAPAD) XX, SPIE, Denver, United States, 2018: p. 29. https://doi.org/10.1117/12.2297082.
[62] W.-M. Zhang, H. Yan, Z.-K. Peng, G. Meng, Electrostatic pull-in instability in MEMS/NEMS: A review, Sensors and Actuators A: Physical. 214 (2014) 187–218. https://doi.org/10.1016/j.sna.2014.04.025.
[63] E. Hajiesmaili, D.R. Clarke, Dielectric elastomer actuators, Journal of Applied Physics. 129 (2021) 151102. https://doi.org/10.1063/5.0043959.
[64] N. Kellaris, V.G. Venkata, P. Rothemund, C. Keplinger, An analytical model for the design of Peano-HASEL actuators with drastically improved performance, Extreme Mechanics Letters. 29 (2019) 100449. https://doi.org/10.1016/j.eml.2019.100449.
[65] B. Behzadnezhad, B.D. Collick, N. Behdad, A.B. McMillan, Dielectric properties of 3D-printed materials for anatomy specific 3D-printed MRI coils, Journal of Magnetic Resonance. 289 (2018) 113–121. https://doi.org/10.1016/j.jmr.2018.02.013.
[66] S. Simula, S. Ikäläinen, K. Niskanen, T. Varpula, H. Seppä, A. Paukku, Measurement of the Dielectric Properties of Paper, 43 (1999) 6.
[67] PolyK technologies, P(VDF-TrFE-CTFE) datasheet., High Dielectric Constant P(VDF-TrFE-CTFE) Terpolymer Film. (n.d.). https://piezopvdf.com/ctfe-terpolymer-film-low-ctfe-18-um/.
[68] G. Kofod, P. Sommer-Larsen, R. Kornbluh, R. Pelrine, Actuation Response of Polyacrylate Dielectric Elastomers, Journal of Intelligent Material Systems and Structures. 14 (2003) 787–793. https://doi.org/10.1177/104538903039260.
[69] S. Park, K. Mondal, R.M. Treadway, V. Kumar, S. Ma, J.D. Holbery, M.D. Dickey, Silicones for Stretchable and Durable Soft Devices: Beyond Sylgard-184, ACS Appl. Mater. Interfaces. 10 (2018) 11261–11268. https://doi.org/10.1021/acsami.7b18394.
[70] Dow Corning, Sylgard 184 Silicone Elastomer datasheet., (n.d.). https://www.dow.com/documents/en-us/productdatasheet/11/11-31/11-3184-sylgard-184-elastomer.pdf.
[71] F.B. Albuquerque, H. Shea, Influence of humidity, temperature and prestretch on the dielectric breakdown strength of silicone elastomer membranes for DEAs, Smart Mater. Struct. 29 (2020) 105024. https://doi.org/10.1088/1361-665X/aba5e3.
[72] D. Ruffatto, J. Shah, M. Spenko, Increasing the adhesion force of electrostatic adhesives using optimized electrode geometry and a novel manufacturing process, Journal of Electrostatics. 72 (2014) 147–155. https://doi.org/10.1016/j.elstat.2014.01.001.
[73] S.B. Diller, S.H. Collins, C. Majidi, The effects of electroadhesive clutch design parameters on performance characteristics, Journal of Intelligent Material Systems and Structures. 29 (2018) 3804–3828. https://doi.org/10.1177/1045389X18799474.
[74] K. Kendall, Thin-film peeling-the elastic term, J. Phys. D: Appl. Phys. 8 (1975) 1449–1452. https://doi.org/10.1088/0022-3727/8/13/005.
[75] S. Ponce, J. Bico, B. Roman, Effect of friction on the peeling test at zero-degrees, Soft Matter. 11 (2015) 9281–9290. https://doi.org/10.1039/C5SM01203A.
[76] V. Ramachandran, F. Schilling, A.R. Wu, D. Floreano, Smart Textiles that Teach: Fabric-Based Haptic Device Improves the Rate of Motor Learning, Advanced Intelligent Systems. 3 (2021) 2100043. https://doi.org/10.1002/aisy.202100043.
[77] S. Diller, C. Majidi, S.H. Collins, A lightweight, low-power electroadhesive clutch and spring for exoskeleton actuation, in: 2016 IEEE International Conference on Robotics and Automation (ICRA), IEEE, Stockholm, Sweden, 2016: pp. 682–689. https://doi.org/10.1109/ICRA.2016.7487194.
[78] G.L. Hazelton, A force amplifier: the capstan, The Physics Teacher. 14 (1976) 432–433. https://doi.org/10.1119/1.2339442.
[79] E. Oborin, Y. Vetyukov, I. Steinbrecher, Eulerian description of non-stationary motion of an idealized belt-pulley system with dry friction, International Journal of Solids and Structures. 147 (2018) 40–51. https://doi.org/10.1016/j.ijsolstr.2018.04.007.
[80] M.M. Starkey, R.L. Williams, Capstan as a Mechanical Amplifier, in: Volume 6: 35th Mechanisms and Robotics Conference, Parts A and B, ASMEDC, Washington, DC, USA, 2011: pp. 1309–1316. https://doi.org/10.1115/DETC2011-48262.
[81] M. Trejo, C. Fretigny, A. Chateauminois, Friction of viscoelastic elastomers with rough surfaces

under torsional contact conditions, Phys. Rev. E. 88 (2013) 052401. https://doi.org/10.1103/PhysRevE.88.052401.
[82] M. Takata, T. Yamaguchi, J. Ping Gong, M. Doi, Electric Field Effect on the Sliding Friction of a Charged Gel, J. Phys. Soc. Jpn. 78 (2009) 084602. https://doi.org/10.1143/JPSJ.78.084602.
[83] M. Takata, T. Yamaguchi, M. Doi, Friction Control of a Gel by Electric Field in Ionic Surfactant Solution, J. Phys. Soc. Jpn. 79 (2010) 063602. https://doi.org/10.1143/JPSJ.79.063602.
[84] M. Wada, K. Yamada, T. Kameyama, N. Yamada, K. Yoshida, A. Saito, M. Makino, A. Khosla, M. Kawakami, H. Furukawa, Electric control of friction on surface of high-strength hydrogels, Microsyst Technol. 24 (2018) 639–646. https://doi.org/10.1007/s00542-017-3417-6.
[85] Z. Shen, F. Chen, X. Zhu, K.-T. Yong, G. Gu, Stimuli-responsive functional materials for soft robotics, J. Mater. Chem. B. 6 (2020) 8972–8991. https://doi.org/10.1039/D0TB01585G.
[86] J.P. Gong, Friction and lubrication of hydrogels—its richness and complexity, Soft Matter. 2 (2006) 544–552. https://doi.org/10.1039/B603209P.
[87] R.J. Hinchet, H. Shea, Glove- and Sleeve-Format Variable-Friction Electrostatic Clutches for Kinesthetic Haptics, Advanced Intelligent Systems. 4 (2022) 2200174. https://doi.org/10.1002/aisy.202200174.
[88] J. Gong, Y. Iwasaki, Y. Osada, K. Kurihara, Y. Hamai, Friction of Gels. 3. Friction on Solid Surfaces, J. Phys. Chem. B. 103 (1999) 6001–6006. https://doi.org/10.1021/jp9902553.
[89] J.P. Gong, G. Kagata, Y. Osada, Friction of Gels. 4. Friction on Charged Gels, J. Phys. Chem. B. 103 (1999) 6007–6014. https://doi.org/10.1021/jp990256v.
[90] T. Narita, A. Knaebel, J.-P. Munch, S.J. Candau, J.P. Gong, Y. Osada, Microrheological Investigation of Substrate-Induced Gradient Structure in Hydrogels, Macromolecules. 34 (2001) 5725–5726. https://doi.org/10.1021/ma010364r.
[91] J. Gong, Y. Osada, Gel friction: A model based on surface repulsion and adsorption, The Journal of Chemical Physics. 109 (1998) 8062–8068. https://doi.org/10.1063/1.477453.
[92] Y. Liu, P. Wang, X. Su, L. Xu, Z. Tian, H. Wang, G. Ji, J. Huang, Electrically Programmable Interfacial Adhesion for Ultrastrong Hydrogel Bonding, Advanced Materials. 34 (2022) 2108820. https://doi.org/10.1002/adma.202108820.
[93] L.K. Borden, A. Gargava, S.R. Raghavan, Reversible electroadhesion of hydrogels to animal tissues for suture-less repair of cuts or tears, Nat Commun. 12 (2021) 4419. https://doi.org/10.1038/s41467-021-24022-x.
[94] A. Wiranata, Y. Ohsugi, A. Minaminosono, Y. Kuwajima, S. Maeda, Electromechanical tensile test equipment for stretchable conductive materials, HardwareX. 11 (2022) e00287. https://doi.org/10.1016/j.ohx.2022.e00287.
[95] D.F. Moore, Principles and applications of tribology, 1st ed., Pergamon Press, Oxford, New York, 1975.
[96] K.R. Makinson, D. Tabor, The friction and transfer of polytetrafluoroethylene, Proceedings of the Royal Society A: Mathematical and Physical Sciences. 281 (1964) 49–61.
[97] M.L. White, THE PERMEABILITY OF AN ACRYLAMIDE POLYMER GEL, J. Phys. Chem. 64 (1960) 1563–1565. https://doi.org/10.1021/j100839a055.
[98] E.M. Ahmed, Hydrogel: Preparation, characterization, and applications: A review, Journal of Advanced Research. 6 (2015) 105–121. https://doi.org/10.1016/j.jare.2013.07.006.
[99] S. Seiffert, W. Oppermann, K. Saalwächter, Hydrogel formation by photocrosslinking of dimethylmaleimide functionalized polyacrylamide, Polymer. 48 (2007) 5599–5611. https://doi.org/10.1016/j.polymer.2007.07.013.
[100] Jaya Maitra, Vivek Kumar Shukla, Cross-linking in Hydrogels - A Review, American Journal of Polymer Science. (n.d.). https://doi.org/10.5923/j.ajps.20140402.01.
[101] E. Nicol, Photopolymerized Porous Hydrogels, Biomacromolecules. 22 (2021) 1325–1345. https://doi.org/10.1021/acs.biomac.0c01671.
[102] C. Keplinger, J.-Y. Sun, C.C. Foo, P. Rothemund, G.M. Whitesides, Z. Suo, Stretchable, Transparent, Ionic Conductors, Science. 341 (2013) 984–987. https://doi.org/10.1126/science.1240228.
[103] G. Gu, H. Xu, S. Peng, L. Li, S. Chen, T. Lu, X. Guo, Integrated Soft Ionotronic Skin with Stretchable and Transparent Hydrogel–Elastomer Ionic Sensors for Hand-Motion Monitoring, Soft Robotics. 6 (2019) 368–376. https://doi.org/10.1089/soro.2018.0116.

[104] Y. Bai, B. Chen, F. Xiang, J. Zhou, H. Wang, Z. Suo, Transparent hydrogel with enhanced water retention capacity by introducing highly hydratable salt, Appl. Phys. Lett. 105 (2014) 151903. https://doi.org/10.1063/1.4898189.
[105] C. Yang, Z. Suo, Hydrogel ionotronics, Nat Rev Mater. 3 (2018) 125–142. https://doi.org/10.1038/s41578-018-0018-7.
[106] J. Yang, R. Bai, B. Chen, Z. Suo, Hydrogel Adhesion: A Supramolecular Synergy of Chemistry, Topology, and Mechanics, Adv. Funct. Mater. 30 (2020) 1901693. https://doi.org/10.1002/adfm.201901693.
[107] H. Yuk, T. Zhang, S. Lin, G.A. Parada, X. Zhao, Tough bonding of hydrogels to diverse non-porous surfaces., Nat Mater. 15 (2016) 190–196. https://doi.org/10.1038/nmat4463.
[108] S. Ebnesajjad, Chapter 12 - Adhesion Promoters, in: S. Ebnesajjad (Ed.), Surface Treatment of Materials for Adhesive Bonding (Second Edition), Second Edition, William Andrew Publishing, Oxford, 2014: pp. 301–329. https://doi.org/10.1016/B978-0-323-26435-8.00012-5.

List of Publications

Journal papers

- **Massimiliano Mastrangelo**, Fabio Caruso, Giuseppe Carbone, and Vito Cacucciolo, "Electroadhesion zipping with soft grippers on curved objects", *Extreme Mechanics Letters* (2023). DOI: https://doi.org/10.1016/j.eml.2023.101999.

Conference proceedings

- **Massimiliano Mastrangelo** and Vito Cacucciolo, "High-Force Soft Grippers with Electroadhesion on Curved Objects", *2022 IEEE 5th International Conference on Soft Robotics (RoboSoft)*, pages 384-389, 2022. DOI: 10.1109/RoboSoft54090.2022.9762116.
- **Massimiliano Mastrangelo**, Giuseppe Carbone, and Vito Cacucciolo, "Electroadhesion tribology: 4-orders-of-magnitude increase in the holding force of a soft robotic gripper by changing the grasping angle from peeling to wrapping", *8° Workshop AIT "Tribologia e Industria"*, 2022.

In preparation

- **Massimiliano Mastrangelo**, Gabriele Pupillo, Giuseppe Lorusso and Vito Cacucciolo, "Electroadhesion on Curved Objects: Principles and Applications"
- **Massimiliano Mastrangelo**, Shunsuke Kanzawa, Daichi Sakamoto, Vito Cacucciolo, and Shingo Maeda. Topic: Electric modulation of hydrogel contact force and application in soft robotics.